8-2016

An R-Matrix, Quantum Defect Theory Approach to the Photoionization of Molecular Nitrogen

Gaetan L. VanGyseghem
Western Michigan University, gaetan.vangyseghem@gmail.com

AN R-MATRIX, QUANTUM DEFECT THEORY APPROACH TO THE PHOTOIONIZATION OF MOLECULAR NITROGEN

Gaetan L. VanGyseghem, Ph.D.

Western Michigan University, 2016

When radiation interacts with a molecule, several processes may occur. One of these, photoionization, is the topic of this study. The system is broken down into two nuclei and N electrons, the wavefunctions of which are entirely codependent. Operating under the Born-Oppenheimer approximation[1,2] allows for the nuclear and electronic wavefunctions to be separable, which greatly simplifies the situation. The task, then, is to freeze the nuclei and find the electronic wavefunctions . These fixed-nuclei wavefunctions are found, in this study, using the UK molecular R-Matrix (UKRmol) suite of codes[3,4,5,6,7,8], which solves for the wavefunctions separately near the nuclei and far from the nuclei, then matches the solutions smoothly at the boundary of these regions.
The Born-Oppenheimer approximation , which allows such a separation of nuclear and electronic motion, is, however, only applicable when the electronic motion is very fast compared to the nuclear motion. Near the nuclei, the electron's kinetic energy is great, and this approximation is sufficient. When a low-energy electron is far from the nuclei, its speed is significantly decreased, and the Born-Oppenheimer approximation breaks down. To account for this, the quantum defects, which characterize the complicated inner region, i.e., the region in which the Born-Oppenheimer approximation is valid, on the boundary, are extracted from the frozen-nuclei results and used to form an unphysical reactance matrix $\underline{\underline{\mathbf{K}}}(R)$ and dipole matrix $\vec{d}(R)$. From these, a vibrational frame transformation is applied, and a more prudent result is achieved.
The primary focus of this study is the photoabsorption of molecular nitrogen (N_2) near the first ionization threshold. Beginning with an existing photoionization model[9], a self-consistent field (SCF) representation and a configuration-interaction (CI) representation have been treated using the UKRmol suite of codes. This has been used to construct photoionization cross sections σ_{PI}, as well as R-matrices $\underline{\underline{\mathbf{R}}}$, physical and unphysical reactance matrices $\underline{\underline{\mathbf{K}}}^{(\text{phys})}$ and $\underline{\underline{\mathbf{K}}}$ as functions of energy, and dipole matrices $\vec{d}$ [10,11,12]. From the reactance matrices, the eigenquantum defects μ were extracted and plotted against energy. These eigenquantum defects or reactance matrices are needed as a function of internuclear separation R to enact a vibrational frame transformation via potential energy curves, which were constructed for both $N_2$and N_2^+.

AN R-MATRIX, QUANTUM DEFECT THEORY APPROACH TO THE PHOTOIONIZATION OF MOLECULAR NITROGEN

by

Gaetan L. VanGyseghem

A dissertation submitted to the Graduate College
in partial fulfillment of the requirements
for the degree of Doctor of Philosophy
Physics
Western Michigan University
August 2016

Doctoral Committee:

Thomas Gorczyca, Ph.D., Chair
Manuel Bautista, Ph.D.
Elena Litvinova, Ph.D.
Chris Greene, Ph.D.

To my wonderful wife, Julie, and to our endlessly amazing kids, Tristan, Lucy, and Norah. I love you dearly. Thank you.

ACKNOWLEDGEMENTS

"The compelling thing about making art - or making anything, I suppose - is the moment when the vaporous, insubstantial idea becomes a solid there, a thing, a substance in a world of substances." -Audrey Niffenegger

There are so many people that I'd like to thank, and I'm sure to miss several. This has been a big undertaking, and there is no way I could have done this without the help of many. So to those below, and to those I miss, thank you, sincerely, for helping, guiding, encouraging, sculpting, feeding, inspiring, and pushing me. Here's to you.

To my advisor, Dr. Tom Gorczyca:
Thank you for your patience. I'm sure there are many frustrations that come with being an advisor, but you've stuck with me. Thank you also for not being a single-faceted advisor, but being someone with whom I could talk about life, jokes, politics, and whatever happened to come up. I've learned much from you, and it's by no means limited to physics. Thank you.

To Connor:
Thank you for all you've done. Your visits were immeasurably helpful, and I would not have been able to get a foothold in all this code without you. Thank you.

To my mom:
Thank you for your interest and encouragement. You never doubted me, and you always made a big deal out of small victories. Thank you.

To Don and Terrie:
Thank you for all your support. Thank you for believing in me.

To my wonderful, tireless, ever-encouraging wife, Julie:
Thank you. Thank you for always being there to celebrate the highs and to commiserate in times of frustration. Thank you for putting up with my long nights of work. Thank you for driving so that I could finish a thought on the road. Thank you for enduring

the “almost done” meetings that lasted an extra hour. Thank you for being my voice of encouragement, not just when I was struggling, but also when everything was running smoothly. Thank you. Thank you.

To Tristan:
Thank you for being my brilliant boy. Thank you for asking questions, for playing with me, and for all your cards and hugs and excitement and love. I love you.

To Lucy:
Thank you for being the amazing girl you are. Thank you for holding things together. You’re such a sweetheart, and nothing ever escapes you. I love you.

To Norah:
Thank you. I’ve been in grad school for your entire life so far, and you’ve been there with all of your clever, heartfelt, and absolutely crazy ways. You bring so much joy. I love you.

This has been quite the journey, and I deeply appreciate all the help I’ve had along the way. Now, with the close of this, comes the beginning of the next adventure. Finally, there is only one thing left to say: allons-y!

Gaetan L. VanGyseghem

TABLE OF CONTENTS

LIST OF FIGURES

1

Introduction

While an immense amount of theoretical work has been done in the realm of atomic photoionization, considerably less has been done in molecular photoionization. This is, of course, due to the computational demand inherent in molecular calculations. Where an atom exhibits three degrees of freedom, a molecule possesses more. A diatomic molecule has the same three translational degrees of freedom as an atom, but additionally has two rotational degrees of freedom, both about axes perpendicular to the internuclear axis, and a vibrational degree of freedom along said internuclear axis. Consequently, even a homonuclear molecule exhibits six degrees of freedom, thereby significantly increasing the time required for computation. It comes as no surprise, then, that the most well-studied molecule is hydrogen H_2, and that the study of molecules with larger nuclei, and, more importantly, more electrons, is relatively new.

The near-threshold, vibrationally-resolved photoionization spectrum of molecular ni-

trogen is not well understood, though a considerable amount of experimental spectral data exists[13,17,18,14,13]. Besides its puzzling photoionization spectrum, nitrogen is of particular interest due to its prevalance in Earth's atmosphere, as well as in the atmospheres of other planets and moons. Stemming from an existing photoionization model[9], this study applies quantum defect theory and a vibrational frame transformation to the photoionization calculations. This allows for a vibrationally-resolved photoionization cross section to be calculated and compared to the works of O'Keeffe, et al.[13], and Heays, et al.[14]

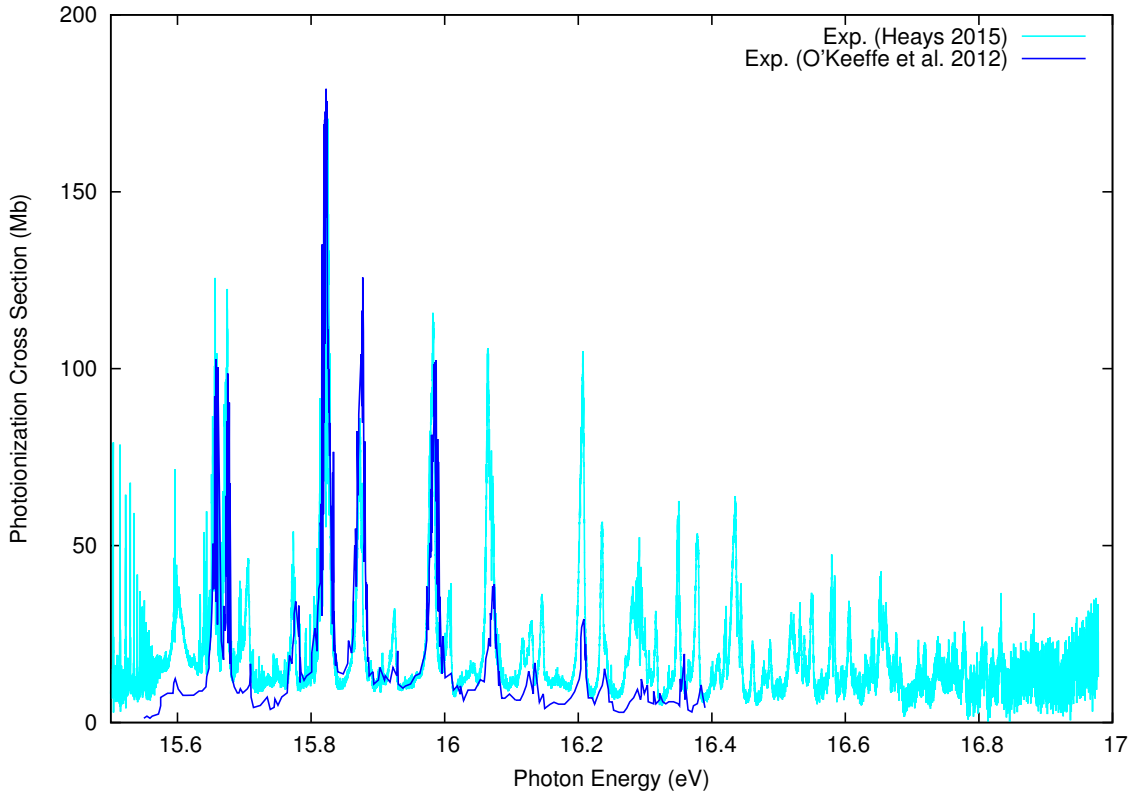

Figure 1.0.1: Experimental photoionization cross sections for N_2. The blue curve shows the experimental photoionization cross section of O'Keeffe, et al.[13], while the cyan curve shows the experimental photoabsorption cross section of Heays, et al.[14] These are the experimental works to which this theoretical study will be compared.

1.1 The R-matrix: A Brief History

The underlying principle to the R-matrix method originated with Kapur and Peierls in 1938,[19] who were attempting to describe nuclear phenomena. The idea utilized was that configuration space may be divided into two regions so as to exploit certain relations. In the inner region, they used a square-integrable basis, greatly simplifying the short-range properties of the wavefunction. The inner region wavefunction is found, subject to interactions prominent in the inner region, and the outer region wavefunction is found by neglecting the short-range inner region interactions in favor of those dominating at longer ranges. The two logarithmic derivatives are matched at the boundary, and the total wavefunction is constructed through this matching. The R-matrix, in fact, is nothing more than the inverse of the logarithmic derivative of the wavefunction at the boundary. Unfortunately for Kapur and Peierls, however, the energy dependence in their basis was nontrivial and therefore problematic. In 1947, Wigner and Eisenbud[20], building on and refining the work of Kapur and Peierls, introduced the R-matrix method. Rather than use the troublesome basis of their predecessors, Wigner and Eisenbud employed an energy-independent inner region basis. As a consequence, their R-matrix relied only on real, energy-independent quantities.

While both Wigner and Eisenbud and Kapur and Peierls had focused on nuclear resonances, Lane and Thomas[21] recognized the applicability of the R-matrix method to the non-resonant portions of cross sections. This incarnation would become known as the phenomenological R-matrix, and, while it is still used in nuclear astrophysics, it is not of any further direct consequence to this study.

Where the phenomenological R-matrix looks to parameterize low-energy cross sections, the so-called calculable R-matrix seeks to efficiently solve the Schrödinger equation at

both positive and negative energies. This was greatly simplified by the work of Bloch[22], who, in 1957, proposed an operator that allowed a more elegant approach. The work of Bloch was at least partially responsible for casting the R-matrix method in a new light, and perhaps sparked the evolution of the method to phenomena beyond nuclear scattering and resonances. Developed in 1965 by Haglund and Robson[23], the calculable R-matrix was ultimately expanded to atomic and, eventually, molecular applications. Haglund and Robson had applied the R-matrix method to square well potentials, but it was Buttle[24] who, in 1967, first applied the R-matrix to a real system. While the phenomenological R-matrix has remained, for the most part, in the realm of nuclear systems, the calculable R-matrix has since been adapted to atomic physics[25].

The adaptation of the R-matrix method to electron-atom collisions[26,27,28] came about in the 1960s and 1970s through the work of many, including Fano[29], Cooper, et al.[30], Burke, et al.[31], and Burke[32,33,34,35,36]. Work by Allison, et al.[37,38], Robb[39], and Burke and Taylor[40] introduced the extensions of the R-matrix framework to atomic polarizabilities, van der Waal's coefficients, and photoionization[8]. Later, the R-matrix methodology was further generalized and applied to electron-molecule collisions by Schneider, et al.[41,42,43] and Burke, et al.[44]. Much work has been done since to refine and optimize these methods, and R-matrix theory has become a very robust tool to treat nuclear, atomic, and molecular collision processes. A more detailed account is provided by Barrett, et al.[45], Aymar, et al.[46], Burke and Robb[47], Descouvemont and Baye[25], and Burke[8].

1.2 Quantum Defect Theory: A Brief History

The origins of quantum defect theory can be traced back to Rydberg himself. In Rydberg's 1890 paper[48], he presented the now-famous formula for the quantization of bound

atomic energy levels

$$E_n = -\frac{R_y}{(n-\delta_l)^2} \quad n = 1, 2, 3, \ldots,$$

where R_y is the Rydberg constant and δ_l is the quantum defect. The quantum defect, then, is an angular momentum-dependent quantity that acts as a nonhydrogenic correction on the energy of the outer electron. Later works by Seaton[49,50,51,52,12] and Fano and Rau[53] adopted the use of μ_l, or simply μ, for the quantum defect, and δ_l for the phase shift, and it is this notation that will be used henceforth.

The main aspect of quantum defect theory (QDT) is thus. The electron is, in general, subject to a long-range Coulombic field and a myriad of short-range multiparticle interactions. Near the ionic core, be it atomic or molecular, the electron is subject to very strong potentials, so that its total energy lies far above the potential "floor", and its kinetic energy is sufficiently large. In this region, then, the electron is not particularly sensitive to small changes in either energy or potential energy. Far from the ionic core, on the other hand, the short-range interparticle interactions die off, and the long-range Coulomb field dominates. In this region, for low-energy electrons, the energy of the electron lies close to the potential "floor," so that small changes in potential might effect very large changes in the electronic wavefunction, so much so that a formerly continuum state may even become bound for a small change in energy, leading to resonances that would otherwise have been missed. Rather than determine the nature of the state a priori, then, MQDT treats all channels as open, closing energetically unavailable channels only after all other transformations have been enacted, thereby preserving resonance series.

Theoretical treatises by Hartree[54,55,56,57], Ham[58], and Seaton[49,50,51] greatly expanded quantum defect theory, so that it had become used to calculate asymptotic wavefunctions

and phases, which facilitated the use of QDT for atomic collision problems[51], including photoionization[59]. Further work by Ross and Shaw[60], Gailitis[61], and Bely, et al.[62] laid out the groundwork for multichannel quantum defect theory (MQDT), and Seaton's 1966 paper[52] provided a more comprehensive theoretical account thereof. The advent of MQDT brought about scores of studies in atomic physics, and MQDT is widely used today.

It was Fano's 1970 paper[63] that first applied MQDT to diatomic hydrogen, thereby paving the way for MQDT to be used to treat molecular processes. Rovibrational effects on the photoabsorption spectra of H_2 were then investigated by Fano[63,64], Jungen and Atabek[65,66], and by Atabek, Dill, and Jungen[67], whose photoionization results agreed well with experimental data from Dehmer and Chupka[68]. Vibrational preionization was later included for H_2 by Jungen and Dill[69], Jungen[70], and later Stephens and Greene[71]. A detailed account of the development of MQDT, especially in the context of molecules, is given by Greene and Jungen[72].

1.3 Current Work

The powerful methods of the R-matrix approach and MQDT each exploit differences in the potential experienced by an electron close to and far from the nucleus. It is only natural, then, that the marriage of these two methods is often found in theoretical studies. For molecules, the R-matrix method, MQDT, and frame transformations have each been used individually, and two of these three have been combined with some frequency since the late 1980s, including works by Tennyson[73], Shimamura, Noble, and Burke[74], Yoo[75], Little, et al.[76], Čurík and Greene[77], Hiyama and Kosugi[78], and Telmini, Bezzaouia, and Jungen[79], to name a few. However, the concurrent application of the three methods to molecular problems is much more infrequent, featuring works like those of Haxton and

Greene[80] and O'Mahony and Mota-Furtado[81].

The current study employs the R-matrix method through the UKRmol suite of codes to calculation of the photoionization of molecular nitrogen N_2. The R-matrix calculations are performed under the Born-Oppenheimer approximation , so that the nuclei are frozen. Rather than carry this set of calculations to completion in this manner, an unphysical reactance matrix $\underline{\underline{\mathbf{K}}}$ is calculated and written out separately, from which the eigenquantum defects μ are obtained. The eigenquantum defects, together with the transformation matrix between eigenchannel and fragmentation channel, contain all of the electron's pertinent short-range information[63], and vary slowly with energy, i.e., are minimally energy-dependent. These calculations are performed for a wide range of internuclear separation distances R, and potential energy curves are constructed therefrom, for both the neutral N_2 molecule and multiple electronic states of the N_2^+ ion. These potential curves are fit with a Morse function, from which analytic nuclear wavefunctions χ_v are constructed. Following this, the nuclear wavefunctions are used to enact a vibrational frame transformation upon the K-matrix and dipole matrix $\vec{d}$. Finally, the energetically unavailable channels are closed and physical, vibrationally-resolved photoionization cross sections calculated.

2

Theoretical Methodology

2.1 The Coulomb Potential

In order to address molecular photoionization, or molecular dynamics at all, one must first have a firm grasp on atomic principles, from which molecular discussions must spring. The natural starting point is the scattering of an electron off a Coulomb potential.

The time-independent Schrödinger equation for an electron scattering off a positive charge of $+Z$ is:

$$-\frac{\hbar^2}{2m_e}\nabla^2\psi(\vec{r}) - \frac{Z}{4\pi\epsilon_0 r}\psi(\vec{r}) = E\psi(\vec{r}), \tag{2.1.1}$$

where m_e is the mass of the electron. This may be expressed in atomic units:

$$m_e = e = \hbar = \frac{1}{4\pi\epsilon_0} = 1$$

to give:

$$-\frac{1}{2}\nabla^2\psi(\vec{r}) - \frac{Z}{r}\psi(\vec{r}) = E\psi(\vec{r}). \tag{2.1.2}$$

Expressed more explicitly,

$$\begin{aligned}\hat{\mathscr{H}} &= -\frac{1}{2}\nabla^2 - \frac{Z}{r} \\ &= -\frac{1}{2}\left[\frac{1}{r^2}\frac{\partial}{\partial r}\left(r^2\frac{\partial}{\partial r}\right) + \frac{1}{r^2\sin\theta}\frac{\partial}{\partial\theta}\left(\sin\theta\frac{\partial}{\partial\theta}\right) + \frac{1}{r^2\sin^2\theta}\frac{\partial^2}{\partial\phi^2}\right] - \frac{Z}{r}\end{aligned} \tag{2.1.3}$$

so that

$$-\frac{1}{2}\left[\frac{1}{r^2}\frac{\partial}{\partial r}\left(r^2\frac{\partial}{\partial r}\right) + \frac{1}{r^2 sin\theta}\frac{\partial}{\partial\theta}\left(\sin\theta\frac{\partial}{\partial\theta}\right) + \frac{1}{r^2\sin^2\theta}\frac{\partial^2}{\partial\phi^2} + \frac{2Z}{r}\right]\psi(\vec{r}) = E\psi(\vec{r}).$$

From here, the angular and radial portions of the wavefunction will be treated separately.

2.1.1 Angular Momentum

The classical orbital angular momentum of a particle is given by $\vec{L} = \vec{r} \times \vec{p}$, with $\vec{r}$ and $\vec{p}$ being the position and momentum vectors of the particle, respectively. With the momentum operator (in atomic units) defined as $\vec{p} = -i\vec{\nabla}$, this gives

$$\vec{L} = i\left(\hat{\theta}\frac{1}{\sin\theta}\frac{\partial}{\partial\phi} - \hat{\phi}\frac{\partial}{\partial\theta}\right)$$

where $\hat{\theta}$ and $\hat{\phi}$ are related back to Cartesian coorinates by

$$\begin{aligned}\hat{\theta} &= [\cos\theta\cos\phi]\,\hat{x} + [\cos\theta\sin\phi]\,\hat{y} - [\sin\theta]\,\hat{z} \\ \hat{\phi} &= [-\sin\phi]\,\hat{x} + [\cos\phi]\,\hat{y}.\end{aligned}$$

The angular momentum, then, may be written

$$\begin{aligned}\vec{L} &= i\left(\left[\,[\cos\theta\cos\phi]\,\hat{x} + [\cos\theta\sin\phi]\,\hat{y} - [\sin\theta]\,\hat{z}\right]\frac{1}{\sin\theta}\frac{\partial}{\partial\phi} - \left[\,[-\sin\phi]\,\hat{x} + [\cos\phi]\,\hat{y}\right]\frac{\partial}{\partial\theta}\right) \\ &= i\left(\left[\sin\phi\frac{\partial}{\partial\theta} - \cot\theta\cos\phi\frac{\partial}{\partial\phi}\right]\hat{x} + \left[-\cos\phi\frac{\partial}{\partial\theta} + \cot\theta\sin\phi\frac{\partial}{\partial\phi}\right]\hat{y} + \left[-\frac{\partial}{\partial\phi}\right]\hat{z}\right)\end{aligned} \tag{2.1.4}$$

so that, after some algebra,

$$|\vec{L}|^2 = L^2 = -\left(\frac{1}{\sin\theta}\frac{\partial}{\partial\theta}\left(\sin\theta\frac{\partial}{\partial\theta}\right) + \frac{1}{\sin^2\theta}\frac{\partial^2}{\partial\phi^2}\right). \tag{2.1.5}$$

Inspecting the Hamiltonian 2.1.3, the square of the angular momentum 2.1.5 is seen:

$$\begin{aligned}\hat{\mathscr{H}} &= -\frac{1}{2}\left[\frac{1}{r^2}\frac{\partial}{\partial r}\left(r^2\frac{\partial}{\partial r}\right) + \frac{1}{r^2}\underbrace{\left(\frac{1}{\sin\theta}\frac{\partial}{\partial\theta}\left(\sin\theta\frac{\partial}{\partial\theta}\right) + \frac{1}{\sin^2\theta}\frac{\partial^2}{\partial\phi^2}\right)}_{L^2}\right] - \frac{Z}{r} \\ &= -\frac{1}{2}\left[\frac{1}{r^2}\frac{\partial}{\partial r}\left(r^2\frac{\partial}{\partial r}\right) - \frac{1}{r^2}L^2\right] - \frac{Z}{r}.\end{aligned} \tag{2.1.6}$$

And thus, all the angular dependence in the Hamiltonian is manifest in the square of the angular momentum. The Schrödinger equation , then, becomes a separable differential equation, so that the wavefunction may be written as a product of a radial and an angular function:

$$\psi(r,\theta,\phi) = \mathscr{R}(r)\mathscr{Y}(\theta,\phi) \tag{2.1.7}$$

As such, each component, as well as the square of the angular momentum vector, necessarily commutes with the Hamiltonian, as well as with one another, i.e.,

$$\begin{aligned}\left[\hat{\mathscr{H}}, L_i\right] &= 0 \\ \left[\hat{\mathscr{H}}, L^2\right] &= 0 \\ \left[L_i, L^2\right] &= 0. \end{aligned} \tag{2.1.8}$$

It is therefore possible to construct a set of functions that are simultaneous eigenfunctions of the Hamiltonian, the square of the angular momentum vector, and any one component of the angular momentum. As can be seen from 2.1.4, however, the individual components of the angular momentum do not commute with one another

$$[L_i, L_j] \neq 0 \quad \text{for} \quad i \neq j,$$

so there can exist no simultaneous eigenfunctions of the Hamiltonian, the angular momentum vector *in its entirety*, and its square. Consequently, one component of the angular momentum vector must be chosen. With no preferred orientation in space, the z-axis may be chosen as the commuting component. The functions that accomplish this are the familiar spherical harmonics $Y_{lm}(\theta, \phi)$, for which

$$\begin{aligned} L^2 Y_{lm}(\theta, \phi) &= \left[l(l+1)\right] Y_{lm}(\theta, \phi) \\ L_z Y_{lm}(\theta, \phi) &= m Y_{lm}(\theta, \phi). \end{aligned} \tag{2.1.9}$$

Having established the angular portion of the wavefunction 2.1.7, the radial portion may now be addressed.

2.1.2 The Radial Wavefunction

The wavefunction for an electron scattering off a Coulomb potential may then be written, as per 2.1.7, as:

$$\psi(r,\theta,\phi) = \mathscr{R}(r)Y_{lm}(\theta\phi),$$

where $\mathscr{R}(r)$ is the radial portion of the wavefunction, which has yet to be discussed. The differential equation for the radial portion of the wavefunction was established in 2.1.6, and, with the eigenvalues of L^2 and L_z established in 2.1.9, is written:

$$\begin{aligned}\hat{\mathscr{H}}\psi(r,\theta,\phi) &= \left(-\frac{1}{2}\left[\frac{1}{r^2}\frac{\partial}{\partial r}\left(r^2\frac{\partial}{\partial r}\right) - \frac{1}{r^2}L^2\right] - \frac{Z}{r}\right)\mathscr{R}(r)Y_{lm}(\theta,\phi) \\ &= -\left(\frac{1}{2}\left[\frac{1}{r^2}\frac{\partial}{\partial r}\left(r^2\frac{\partial}{\partial r}\right) - \frac{l(l+1)}{r^2}\right] + \frac{Z}{r}\right)\mathscr{R}(r)Y_{lm}(\theta,\phi). \qquad (2.1.10)\end{aligned}$$

With the angular contribution already determined, this leaves

$$\left(-\frac{1}{2r^2}\frac{\partial}{\partial r}\left(r^2\frac{\partial}{\partial r}\right) + \frac{l(l+1)}{2r^2} - \frac{Z}{r}\right)\mathscr{R}(r) = E\mathscr{R}(r),$$

which may be further simplified by defining a function $u(R)$ such that

$$u(r) \equiv r\mathscr{R}(r). \qquad (2.1.11)$$

This changes 2.1.10 to a more familiar differential equation

$$\left(-\frac{1}{2}\frac{d^2}{dr^2} + \frac{l(l+1)}{2r^2} - \frac{Z}{r} \right) u(r) = Eu(r)$$

or

$$\left(\frac{d^2}{dr^2} + 2E + \frac{2Z}{r} - \frac{l(l+1)}{r^2} \right) u(r) = 0, \tag{2.1.12}$$

where the partial derivatives have become full derivatives in r. Defining an effective potential

$$V_{eff}(r) = \frac{l(l+1)}{2r^2} - \frac{Z}{r} \tag{2.1.13}$$

shows the radial part of the Schrödinger equation to be nothing more than

$$\left(-\frac{1}{2}\frac{d^2}{dr^2} + V_{eff}(r) \right) u(r) = Eu(r),$$

so that $V_{eff}(r)$ contains the so-called centrifugal barrier

$$V_{\text{(centrifugal)}} = \frac{l(l+1)}{2r^2},$$

as is the common practice in any quantum mechanics text. This effective potential is shown in Figure 2.1.2 for several angular momentum values. The solutions to 2.1.12 are the regular Coulomb functions $S_l(kr)$, which behave sine-like for large r, and the irregular Coulomb functions $C_l(kr)$, which behave cosine-like for large r. Including normalization, the Coulomb functions are, as discussed by Abramowitz and Stegun[82],

$$\begin{aligned} S_l(\eta,\rho) &= C_l(\eta)\rho^{l+1}e^{-i\rho}{}_1F_1\left(l+1-i\eta, 2l+2, 2i\rho\right) \\ C_l(\eta,\rho) &= \frac{2\eta}{C_0^2(\eta)}S_l(\eta,\rho)\left[\ln(2\rho) + \frac{q_l(\eta)}{p_l(\eta)}\right] + \theta_l(\eta,\rho) \end{aligned} \tag{2.1.14}$$

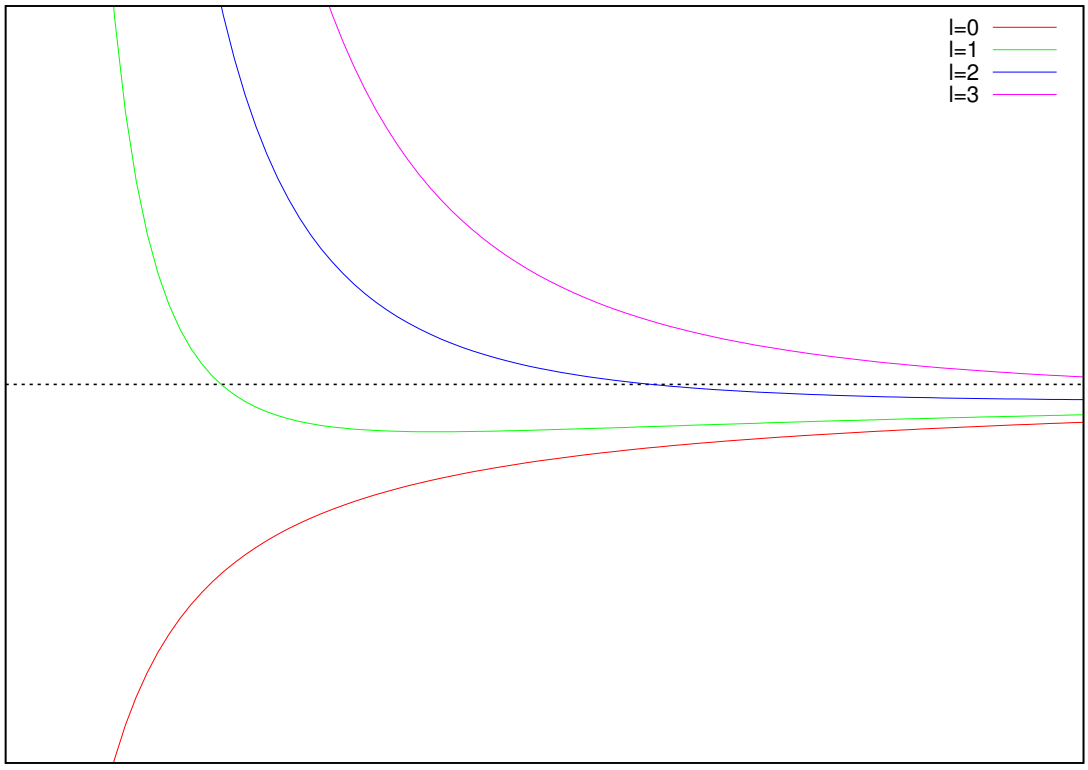

Figure 2.1.1: The Coulomb potential with a centrifugal barrier. The effective Coulomb potential, as written in 2.1.13, is a long-range attractive potential, as can be easily seen from the $l = 0$ curve. A centrifugal barrier is introduced with increased angular momentum. The dashed line is the asymptotic limit of the total effective potential.

with scaled quantities

$$\rho \equiv \sqrt{2E}r$$
$$\eta \equiv \frac{Z}{\sqrt{2E}}.$$

A brief description of these functions may be found in Appendix A, and a plot of the first few regular and irregular Coulomb functions is provided in Figure 2.1.2. The derivation and normalization of these wavefunctions is presented elegantly by Altunata[83].

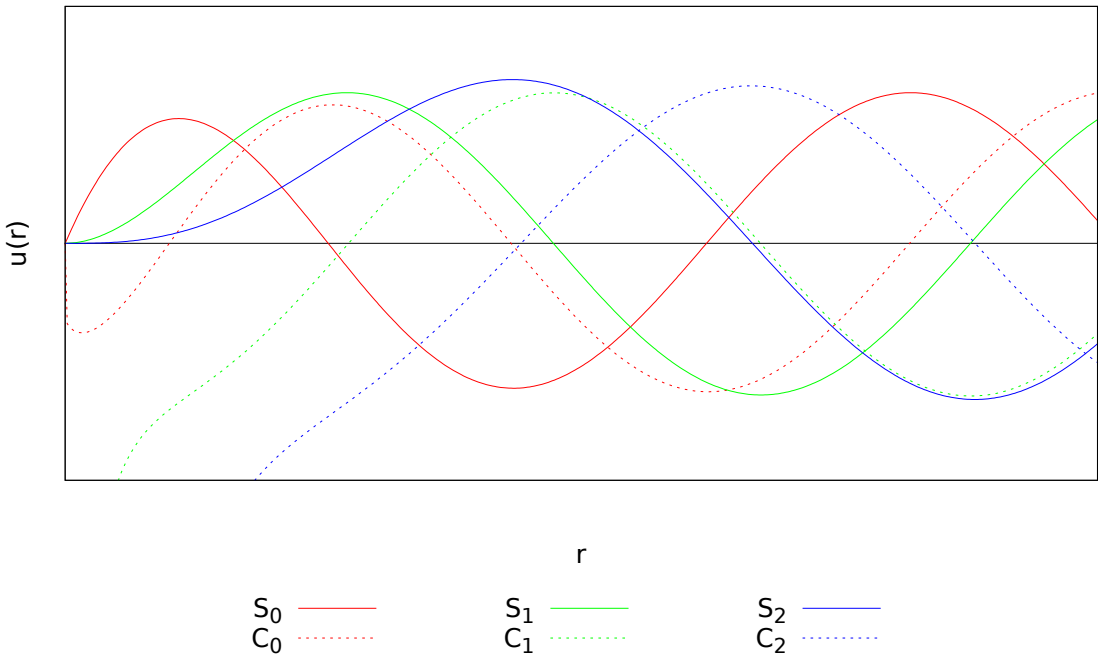

Figure 2.1.2: Regular and irregular Coulomb functions for positive energy. The regular Coulomb functions are plotted with solid lines for angular momentum values of $l = 0, 1,$ and 2. The corresponding irregular Coulomb functions are plotted with dashed lines. The functions are color-coded by angular momentum.

2.2 Symmetry of a Diatomic Molecule

Atoms are spherically symmetric, and so, then, are the electronic wavefunctions associated therewith. As a result, the electronic Hamiltonian for an atom, neglecting spin-orbit and other hyperfine corrections, commutes (separately) with each component of the angular momentum $\vec{L}$, as well as with the square of the full angular momentum vector $\vec{L}^2$, with corresponding eigenvalues E, M_L, and $L(L+1)\hbar^2$, respectively. This makes both L and M_L "good" quantum numbers, i.e., these are conserved quantities.

A diatomic molecule, on the other hand, does *not* exhibit spherical symmetry, and there exists a clear preferred orientation in space. In a fixed molecular "body frame,"[84,85] the internuclear axis is typically chosen along the $\hat{z}$-internuclear axis, and thus the molecule

exhibits *cylindrical* symmetry about $\hat{z}$; the molecular Hamiltonian is then invariant under rotations about $\hat{z}$, but not about $\hat{x}$ or $\hat{y}$. Consequently, L_z is a conserved quantity, but L_x and L_y, and thus, $\vec{L}^2$, are not. The electronic wavefunctions may then be constructed so as to be simultaneously eigenfunctions of $\hat{\mathscr{H}}$ and L_z. For molecules, a new quantum number Λ is defined, such that $\Lambda = |L_z|$[2]. This is, again, the projection of the electronic angular momentum onto the internuclear $\hat{z}$-axis. The reason for the use of the absolute value of L_z, rather than L_z outright, will be discussed shortly. The azimuthal part of the electronic wavefunction , then, is of the form:

$$\Phi_q^{(az)} \sim \frac{1}{2\pi} \cdot e^{\pm \Lambda \phi}. \tag{2.2.1}$$

The spectroscopic designations used with atoms, e.g., S, P, D, and F, for $L = 0, 1, 2,$ and 3, respectively, are also no longer valid. Instead, a molecular spectroscopic notation is used. To summarize the redesignation from the atomic to molecular case:

Atomic			Molecular		
$L^2 \lvert \Phi_s \rangle$	=	$L(L+1)\hbar^2 \lvert \Phi_s \rangle$	$L_z^2 \lvert \Phi_s \rangle$	=	$\Lambda^2 \hbar^2 \lvert \Phi_s \rangle$
$L_z \lvert \Phi_s \rangle$	=	$M\hbar \lvert \Phi_s \rangle$			
(L, M = integer)			(Λ = integer)		

and

Atomic					Molecular				
L	0	1	2	3	Λ	0	1	2	3
Letter	S	P	D	F	Letter	Σ	Π	Δ	Φ
(L = integer)					(Λ = positive integer)				

or, for an individual electron, $\lambda = |m|$ and

Atomic				
ℓ	0	1	2	3
letter	s	p	d	f
(ℓ = integer)				

Molecular				
λ	0	1	2	3
letter	σ	π	δ	ϕ
(λ = integer)				

Additionally, the electronic Hamiltonian $\hat{\mathscr{H}}_{\text{(el)}}$ is invariant under a reflection within a plane containing the $\hat{z}$-axis, e.g., the xz-plane[86]. A reflection in this plane yields the electronic transformation $y_i \rightarrow -y_i$

$$\begin{aligned} \hat{\mathbf{\Pi}}_y y &= -y\hat{\mathbf{\Pi}}_y \\ \hat{\mathbf{\Pi}}_y p_y &= -p_y\hat{\mathbf{\Pi}}_y. \end{aligned} \tag{2.2.2}$$

This, then, means that the effect of $\hat{\mathbf{\Pi}}_y$ acting on some state characterized by magnetic quantum number m is

$$\hat{\mathbf{\Pi}}_y \left| m \right\rangle = \left| -m \right\rangle . \tag{2.2.3}$$

If the operator $\hat{\mathbf{\Pi}}_y$ is responsible for this reflection, then the invariance of $\hat{\mathscr{H}}_{\text{(el)}}$ under $\hat{\mathbf{\Pi}}_y$ signifies that

$$\left[\hat{\mathbf{\Pi}}_y, \hat{\mathscr{H}}_{\text{(el)}}\right] = 0. \tag{2.2.4}$$

In order to construct simultaneous eigenfunctions of $\hat{\mathscr{H}}_{\text{(el)}}$, $\hat{\mathbf{\Pi}}_y$, and L_z, it is required not only that both $\hat{\mathbf{\Pi}}_y$ and L_z commute with the Hamiltonian, but also that they commute with one another. First, L_z is defined as

$$\begin{aligned} L_z &\equiv \left(\vec{r} \times \vec{p}\right) \cdot \hat{z} \\ &= -i\hbar(x\frac{\partial}{\partial y} - y\frac{\partial}{\partial x}). \end{aligned} \tag{2.2.5}$$

With 2.2.2, this gives

$$\begin{aligned}\hat{\mathbf{\Pi}}_y L_z &= -i\hbar\left(\hat{\mathbf{\Pi}}_y(x\frac{\partial}{\partial y}) - \hat{\mathbf{\Pi}}_y(y\frac{\partial}{\partial x})\right)\\ &= -i\hbar\left(x(-\frac{\partial}{\partial y})\hat{\mathbf{\Pi}}_y - (-y)\frac{\partial}{\partial x}\hat{\mathbf{\Pi}}_y\right)\\ &= -L_z\hat{\mathbf{\Pi}}_y, \end{aligned} \tag{2.2.6}$$

so that

$$\begin{aligned}\left[\hat{\mathbf{\Pi}}_y, L_z\right] &= \hat{\mathbf{\Pi}}_y L_z - L_z\hat{\mathbf{\Pi}}_y\\ &= 2\hat{\mathbf{\Pi}}_y L_z \neq 0, \end{aligned} \tag{2.2.7}$$

in general. Thus, both $\hat{\mathbf{\Pi}}_y$ and L_z commute with the Hamiltonial $\hat{\mathscr{H}}_{\text{(el)}}$

$$\left[\hat{\mathbf{\Pi}}_y, \hat{\mathscr{H}}_{\text{(el)}}\right] = \left[L_z, \hat{\mathscr{H}}_{\text{(el)}}\right] = 0,$$

but not with one another

$$\left[\hat{\mathbf{\Pi}}_y, L_z\right] \neq 0.$$

Consequently, there can exist no simultaneous eigenfunction of $\hat{\mathscr{H}}_{\text{(el)}}$, L_z, and $\hat{\mathbf{\Pi}}_y$. However, 2.2.7 suggests a different conserved quantity that commutes with $\hat{\mathbf{\Pi}}_y$. If the z-component of the angular momentum commutes with the Hamiltonian, then it follows that its square will do likewise

$$\left[L_z, \hat{\mathscr{H}}_{\text{(el)}}\right] = 0 \implies \left[L_z^2, \hat{\mathscr{H}}_{\text{(el)}}\right] = 0.$$

Looking at 2.2.6, it is clear that

$$\hat{\mathbf{\Pi}}_y L_z^2 = L_z^2 \hat{\mathbf{\Pi}}_y$$

and therefore

$$\left[\hat{\mathbf{\Pi}}_y, L_z^2\right] = 0. \tag{2.2.8}$$

As such, there *does* exist a simultaneous eigenfunction, not of $\hat{\mathscr{H}}_{\text{(el)}}$, $\hat{\mathbf{\Pi}}_y$, and L_z, but of $\hat{\mathscr{H}}_{\text{(el)}}$, $\hat{\mathbf{\Pi}}_y$, and L_z^2. This, then, is why $\Lambda = |M|$ is chosen in the beginning of this section.

As this reflection operator $\hat{\mathbf{\Pi}}_y$ commutes with the electronic Hamiltonian $\hat{\mathscr{H}}_{\text{(el)}}$, i.e., $\left[\hat{\mathbf{\Pi}}_y, \hat{\mathscr{H}}_{\text{(el)}}\right]$, the energies of the states $|\,\Phi_s\rangle$ and $\hat{\mathbf{\Pi}}_y\,|\,\Phi_s\rangle$ are equal, i.e., the energy of the wavefunction is independent of the sign of the z-component of angular momentum:

$$\left(\hat{\mathscr{H}}_{\text{(el)}} - E\right)|\,\Phi_s^{\pm}\rangle = \left(\hat{\mathscr{H}}_{\text{(el)}} - E\right)|\,\Phi_s^{\pm}\rangle = 0$$

or

$$\hat{\mathscr{H}}_{\text{(el)}}\,|\,\Phi_s^{\pm}\rangle = E\,|\,\Phi_s^{\pm}\rangle$$

Because both the $+m$ and $-m$ wavefunctions are valid solutions to the Schrödinger equation , so is a linear combination thereof. To guarantee even or odd parity, then, wavefunctions $\Phi_s^{\pm}$ are chosen such that

$$|\,\Phi_s^{\pm}\rangle \equiv \frac{|m\rangle \pm |-m\rangle}{\sqrt{2}} \quad \text{for } m \neq 0,$$

where the factor of $1/\sqrt{2}$ is included to maintain normalization. As discussed, these

wavefunctions satisfy three eigenvalue equations

$$\begin{aligned} \hat{\mathscr{H}}_{(\mathrm{el})} \left| \Phi_s^{\pm} \right\rangle &= E \left| \Phi_s^{\pm} \right\rangle \\ L_z^2 \left| \Phi_s^{\pm} \right\rangle &= \hbar^2 \Lambda^2 \left| \Phi_s^{\pm} \right\rangle \\ \hat{\mathbf{\Pi}}_y \left| \Phi_s^{\pm} \right\rangle &= \pm \left| \Phi_s^{\pm} \right\rangle . \end{aligned} \tag{2.2.9}$$

Thus the electronic states with $\Lambda \neq 0$ are doubly degenerate. The energy of the state with an L_z eigenvalue of $+\Lambda\hbar$ is equal to that with eigenvalue $-\Lambda\hbar$, meaning the direction of the projections of $\vec{L}$ onto the $\hat{z}$-axis has no effect on the energy of the state. This is, of course, an approximation, and, in reality, the energies of the states with L_z eigenvalues of $\pm\Lambda\hbar$ are not *precisely* equal, but they are very nearly so. Because of this (approximate) energy degeneracy, the additional $\pm$ notation is not typically specified for $\Lambda \neq 0$ states.

For the $\Lambda = 0$ case (the Σ states), there is no such degeneracy. Because the second eigenvalue equation in 2.2.9 has an eigenvalue of zero, and likewise, the eigenvalue of the z-component of angular momentum is zero

$$L_z^2 \left| \Lambda = 0 \right\rangle = 0 \implies L_z \left| \Lambda = 0 \right\rangle = 0.$$

It follows, then, that $\Lambda = 0$ (Σ) states may be constructed to be simultaneous eigenfunctions of $\hat{\mathscr{H}}_{(\mathrm{el})}$, $\hat{\mathbf{\Pi}}_y$, and L_z. These states are non-degenerate, so that the Σ^+ and Σ^- states have different energies. Because of this, the additional $\pm$ indicator is explicitly included for Σ states.

The electronic wavefunctions Φ_s are constructed so as to be simultaneously eigenfunctions of $\hat{\mathscr{H}}_{(\mathrm{el})}$, L_z^2, and $\hat{\mathbf{\Pi}}_y$. Because $\hat{\mathbf{\Pi}}_y$ represents a reflection in the xz-plane, an even number

of consecutive instances of this operator acts as the identity operator $\hat{\mathbb{1}}$:

$$\left(\hat{\mathbf{\Pi}}_y\right)^2 |\,\Phi_s\rangle = |\,\Phi_s\rangle \tag{2.2.10}$$

which indicates that $\hat{\mathbf{\Pi}}_y$ has eigenvalues of ± 1. States with the eigenvalue $+1$ are of even parity in $\hat{\mathbf{\Pi}}_y$, and are denoted Σ^+, while those with the eigenvalue -1 are of odd parity in $\hat{\mathbf{\Pi}}_y$, and are denoted Σ^-.[2]

In the case of a *homonuclear* diatomic molecule, there is an additional point of symmetry, which is taken as the origin. This point is located at the center of mass of the molecule, and has been previously denoted O. As with $\hat{\mathbf{\Pi}}_y$, a reflection through this point may be represented by some operator $\hat{\mathbf{\Pi}}_{\vec{r}}$, so that $\hat{\mathbf{\Pi}}_{\vec{r}}$, acting on $|\,\Phi_s\rangle$, enacts the transformation $\vec{r}_i \rightarrow -\vec{r}_i$. Again, this reflection operator commutes with the Hamiltonian:

$$\left[\hat{\mathbf{\Pi}}_{\vec{r}}, \hat{\mathscr{H}}_{(\mathrm{el})}\right] = 0 \tag{2.2.11}$$

and with L_z:

$$\left[\hat{\mathbf{\Pi}}_{\vec{r}}, L_z\right] = 0. \tag{2.2.12}$$

The eigenvalues of $\hat{\mathbf{\Pi}}_{\vec{r}}$ are, as with $\hat{\mathbf{\Pi}}_y$, equal to ± 1, and the parity in $\hat{\mathbf{\Pi}}_{\vec{r}}$ of these states adds a subscript of g or u, for *gerade*, German for *even* or *intuitive*, and *ungerade*, German for *odd* or *counterintuitive*, respectively. Note that this symmetry is not specific to Σ states, but may be applied to Π, Δ, and Φ states, as well. Consequently, a diatomic molecule may exhibit the degenerate states:

$$\Pi_{g/u} \quad \Delta_{g/u} \quad \Phi_{g/u}$$

and so on, along with the four *non*degenerate Σ states[86,2]:

$$\Sigma_g^+ \quad \Sigma_u^+ \quad \Sigma_g^- \quad \Sigma_u^-.$$

2.3 The Electronic Hamiltonian

The time-independent Schrödinger equation for the molecule is

$$\hat{\mathscr{H}}\Psi\left(\vec{R};\vec{r}_1,\vec{r}_2,\ldots,\vec{r}_N\right) = E\Psi\left(\vec{R};\vec{r}_1,\vec{r}_2,\ldots,\vec{r}_N\right) \tag{2.3.1}$$

where $\vec{R}$ is the nuclear separation vector and $\left\{\vec{r}_i\right\}$ are the position vectors of the electrons. In order to treat this, Ψ is expanded in terms of some set of basis functions. One such convenient set is the set of electronic wavefunctions for the fixed-nuclei, i.e., constant $\vec{R}$, case. The corresponding solution to the Schrödinger equation is known as the *electronic wavefunction*:

$$\hat{\mathscr{H}}_{\text{(el)}}\Phi_q\left(\vec{R};\vec{r}_1,\vec{r}_2,\ldots,\vec{r}_N\right) = E_q(R)\left(\vec{R};\vec{r}_1,\vec{r}_2,\ldots,\vec{r}_N\right), \tag{2.3.2}$$

where $\hat{\mathscr{H}}_{\text{(el)}}$ is the electronic Hamiltonian:

$$\hat{\mathscr{H}}_{\text{(el)}} = \hat{\mathbf{T}}_{(el)} + \hat{\mathbf{V}},$$

and $\hat{\mathbf{T}}_{(el)}$ and $\hat{\mathbf{V}}$ are the kinetic and potential energy operators, respectively.

It should be noted that the energies $E_q(R)$ depend on $R = |\vec{R}|$, not on $\vec{R}$, i.e., there is no dependence on the *orientation* of $\vec{R}$, but rather on its magnitude alone. Contrary to this, however, the wavefunctions Φ_q *do* depend on $\vec{R}$, i.e., on the magnitude *and* ori-

entation of $\vec{R}$[2,85,86].

For each internuclear separation vector $\vec{R}$, the electronic wavefunctions Φ_q form a complete orthgonal set. Normalizing these gives:

$$\langle \Phi_q | \Phi_p \rangle \equiv \int \Phi_q^* \Phi_p \, d\vec{r}_1 d\vec{r}_2 \ldots d\vec{r}_N = \delta_{qp}$$

where Φ_q^* and Φ_p are understood to depend on $\vec{R}$ and $\left\{\vec{r}_i\right\}$. While both Φ_q and Φ_p depend on the magnitude *and* orientation of $\vec{R}$, the inner product depends only on the magnitude, not the orientation, of $\vec{R}$, which must be the case as the inner product is a scalar, i.e., invariant under rotations. As $\{\Phi_q\}$ is complete, it may serve as a basis in which the molecular wavefunction Ψ may be expanded:

$$\Psi\left(\vec{R}; \vec{r}_1, \vec{r}_2, \ldots, \vec{r}_N\right) = \sum_q F_q\left(\vec{R}\right) \Phi_q(\vec{r}_1, \vec{r}_2, \ldots, \vec{r}_N), \tag{2.3.3}$$

where the expansion coefficients $F_q\left(\vec{R}\right)$ are wavefunctions representing the nuclear motion when the molecule occupies some electronic state q.

Previously, the electronic Hamiltonian was defined:

$$\hat{\mathscr{H}}_{\text{(el)}} = \hat{\mathbf{T}}_{(el)} + \hat{\mathbf{V}}_{(el)}.$$

The total Hamiltonian for the molecule, however, includes nuclear motion, so a nuclear term must be incorporated. Of course, there are two nuclei, so there is also a potential term between the two nuclei:

$$\hat{\mathbf{V}}_{\text{(nuc)}} = \frac{Z_A Z_B}{R} \frac{e^2}{4\pi\epsilon_0},$$

so that the total Hamiltonian is

$$\begin{aligned}\hat{\mathscr{H}} &= \left(\hat{\mathbf{T}}_{(el)} + \hat{\mathbf{V}}_{(el)}\right) + \left(\hat{\mathbf{T}}_{(nuc)} + \hat{\mathbf{V}}_{(\text{nuc})}\right) \\ &= \hat{\mathscr{H}}_{(\text{el})} + \hat{\mathscr{H}}_{(\text{nuc})}.\end{aligned}$$

Substituting this expression, along with the expansion of Ψ, into the Schrödinger equation

$$\hat{\mathscr{H}}\Psi\left(\vec{R};\vec{r}_1,\vec{r}_2,\ldots,\vec{r}_N\right) = E\Psi\left(\vec{R};\vec{r}_1,\vec{r}_2,\ldots,\vec{r}_N\right)$$

gives

$$\left[\hat{\mathscr{H}}_{(\text{el})} + \hat{\mathscr{H}}_{(\text{nuc})}\right]\sum_q F_s(\vec{R})\Phi_q = E\sum_q F_s(\vec{R})\Phi_q, \tag{2.3.4}$$

or

$$\sum_q \left[\hat{\mathscr{H}}_{(\text{el})} + \hat{\mathscr{H}}_{(\text{nuc})} - E\right]|\,\Phi_q\rangle\; F_q(\vec{R}) = 0. \tag{2.3.5}$$

Taking the inner product with $\langle\Phi_s\,|$, where s is an integer, yields:

$$\sum_q \langle\Phi_s\,|\,\hat{\mathscr{H}}_{(\text{el})} + \hat{\mathscr{H}}_{(\text{nuc})} - E\,|\,\Phi_q\rangle\; F_q(\vec{R}) = 0,$$

or, more explicitly,

$$\begin{aligned}&\sum_q \Bigg[\langle\Phi_s\,|\,\hat{\mathscr{H}}_{(\text{el})} - E\,|\,\Phi_q\rangle \\ &+ \left\langle\Phi_s\left|-\frac{\hbar^2}{2m}\frac{1}{R^2}\frac{\partial}{\partial R}\left(R^2\frac{\partial}{\partial R}\right) + \frac{\vec{N}^2}{2mR^2} + \frac{Z_A Z_B}{R}\frac{e^2}{4\pi\epsilon_0}\right|\Phi_q\right\rangle\Bigg] F_q(\vec{R}) = 0\end{aligned} \tag{2.3.6}$$

where the last term is $\left\langle \Phi_s \left| \hat{\mathscr{H}}_{(\text{nuc})} \right| \Phi_q \right\rangle$. It should be noted, at this point, that the mass in 2.3.6 is not precisely the mass of the electron, but rather its reduced mass in the electron-nucleus system

$$m \equiv \frac{M_{(\text{nuc})}\, m_{e^-}}{M_{(\text{nuc})} + m_{e^-}}.$$

With the mass of the electron being so much smaller than the mass of the nucleus, this reduced mass is very near the electron's mass. It is typical to use μ to denote the reduced mass, but in the interest of clear distinction between this and eigenquantum defects, m will be used henceforth for the former. The first terms are simplified:

$$\begin{aligned}
\left\langle \Phi_s \left| \hat{\mathscr{H}}_{(\text{el})} \right| \Phi_q \right\rangle &= \langle \Phi_s | \left(\hat{\mathscr{H}}_{(\text{el})} | \Phi_q \rangle \right) \\
&= E_q(R) \langle \Phi_s | \Phi_q \rangle \\
&= E_q(R) \delta_{sq} \\
&= E_s(R)
\end{aligned}$$

and

$$\begin{aligned}
\langle \Phi_s | E | \Phi_q \rangle &= E \langle \Phi_s | \Phi_q \rangle \\
&= E\, \delta_{sq}.
\end{aligned}$$

The delta function in these selects $F_s(\vec{R})$ from the summation as the only nonzero contribution. The Schrödinger equation then reads:

$$\sum_q \left\langle \Phi_s \left| -\frac{\hbar^2}{2m} \frac{1}{R^2} \frac{\partial}{\partial R} \left(R^2 \frac{\partial}{\partial R} \right) + \frac{\vec{N}^2}{2mR^2} + \frac{Z_A Z_B}{R} \frac{e^2}{4\pi\epsilon_0} \right| \Phi_q \right\rangle \Bigg] F_q(\vec{R}) + \left[E_s(R) - E \right] F_s(\vec{R}) = 0. \qquad (2.3.7)$$

As Φ_q depends on $\vec{R}$, all partial derivatives, including the angular derivatives contained in $\vec{R}$, must act on the *product* $\Phi_q F_q(\vec{R})$.

2.4 The Born-Oppenheimer Approximation

The electrostatic forces on the nuclei are comparable to those on the electrons. However, the mass of the nucleus is much larger than that of the electron. Consequently, the electrons, in general, move with much greater speeds than the nuclei. The electronic wavefunctions Φ_q, therefore, vary much more slowly with respect to the internuclear separation vector $\vec{R}$ than do the nuclear wavefunctions $F_q(\vec{R})$:

$$\left|\frac{\partial}{\partial R}(\Phi_q)\right| \ll \left|\frac{\partial}{\partial R}(F_q)\right|,$$

and only the diagonal angular momentum matrix element is significant[2,85]:

$$\left\langle \Phi_s \left| \vec{N}^2 \right| \Phi_q \right\rangle \approx 0 \qquad \forall \qquad s \neq q.$$

The Schrödinger equation, after applying these approximations, reads:

$$\left[-\frac{\hbar^2}{2m}\frac{1}{R^2}\frac{\partial}{\partial R}\left(R^2\frac{\partial}{\partial R}\right) + \frac{\left\langle \Phi_s \left| \vec{N}^2 \right| \Phi_s \right\rangle}{2mR^2} + (E_s(R) - E) \right] F_s(\vec{R}) = 0 \qquad (2.4.1)$$

with a as an integer. As all indices are now the same, i.e., there are no cross terms, and the previously coupled equations are now uncoupled. These uncoupled equations describe the nuclear motion for a given electronic state s, and are known as the *nuclear wave equations*. Together, they comprise the Born-Oppenheimer, or adiabatic, approximation[2,85]. The major consequence of this is that the total wavefunction for the molecule may be

separated into an electronic and a nuclear wavefunction:

$$\Psi_s = F_s(\vec{R})\Phi_q(\vec{R};\vec{r}_1,\vec{r}_2,\ldots,\vec{r}_N), \tag{2.4.2}$$

where the electronic wavefunction contains information of both the electronic state of the N_2^+ target and the outer electron

$$\Phi_q\left(\vec{R};\vec{r}_1,\vec{r}_2,\ldots,\vec{r}_N\right) = \sum_{q,\ell}\left[\phi_q\left(R;r_1,r_2,\ldots,r_{N-1},\hat{r}_N;\sigma_1,\sigma_2,\ldots,\sigma_{N-1},\sigma_N\right) f_\ell\left(R;r_N\right)\right].$$

Here, the summation is allowed to sample all the electronic states q of the ionic target and all partial waves of the outer electron l.

It remains, then, to solve for the outer electronic wavefunctions f_q. This is done, again, by solving the fixed-nuclei electronic Schrödinger equation:

$$\begin{gathered}\hat{\mathscr{H}}_{(\mathrm{el})}\Phi_q(\vec{R};\vec{r}_1,\vec{r}_2,\ldots,\vec{r}_N) = E_q(R)\Phi_q(\vec{R};\vec{r}_1,\vec{r}_2,\ldots,\vec{r}_N)\\ \downarrow\\ \hat{\mathscr{H}}_{(\mathrm{el})}\Phi_q(\vec{r}_1,\vec{r}_2,\ldots,\vec{r}_N) = E_q\Phi_q(\vec{r}_1,\vec{r}_2,\ldots,\vec{r}_N).\end{gathered} \tag{2.4.3}$$

Note that although $\vec{R}$ is included as a parameter in the first line of 2.4.3, the nuclei are fixed, so that $\vec{R}$ does not vary. Thus, in the interest of clarity, the parameter $\vec{R}$ will henceforth be suppressed when it is fixed. Solving 2.4.3 is not, however, a trivial task, as the outer electron interacts significantly with both the other electrons and the nuclei. To address this, the R-matrix method is employed.

2.5 The Molecular R-Matrix Approach

The molecular R-matrix method[20,87,88,89,8] separates space into two regions, where different representations of the wavefunction are used in each region so as to exploit different physical properties, after which these wavefunctions are joined at the boundary[20]. In the case of the molecular R-matrix method, space is usually divided into an inner region $r < a$, in which the charge distributions of the target eigenstates are, for all intents and purposes, entirely contained, and an outer region $r > a$, in which only the long-range potentials, in this case, the Coulomb potential and angular momentum barrier, are important[8].

Electrons in the inner region are close enough to the nuclei so that the Born-Oppenheimer approximation provides an adequate description of the total, i.e., electronic plus nuclear, wavefunctions. In essence, the scattering electron, or, in this case, the photoelectron, has a total energy so much greater than its potential energy that it adjusts nearly instantaneously to a change in the orientation of the nuclei. Perhaps a more direct phrasing is that the electron has a much greater kinetic energy than do the nuclei, so that the relative time scales of the two render the nuclei frozen relative to the electron. Beside the Coulombic attraction to the nuclei, the photoelectron is subject to potential terms stemming from electrostatic interactions with each other electron. Additionally, electron exchange effects must be considered. These interactions, with the exception of the Coulomb potential exuded by the nuclei, are prominent only within a small distance of the nuclei, i.e., in the inner region $r < a$. In order to handle all of these short-range interactions, a close-coupling configuration interaction expansion is adopted. This is the subject of the next section.

In the outer region, electron exchange and correlation effects are small enough to ig-

nore. Here, the photoelectron is outside the charge distribution of the target eigenstates, and the wavefunctions are found in the influence of the long-range multipole potential of the target alone[8,90,91,25].

Ultimately, the R-matrix suite of programs connects the wavefunctions and their derivatives at the boundary $r = a$,

$$\psi^{(inner)}(r = a) = \psi^{(outer)}(r = a)$$
$$\frac{\partial}{\partial r}\psi^{(inner)}\bigg|_{r=a} = \frac{\partial}{\partial r}\psi^{(outer)}\bigg|_{r=a},$$

and by exploiting different representations in each region. This is illustrated rather nicely through a simpler example in Appendix C.

2.5.1 The Close-Coupling Expansion

A discussion of the R-matrix process must begin with the close coupling equations. The idea of the close coupling expansion began with Massey and Mohr[92,93] and Mott and Massey[94], who expressed the N-electron wavefunction as a product of the $(N-1)$-electron core and the N^{th} outer electron, i.e.,

$$\psi(\vec{r}_1\sigma_1, \ldots, \vec{r}_{(N-1)}\sigma_{(N-1)}, \vec{r}_N\sigma_N) = \sum\!\!\!\!\!\!\int_{i=1}^{(N-1)} \Phi_i\left(\vec{r}_1\sigma_1, \ldots, \vec{r}_{(N-1)}\sigma_{(N-1)}\right) F_i\left(\vec{r}_N\sigma_N\right), \tag{2.5.1}$$

where σ_i is the spin of the i_{th} electron. The summation is over the bound target eigenstates and the integral is over the continuum target eigenstates. The target eigenstates, both bound and continuum, are represented in 2.5.1 by Φ_i, and the outer electron by F_i. Rather than explicitly carry all of these indices, a notation will be adopted henceforth so

that

$$\vec{q}_{(N-1)} \equiv \vec{r}_1\sigma_1, \vec{r}_2\sigma_2, \ldots, \vec{r}_{(N-1)}\sigma_{(N-1)} \tag{2.5.2}$$

The electronic Hamiltonian, in atomic units, is

$$\begin{aligned}\hat{\mathscr{H}}_N &= -\sum_{i=1}^{N}\left(\frac{\nabla_i^2}{2} + \sum_{k=1}^{n_{nuc}}\frac{Z_k}{r_{ik}}\right) + \sum_{i>j}\sum_{j=1}^{N}\frac{1}{|\vec{r}_i - \vec{r}_j|} \\ &= \hat{\mathscr{H}}_{(N-1)} - \frac{1}{2}\nabla_N^2 - \sum_{k=1}^{n_{nuc}}\frac{Z_k}{r_{Nk}} + \sum_{i=1}^{N-1}\frac{1}{|\vec{r}_i - \vec{r}_N|}.\end{aligned} \tag{2.5.3}$$

Here, the first summation over i represents the one-electron and electron-nuclear interactions between the electrons and the nuclei, with the nested summation over k running over the individual nuclei, while the second double summation handles the two-electron interactions (between any two electrons). This yields a Schrödinger equation

$$\begin{aligned}\left[-\sum_{i=1}^{N}\left(\frac{\nabla_i^2}{2} + \sum_{k=1}^{n_{nuc}}\frac{Z_k}{r_{ik}}\right) + \sum_{i>j}\sum_{j=1}^{N}\frac{1}{r_{ij}} - E\right]\psi(\vec{q}_N) = 0 \\ \left[\sum_{i=1}^{N}\left(\nabla_i^2 - \sum_{k=1}^{n_{nuc}}\frac{2Z_k}{r_{ik}}\right) - \sum_{i>j}\sum_{j=1}^{N}\frac{2}{r_{ij}} + 2E\right]\psi(\vec{q}_N) = 0,\end{aligned} \tag{2.5.4}$$

wherein a shorthand notation has been adopted inside the double summation, such that

$$r_{ij} \equiv \left|\vec{r}_i - \vec{r}_j\right|. \tag{2.5.5}$$

The energy term in 2.5.4 may be broken down into a term entirely dependent on the target states $\Phi_i(\vec{q}_{(N-1)})$, and a sort of cross term. The target states are eigenfunctions of the $(N-1)$-electron Hamiltonian, and constitute a complete orthonormal set, so that a partial energy term ϵ may be introduced,

$$\left\langle \Phi_i(\vec{q}_{(N-1)}) \left| \hat{\mathscr{H}}_{(N-1)} \right| \Phi_j(\vec{q}_{(N-1)}) \right\rangle = \epsilon_i\delta_{ij}, \tag{2.5.6}$$

thereby leaving the energy as

$$E = \epsilon_i + \left\langle F_N(\vec{r}_N\sigma_N) \left| \left(-\frac{1}{2}\nabla_N^2 - \sum_{k=1}^{n_{nuc}} \frac{Z_k}{r_{Nk}} + \sum_{i=1}^{N-1} \frac{1}{r_{iN}} \right) \right| F_N(\vec{r}_N\sigma_N) \right\rangle$$
$$= \epsilon_i + \frac{1}{2}k_i^2$$

When the close-coupling expression 2.5.1 is substituted into the electronic Schrödinger equation 2.5.4, the result is an expansion in coupled differential equations

$$\left(\nabla^2 + k_i^2\right) F_i(\vec{r}_N\sigma_N) = 2 \sum\!\!\!\!\!\!\int_j V_{ij}(\vec{r}_N\sigma_N) F_j(\vec{r}_N\sigma_N), \tag{2.5.7}$$

where the potential energy matrix $V_{ij}(\vec{r}_N\sigma_N)$ is

$$V_{ij}(\vec{r}_N\sigma_N) \equiv \left\langle \Phi_i(\vec{q}_{(N-1)} \left| \sum_{i=1}^{N-1} \frac{1}{r_{iN}} - \sum_{k=1}^{n_{nuc}} \frac{Z_k}{r_{Nk}} \right| \Phi_j(\vec{q}_{(N-1)} \right\rangle. \tag{2.5.8}$$

In the inner region, electron exchange effects introduce singularities when integrating over the continuum terms[8,90]. To address this, Seaton[95] used explicitly antisymmetric wavefunctions, so that 2.5.1 becomes

$$\psi(\vec{q}_N) = \hat{\mathscr{A}} \sum_i \Phi_i(\vec{q}_{(N-1)}) F_i(\vec{r}_N\sigma_N), \tag{2.5.9}$$

where $\hat{\mathscr{A}}$ is an antisymmetrization operator

$$\hat{\mathscr{A}} = \frac{1}{\sqrt{N}} \left[1 - \sum_{i=1}^{N-1} \hat{\mathscr{P}}_{iN} \right],$$

with $\hat{\mathscr{P}}_{iN}$ being the operator that interchanges electrons i and N, i.e.,

$$\hat{\mathscr{P}}_{iN}\begin{pmatrix} \vec{r}_1\sigma_1 \\ \vec{r}_2\sigma_2 \\ \vdots \\ \vec{r}_i\sigma_i \\ \vdots \\ \vec{r}_N\sigma_N \end{pmatrix} = \begin{pmatrix} \vec{r}_1\sigma_1 \\ \vec{r}_2\sigma_2 \\ \vdots \\ \vec{r}_N\sigma_N \\ \vdots \\ \vec{r}_i\sigma_i \end{pmatrix}.$$

However, expanding the continuum in a discrete finite basis, along with its subsequent orthoganalization, removes a certain amount of Hilbert space. To recover this, an additional N-electron space is added, leading to an overall close-coupling expansion, in the inner region, of

$$\psi_\alpha = \hat{\mathscr{A}} \sum_{i,m_i} a_{\alpha i m_i} \Phi_i(\vec{q}_{(N-1)}) \eta_{m_{\gamma i}}(\vec{r}_N \sigma_N) + \sum_p b_{\alpha p} \varphi_p(\vec{q}_N). \tag{2.5.10}$$

Here, $\Phi_i(\vec{q}_{(N-1)})$ is the $(N-1)$-electron target state produced by a configuration interaction procedure, and $\eta_{m_{\gamma i}}$ is a continuum orbital constructed from a set of Gaussian-type orbitals[90,96]. The symmetry of this orbital is denoted $m_{\gamma i}$, and is based on the symmetry of the target state and the overall symmetry[90,97]. The operator $\hat{\mathscr{A}}$ handles anti-symmetrization in order to satisfy the Pauli exclusion principle. The N-electron configuration $\varphi_p(\vec{q}_N)$ is orthogonal to $\Phi_i(\vec{q}_{(N-1)})$, and is required to recover a portion of Hilbert space removed by the prior orthogonalization of bound and continuum orbitals. These $\varphi_p(\vec{q}_N)$ are known as L^2 configurations, in which all electrons are in the bound orbital subspace[90]. The coefficients $a_{\alpha i m_i}$ and $b_{\alpha p}$ are determined variationally[97] by diagonalizing 2.5.10. This results in a flexible basis with which to represent the full N-electron wavefunction in the inner region.

2.5.2 The Outer Region

In the outer region, where the electron is subject to the molecule's long-range multipole potential alone, the close-coupling expansion is

$$\Phi_j = \sum_i \Phi_i(\vec{q}_{(N-1)}) Y_{l_i,m_i}(\theta_N, \phi_N) r_N^{-1} F_{ij}(r_N), \tag{2.5.11}$$

with the summation over partial wave channels[90]. Substitution into the Schrödinger equation then gives reduced radial equations

$$\left[\frac{d^2}{dr^2} - \frac{l_i(l_i+1)}{r^2} + \frac{2(Z-(N-1))}{r} + k_i^2\right] F_{ij}(r) = 2\sum_{i'=1}^{N} V_{ii'}(r) F_{i'j}(r) = 0.$$

This radial second-order differential equation has $2N$ linearly independent solutions. The UKRmol suite of codes treats the outer region wavefunction as strictly physical, immediately eliminating energetically closed channels[72,8], so that

$$\underline{\underline{\mathbf{F}}}^{(p)} = \begin{pmatrix} \underline{\underline{\mathbf{S_o}}} \\ 0 \end{pmatrix} + \begin{pmatrix} \underline{\underline{\mathbf{C_o}}} & 0 \\ 0 & \underline{\underline{\mathbf{e_c}}} \end{pmatrix} \begin{pmatrix} \underline{\underline{\mathbf{K_{oo}}}}^{(p)}(E) \\ \underline{\underline{\mathbf{K_{co}}}}^{(p)}(E) \end{pmatrix}, \tag{2.5.12}$$

where the superscript (p) indicates a physical (as opposed to unphysical) quantity. The functions $\underline{\underline{\mathbf{S_o}}}$, $\underline{\underline{\mathbf{S_c}}}$, and $\underline{\underline{\mathbf{e_c}}}$ in 2.5.12 constitute a set of n_o linearly independent vectors $\vec{F}_i$, so that

$$\underline{\underline{\mathbf{F}}}^{(p)} = \begin{pmatrix} \vec{F}_1 & \vec{F}_2 & \dots & \vec{F}_{n_o} \end{pmatrix}. \tag{2.5.13}$$

Written more explicitly, this becomes

$$\underline{\underline{\mathbf{F}}}^{(p)} = \left(\begin{array}{ccc} S_1 & \dots & 0 \\ \vdots & \ddots & \vdots \\ 0 & \dots & S_{n_o} \\ \hline 0 & \dots & 0 \\ \vdots & \ddots & \vdots \\ 0 & \dots & 0 \end{array}\right) \underline{\underline{\mathbf{A}}} + \left(\begin{array}{ccc} C_1 & \dots & 0 \\ \vdots & \ddots & \vdots \\ 0 & \dots & C_{n_o} \\ \hline 0 & \dots & 0 \\ \vdots & \ddots & \vdots \\ 0 & \dots & 0 \end{array}\right) \underline{\underline{\mathbf{B}}} + \left(\begin{array}{ccc} 0 & \dots & 0 \\ \vdots & \ddots & \vdots \\ 0 & \dots & 0 \\ \hline e_1 & \dots & 0 \\ \vdots & \ddots & \vdots \\ 0 & \dots & e_{n_c} \end{array}\right) \underline{\underline{\tilde{\mathbf{D}}}}, \qquad (2.5.14)$$

where $\underline{\underline{\mathbf{A}}}$, $\underline{\underline{\mathbf{B}}}$, and $\underline{\underline{\tilde{\mathbf{D}}}}$ act as proportionality constants

$$\underline{\underline{\mathbf{A}}} = \begin{pmatrix} A_{11} & \dots & A_{1n_o} \\ \vdots & \ddots & \vdots \\ A_{n_o1} & \dots & A_{n_on_o}. \end{pmatrix}$$

The indices n_o and n_c refer to the number of open and closed channels, respectively. The matrices $\underline{\underline{\mathbf{S}}}$, $\underline{\underline{\mathbf{C}}}$, and $\underline{\underline{\mathbf{e}}}$ are constructed from individual vector solutions, so that

$$\begin{aligned} \underline{\underline{\mathbf{S}}} &= \begin{pmatrix} \vec{S}_1 & \vec{S}_2 & \dots & \vec{S}_{n_o} \end{pmatrix} \\ &= \left(\begin{array}{c} S_1 \\ 0 \\ \vdots \\ 0 \\ \hline 0 \\ \vdots \\ 0 \end{array}\right) \left(\begin{array}{c} 0 \\ S_2 \\ \vdots \\ 0 \\ \hline 0 \\ \vdots \\ 0 \end{array}\right) \cdots \left(\begin{array}{c} 0 \\ 0 \\ \vdots \\ S_{n_o} \\ \hline 0 \\ \vdots \\ 0 \end{array}\right). \end{aligned}$$

The matrix $\underline{\underline{\mathbf{F}}}^{(p)}$ in 2.5.14 may be written differently by multiplying on the right by $\underline{\underline{\mathbf{A}}}^{-1}$

$$\begin{aligned}
\underline{\underline{\mathbf{F}}}^{(p)} &= \left[\begin{pmatrix} \underline{\underline{\mathbf{S_o}}} \\ 0 \end{pmatrix} \underline{\underline{\mathbf{A}}} + \begin{pmatrix} \underline{\underline{\mathbf{C_o}}} \\ 0 \end{pmatrix} \underline{\underline{\mathbf{B}}} + \begin{pmatrix} 0 \\ \underline{\underline{\mathbf{e_c}}} \end{pmatrix} \underline{\underline{\tilde{\mathbf{D}}}}\right] \underline{\underline{\mathbf{A}}}^{-1} \\
&= \left[\begin{pmatrix} \underline{\underline{\mathbf{S_o}}} \\ 0 \end{pmatrix} + \begin{pmatrix} \underline{\underline{\mathbf{C_o}}} \\ 0 \end{pmatrix} \underline{\underline{\mathbf{K_{oo}}}} + \begin{pmatrix} 0 \\ \underline{\underline{\mathbf{e_c}}} \end{pmatrix} \underline{\underline{\mathbf{K_{oc}}}}\right] \\
&= \begin{pmatrix} \underline{\underline{\mathbf{S_o}}} \\ 0 \end{pmatrix} + \begin{pmatrix} \underline{\underline{\mathbf{C_o}}} & 0 \\ 0 & \underline{\underline{\mathbf{e_c}}} \end{pmatrix} \begin{pmatrix} \underline{\underline{\mathbf{K_{oo}}}}^{(p)}(E) \\ \underline{\underline{\mathbf{K_{co}}}}^{(p)}(E) \end{pmatrix}, \qquad (2.5.15)
\end{aligned}$$

thereby arriving at the form of 2.5.12.

The functions $\underline{\underline{\mathbf{S_o}}}$ and $\underline{\underline{\mathbf{C_o}}}$ behave asymptotically like sine and cosine functions, respectively, and $\underline{\underline{\mathbf{e_c}}}$ behaves like an exponentially decaying function, i.e.,

$$\begin{aligned}
\lim_{r\to\infty}\left[\underline{\underline{\mathbf{S_o}}}\right]_{ij} &\sim \frac{1}{\sqrt{k}}\sin\left[kr - \frac{l\pi}{a} + \frac{Z}{k}\ln(2kr) + \sigma_l\right] \\
\lim_{r\to\infty}\left[\underline{\underline{\mathbf{C_o}}}\right]_{ij} &\sim \frac{1}{\sqrt{k}}\cos\left[kr - \frac{l\pi}{a} + \frac{Z}{k}\ln(2kr) + \sigma_l\right] \\
\lim_{r\to\infty}\left[\underline{\underline{\mathbf{e_c}}}(r)\right]_{ij} &\sim e^{-k_i r}\delta_{ij} \quad , \qquad (2.5.16)
\end{aligned}$$

where σ_l is the Coulomb phase

$$\sigma_l = arg\left[\Gamma\left(l+1+\frac{iz}{k}\right)\right]$$

These give a physical dipole matrix

$$\vec{d}^{(p)} = \left\langle \psi_i \left| \underline{\underline{\mathbf{D}}} \right| \vec{F} \right\rangle, \qquad (2.5.17)$$

where $\left|\vec{F}\right\rangle$ have been summed over the columns.

2.5.3 The Boundary

Because the R-matrix radius is chosen such that the bound state orbitals of the target vanish within the boundary, the only non-zero orbitals at the boundary are the continuum orbitals. The radial portions of the inner region wavefunctions, evaluated at the R-matrix boundary, are known as the *surface amplitudes* $w_{ik}(a)$, and are constructed by projecting onto the channel functions[90]:

$$w_{ik}(a) = \left\langle \Phi_i^{(N-1)} \left| Y_{l_i,m_i} \right| \psi_k^{(N)} \right\rangle, \tag{2.5.18}$$

where the spherical harmonics Y_{l_i,m_i} are defined in the molecular frame. The superscripts on the wavefunctions in 2.5.18 indicate the number of electrons in each wavefunction, so that $\Phi_i^{(N-1)}$ is the wavefunction of the $(N-1)$-electron target, and $\psi_k^{(N)}$ is the N-electron wavefunction.

The partial wave expansions of the continuumum associate each target state with several degenerate partial wave channels[90] n, where n is the sum of the number of energetically open n_o and closed n_c channels. The R-matrix, which has dimensions $n \times n$, is then:

$$\underline{\underline{\mathbf{R}}}(a) = \frac{1}{2}\underline{\underline{\mathbf{w}}}(a) \left[\underline{\underline{\mathbf{E}}}_k - E\right]^{-1} \underline{\underline{\mathbf{w}}}^T(a), \tag{2.5.19}$$

where $\left[\underline{\underline{\mathbf{E}}}_k - E\right]^{-1}$ is a diagonal matrix, and E_k are the eigenenergies of ψ_k^N, known as the *R-matrix poles*[90]. The projection of the target wavefunctions Φ_i^{N-1} onto a solution Ψ_j of the full Hamiltonian at the boundary gives:

$$F_{ij}(a) = \left\langle \Phi_i^{N-1} \left| Y_{l_i,m_i} \right| \Phi_j \right\rangle, \tag{2.5.20}$$

so that the R-matrix relates $\underline{\underline{\mathbf{F}}}$ to its spatial derivative at the boundary[20,87,88,89,8]:

$$\underline{\underline{\mathbf{F}}}(a) = \underline{\underline{\mathbf{R}}}(a)\underline{\underline{\mathbf{F}}}'(a). \tag{2.5.21}$$

The R-matrix is evaluated for the inner region at the boundary[72,8]

$$\underline{\underline{\mathbf{R}}}(a) = \underline{\underline{\mathbf{F}}}_{(inner)}(a)\left[\frac{d}{dr}\underline{\underline{\mathbf{F}}}_{(inner)}(r)\bigg|_{r=a}\right]^{-1}. \tag{2.5.22}$$

The outer region wavefunction smoothly connects at the boundary, thereby requireing the same definition to hold:

$$\underline{\underline{\mathbf{R}}}(a)\left[\underline{\underline{\mathbf{F}}}'_{(inner)}(r)\bigg|_{r=a}\right] = \underline{\underline{\mathbf{F}}}_{(outer)}(a). \tag{2.5.23}$$

Inserting the functional form of $\underline{\underline{\mathbf{F}}}$ from 2.5.25 gives

$$\underline{\underline{\mathbf{R}}}(a)\left[\underline{\underline{\mathbf{S}}}'(a) + \left(\underline{\underline{\mathbf{C}}}'(a)\right)\underline{\underline{\mathbf{K}}}^{(p)}\right] = \underline{\underline{\mathbf{S}}}(a) + \underline{\underline{\mathbf{C}}}(a)\underline{\underline{\mathbf{K}}}^{(p)}, \tag{2.5.24}$$

where all derivatives are evaluated at $r = a$[72]. The (physical) reactance matrix $\underline{\underline{\mathbf{K}}}^{(p)}$, then, is found from 2.5.24

$$\underline{\underline{\mathbf{K}}}^{(p)}(E) = \frac{\underline{\underline{\mathbf{R}}}\left(\underline{\underline{\mathbf{S}}}'(a)\right) - \underline{\underline{\mathbf{S}}}(a)}{\underline{\underline{\mathbf{C}}}(a) - \underline{\underline{\mathbf{R}}}\left(\underline{\underline{\mathbf{C}}}'(a)\right)},$$

where $\underline{\underline{\mathbf{S}}}$ and $\underline{\underline{\mathbf{C}}}$ are the Coulomb functions, and all functions and derivatives are evaluated, again, at $r = a$.

In summary, then, the radial Schrödinger equation is an n-dimesional second-order differential equation with $2n$ linearly independent solutions, n of which are irregular at the origin. Of the remaining n physically allowed solutions, n_o are finite in the limit of $r \to \infty$. The other n_c solutions diverge, and are therefore also unphysical[90,8].

The boundary conditions of $\underline{\underline{\mathbf{F}}}$, then, require that

$$\underline{\underline{\mathbf{F}}} \sim \left[\underline{\underline{\mathbf{S}}} + \underline{\underline{\mathbf{CK}}}\right], \tag{2.5.25}$$

where $\underline{\underline{\mathbf{S}}}$ behaves sine-like asymptotically and $\underline{\underline{\mathbf{C}}}$ behaves cosine-like for open channels and increases exponentially for closed channels, where $\underline{\underline{\mathbf{K}}}$ is the reactace matrix[90,8]. Note that $\underline{\underline{\mathbf{S}}}$ and $\underline{\underline{\mathbf{C}}}$ have Wronskian $W(C,S) = 1$, i.e., they are linearly independent and Wronskian-normalized[8,2].

The immediate elimination of energetically closed channels, however, is not necessary, and "irons in" any resonance series as fixed artifacts, so that "unfreezing" the nuclei does not affect these resonances properly. In lieu of this premature channel closure, $\underline{\underline{\mathbf{K}}}$ may be found by invoking multichannel quantum defect theory, with unphysical channels included at first.

2.6 Multichannel Quantum Defect Theory

In general, the reactance matrix $\underline{\underline{\mathbf{K}}}$ includes both open and closed channels, i.e., energetically available and unavailable channels, respectively. This reactance matrix has elements:

$$K_{ij} = \sum_{\alpha=1}^{n} \mathscr{U}_{i\alpha} \tan(\pi\mu_\alpha) \mathscr{U}^{\dagger}_{\alpha j}, \tag{2.6.1}$$

where n is the total number of channels, both open and closed, i.e., $n = n_o + n_c$, and the operator $\hat{\mathscr{U}}$ is the unitary, orthogonal, and real eigenvector matrix of $\underline{\underline{\mathbf{K}}}$, with eigenvalues $\tan(\pi\mu_\alpha)$. These n *eigenquantum defects* μ_α are defined in the molecule-fixed frame[10,11,12,98].

The unphysical K-matrix $\underline{\underline{\mathbf{K}}}$, it should be noted, is different from the physical K-matrix

$\underline{\underline{\mathbf{K}}}^{\text{phys}}(E)$. The former ($\underline{\underline{\mathbf{K}}}$) has dimensions $n \times n$, and typically exhibits a smooth variation with energy. The latter $\left(\underline{\underline{\mathbf{K}}}^{phys}(E)\right)$ has dimensions $n \times n_o$, as determined by the number of open channels at the given energy, and has poles near the positions of bound levels[98]. The transformation from $\underline{\underline{\mathbf{K}}}$ to $\underline{\underline{\mathbf{K}}}^{\text{phys}}(E)$ is then enacted through the process of eliminating the closed channels through boundary conditions at infinity. The relation is[12]

$$\underline{\underline{\mathbf{K}}}^{\text{phys}}(E) = \underline{\underline{\mathbf{K}}}^{oo} - \underline{\underline{\mathbf{K}}}^{oc}\left[\underline{\underline{\mathbf{K}}}^{cc} + \tan\left(\beta(E)\right)\right]^{-1}\underline{\underline{\mathbf{K}}}^{co}, \tag{2.6.2}$$

where $\underline{\underline{\mathbf{K}}}^{oo}$ is the submatrix of $\underline{\underline{\mathbf{K}}}$ representing interactions between open channels, $\underline{\underline{\mathbf{K}}}^{cc}$ the interactions between closed channels, and $\underline{\underline{\mathbf{K}}}^{oc}$ and $\underline{\underline{\mathbf{K}}}^{co}$ interactions between open and closed channels. The terms $\beta_i(E)$ are the accumulated phase parameters $\pi\nu_i(E)$, where $\nu_i(E)$ is the effective principle quantum number for each channel[10,11,12,98].
Through these eigenquantum defects, then, the vibrational frame transformation may be effected, producing transformed reactance and dipole matrices

$$\underline{\underline{\mathbf{K}}}^{\text{vib}} = \underline{\underline{\mathbf{U}}}^{\dagger}\,\underline{\underline{\mathbf{K}}}\,\underline{\underline{\mathbf{U}}} \qquad \text{and} \qquad \vec{d}^{\,T}\,\underline{\underline{\mathbf{U}}}.$$

The details of this frame transformation are discussed in Section 2.10. Note that the molecular frame transition dipole matrix $\vec{d}$ between the initial bound state Φ_i^n and final continuum state Φ^-_{f,k_f}, is

$$\vec{d}^{\,T}_{fi}(\vec{k}) = \left\langle \Phi^-_{f,k_f} \left| \hat{\mathbf{d}} \right| \Phi_i^n \right\rangle, \tag{2.6.3}$$

where $\vec{k}_f$ is the momentum of the ejected electron and $\hat{\mathbf{d}}$ is the dipole operator

$$d_q = \sqrt{\frac{4\pi}{3}} \sum_{i=1}^{n} r_i Y_{1,q}(\vec{r}_i). \tag{2.6.4}$$

The subscript q indexes the type of polarization ($q = \pm 1$ for circular polarization, and $q = 0$ for linear polarization).

2.7 QDT Examples

Let the states of the unperturbed Rydberg series, in which the electron and ion core do *not* exchange energy or angular momentum, belong to the same channel as the ionized states above the series with the same ionic core level and angular momentum. For the time being, the radial quantization of discrete states is disregarded, and will be reintroduced later. This is the essence of unphysical multichannel quantum defect theory (MQDT). The configurations of *all* levels of the unperturbed series and the adjoining continuum thus make up a single channel. Rather than allow the configurations to interact, the channels are allowed to do so.

2.7.1 One Channel

Consider the valence electron states of an alkali atom. Let a single channel be constructed for each angular momentum eigenvalue. The valence electron moves in a spherically symmetric Coulomb field surrounding an ionic core. The radial part of the valence electron wavefunction $u(r)$ may be represented, outside of the core, as a superposition of any two independent Coulomb wavefunctions $S(r)$ and $C(r)$. Take $S(r)$ to be regular at $r = 0$, and let $C(r)$ have a phase of 90° behind $S(r)$ at large r:

$$u(r) = S(r)\cos(\pi\mu) + C(r)\sin(\pi\mu). \tag{2.7.1}$$

In the continuous spectrum, $(\pi\mu)$ is the scattering phase shift for electron/ion collisions. Note that μ is slowly varying in energy E.

If the energy is below the ionization threshold, i.e., $E < I$, then $S(r)$ and $C(r)$, and thus $u(r)$, may be expressed as superpositions of a term that converges exponentially in

the limit of $r \to \infty$ and one that diverges exponentially in the limit of $r \to \infty$. The coefficients of said superposition are periodic functions of energy through an effective quantum number ν. Radial quantization, then, consists of requiring the coefficient of the diverging term to vanish. This determines the discrete energy eigenvalues that simultaneously satisfy the set of equations:

$$\sin\left(\pi\left[\nu(E) + \mu(E)\right]\right) = 0 \qquad \text{and} \qquad E = I - \frac{E_{Ryd}}{\left[\nu(E)\right]^2} \tag{2.7.2}$$

the resulting roots of which are

$$E_n = I - \frac{E_{Ryd}}{\left[n - \mu(E_n)\right]^2}.$$

In the above, E_{Ryd} is the Rydberg energy

$$E_{Ryd} = 13.60569 \text{ eV}.$$

The oscillator strength, or probability of absorption, of optical transitions to the n^{th} level of the channel is:

$$\begin{aligned} S_n &= \left(\frac{\partial}{\partial E} S\Big|_{E_n}\right) \frac{\partial}{\partial n} E_n \\ &= \left(\frac{\partial}{\partial E} S\Big|_{E_n}\right) \frac{2E_{Ryd}}{\left[n - \mu(E_n)\right]^3} \end{aligned}$$

from which the photoabsorption cross section σ_{PA} is obtained:

$$\sigma_{PA} = \frac{\pi e^2 h}{mc} \frac{\partial}{\partial E} S, \tag{2.7.3}$$

where the spectral density of the oscillator strength $\dfrac{\partial}{\partial E} S$ is a slowly-varying function.

Thus the main spectral and collisional properties are represented in terms of two parameters, μ and $\frac{\partial}{\partial E}S$, both of which have physical significance. The quantum defect μ represents all the relevant effects of the short-range interaction between the valence electron and the ion core, and it specifies the boundary conditions imposed by the presence of the ion core upon the log derivative $\frac{\partial}{\partial r}\ln(u)$ at the radius a of a sphere surrounding said core[64].

2.7.2 Two Closed Channels

This treatment extends to multiple channels as follows. First, consider the case of two closed channels. Photoabsorption by molecular hydrogen (H_2) serves as a good example. Due to symmetry and conservation arguments, the lowest two states of electronic excitation reached by photoabsorption belong to two series: $1s\sigma np\sigma\ ^1\Sigma_u$ and $1s\sigma np\pi\ ^1\Pi_u$. The electron/core short-range interaction now requires two quantum defects μ_σ and μ_π, and photoabsorption is determined by two oscillator strength densities $\frac{df_\sigma}{dE}$ and $\frac{df_\pi}{dE}$. Each channel is well defined experimentally only within the bounds of the Born-Oppenheimer approximation.

As the electron slows, its motion uncouples from the molecular core, the extreme case of which results in a complete breakdown of the Born-Oppenheimer approximation. In such a case, the interval of successive Rydberg levels is dwarfed by vibrational and rotational quanta of the molecular core[64,72], and entirely new Rydberg series emerge, corresponding to different states of the core. Rotational uncoupling of the ionic H_2^+ core from the orbital momentum of the excited electron causes separate Rydberg series to converge to differing iionization thresholds, corresponding to alternative rotational states of the ion[64,98].

The pair of channels appropriate for short-range interactions is linked to those appropriate for long-range interactions through a unitary transformation, specifically, a

2×2 rotation by an angle θ. In the limiting case of low excitation, the energy level is characterized by a quantum number σ or π, while in the limit of high excitation, the level is characterized by an ionization threshold I_0 or I_2. In general, the electronic state is a superposition of eigenfunctions for these extremes. The level positions are determined by requiring the complete wavefunction to converge in the limit of $r \to \infty$. The resulting eigenvalue equations are:

$$\begin{aligned} E &= I_0 - \frac{E_{Ryd}}{\nu_0^2} \\ \\ &= I_2 - \frac{E_{Ryd}}{\nu_2^2} \end{aligned}$$

and

$$\begin{vmatrix} \cos\theta \sin\left[\pi(\mu_\sigma + \nu_0)\right] & \sin\theta \sin\left[\pi(\mu_\pi + \nu_0)\right] \\ -\sin\theta \sin\left[\pi(\mu_\sigma + \nu_2)\right] & \cos\theta \sin\left[\pi(\mu_\pi + \nu_2)\right] \end{vmatrix} = 0.$$

2.8 Body-Fixed Frame

In the inner region, the internuclear separation $\vec{R}$ is a "good" quantum number, and the Born-Oppenheimer approximation holds for all electrons within the R-matrix "box" $(r < a)$. However, $\vec{R}$ is a body frame, rather than a laboratory frame, value. A vibrational frame transformation connects $\vec{R}$ with laboratory frame quantizations $\mathscr{F}^{s}_{\nu,K}(R)$[72,99]. The formulation of the vibrational interactions is greatly simplified due to the mass of the electron relative to the nucleus. In the inner region, the electrons *do* experience forces comparable to those on the nuclei, i.e., the error in the wavefunctions obtained from the Born-Oppenheimer approximation is very nearly zero. The electron, therefore, reacts almost instantaneously to the changing field of the nuclei, which allows the nuclei to be treated as fixed while the electron is in the inner region. While the Born-Oppenheimer approximation is not accurate for the electron for *all* space, it is entirely sufficient within the R-matrix "box."

Far from the nuclei (large r), the interaction between the electron and the molecule is weak, and is, in fact, nearly central. Consequently, the angular momentum of the electron is almost entirely uncoupled from that of the molecule, as well as from the internuclear separation $R = \left|\vec{R}\right|$. Here, the total angular momentum j and orbital angular momentum ℓ of the outer electron are approximately "good" quantum numbers, and thus a space-fixed, or laboratory, frame is an appropriate environment[99,98,72].

At small distances, the electron is close enough to the nuclei for it to be associated therewith, and the Born-Oppenheimer approximation gives sufficiently accurate wavefunctions. Here, the wavefunctions belonging to the body-fixed frame are the more appropriate[63,72,99].

2.9 Failure of the Born-Oppenheimer Approximation

While the Born-Oppenheimer approximation is particularly useful, it breaks down in certain cases. The assumptions in using this approach are that:

- the electrons and nuclei occupy roughly the same space, i.e., the electrons are spatially relatively close to the nuclei
- the forces on the electrons and nuclei are comparable

which together imply that the electronic motion is significantly faster than the nuclear motion, and that the electrons adjust roughly instantaneously to changes in the nuclear configuration. This leads to uncoupled nuclear and electronic wavefunctions[72,99].

In Rydberg molecules, however, the outer electron is in a highly excited state, and its average distance from the nuclei and from other electrons is much greater than in the

simpler valence state. Consequently, the time scales for nuclear and electronic motion become comparable, and, in fact, the time scale for nuclear motion may surpass that for electronic motion. When these time scales are comparable, the Born-Oppenheimer approximation fails, and a new approach must be adopted.

It also bears mentioning that the Born-Oppenheimer approximation is insufficient in the case where the electronic energy $E_s(R)$ is degenerate, as degenerate states inherently exhibit significant coupling.

2.10 The Vibrational Frame Transformation

The purpose of the frame transformation, then, is to transform the *outer region* wavefunctions to a laboratory-fixed frame, and to ensure that they smoothly connect to the inner region wavefunctions.

In the Born-Oppenheimer approximation, the wavefunction for the lowest n Rydberg states of a diatomic molecule takes the form[98]:

$$\begin{aligned}\Psi &\approx \psi_{el}\psi_{vib} \\ &= \left(\hat{\mathscr{A}}\psi_{core}\psi_{Ryd}\right)\psi_{vib}\end{aligned}$$

where $\hat{\mathscr{A}}$ makes Ψ antisymmetric in all electrons[98]. Mulliken referred to this as the Rydberg-coupled wavefunction[100]. As n increases, the Rydberg electron influences the rotation and vibration of the nuclei less, and the wavefunction takes the form:

$$\Psi \approx \left(\hat{\mathscr{A}}\psi_{core}\psi_{vib}\right)\psi_{Ryd},$$

which Mulliken referred to as the Rydberg-uncoupled wavefunction. Here, ψ_{Ryd} is now separate from the electronic factor of the Born-Oppenheimer approximation[100].

Because the Rydberg electron has such a comparitively large kinetic energy when approaching the positive core, the nuclei do not have time to move noticeably, and the only appreciable change possible is electronic excitation, which is consistent with the Born-Oppenheimer approximation. Changes in rotational and vibrational states of the molecule may occur, but only through the uncoupling of the electron as it moves away from the nuclei[98].

It should be noted at this point that the nuclei exhibit multiple degrees of freedom, and not just vibration. By implementing a *vibrational*, and not *ro*vibrational, frame transformation, an implied approximation is made that, while the nuclei are "unfrozen" with respect to vibration, the orientation of the molecule remains fixed.

Within the framework of the Born-Oppenheimer approximation , the molecular R-matrix suite calculates photon energies $E_i(R)$, an S-matrix $\underline{\underline{\mathcal{S}}}(R)$, and a dipole matrix $d_j(R)$. The energetically unavailable channels are then immediately closed, thus producing a physical S-matrix $\underline{\underline{\mathcal{S}}}^{(phys)}(R)$

$$\underline{\underline{\mathcal{S}}}^{(phys)}(R) = \underline{\underline{\mathcal{S}_{\mathbf{oo}}}}(R) - \underline{\underline{\mathcal{S}_{\mathbf{oc}}}}(R)\left[\underline{\underline{\mathcal{S}_{\mathbf{cc}}}}(R) - e^{-i2\pi\nu}\delta_{cc}\right]^{-1}\underline{\underline{\mathcal{S}_{\mathbf{co}}}}(R). \tag{2.10.1}$$

The dipole matrix undergoes the same treatment

$$\vec{d}_o^{\,(phys)}(R) = \vec{d}_o(R) - \vec{d}_c(R)\left[\underline{\underline{\mathcal{S}_{\mathbf{cc}}}}(R) - e^{-i2\pi\nu}\delta_{cc}\right]^{-1}\underline{\underline{\mathcal{S}_{\mathbf{co}}}}(R). \tag{2.10.2}$$

The term inside the square brackets is presented somewhat awkwardly, but is understood to mean that the complex exponential is represented as a diagonal $n_c \times n_c$ matrix. The

argument of the complex exponential relates to the eigenenergies via

$$\nu_i = \frac{1}{\sqrt{2(E_i - E)}}, \quad E < E_i.$$

From these values, a photoionization cross section σ_{PI} may be calculated so that

$$\sigma_{PI}(R) \propto \left| \vec{d}_o^{\,(phys)}(R) \right|^2 . \tag{2.10.3}$$

While there is an R-dependence in 2.10.3, it should be noted that this photoionization cross section was calculated from fixed-R quantities, so that it is not a true, direct function of the internuclear separation R, but rather a function of the fixed-nuclei quantities E_i, $\underline{\underline{S}}$, and $\vec{d}$.

The idea of the vibrational frame transformation, then, is to move from a position representation, characterized by R, to an energy representation, characterized by the vibrational state of the molecule. This vibrational state is represented by a vibrational quantum number v, so that the quantities $\underline{\underline{\mathbf{S}}}(R)$ and $\vec{d}(R)$ may instead be represented in terms of v

$$\begin{aligned} E_i(R) &\rightarrow E_{iv} \\ S_{ij}(R) &\rightarrow S_{iv,jv'} \\ d_j(R) &\rightarrow d_{jv'}^{(v'')}, \end{aligned} \tag{2.10.4}$$

where the indices v and v' represent vibrational states of the $(N-1)$-electron N_2^+ ion, and v'' represents the vibrational state of the N-electron N_2 molecule. In the fixed-nuclei formulation, the energy was measured relative to the stationary potential energy curves $U(R)$ associated with the N_2 molecule and N_2^+ ion. Allowing the nuclei to move, however, introduces vibrational splitting of these potential energy curves, so that the

fixed-nuclei curve $U(R)$ becomes laden with a series of vibrational levels E_v. To account for this, energy values must be calculated relative to the vibrationally-split potential curve $U_v(R)$

$$E_{iv} = E_i + (E_v - E^{(fixed)}), \tag{2.10.5}$$

where $E^{(fixed)}$ is the energy calculated from the fixed-nuclei scenario. In the position basis, the operator $\hat{\mathbf{R}}$ is diagonal, with

$$\hat{\mathbf{R}} \, |R\rangle = R \, |R\rangle \; .$$

The eigenfunctions $|R\rangle$ are constructed to be orthonormal, so that

$$\langle R \, | R' \rangle = \delta(R - R'), \tag{2.10.6}$$

and they comprise a complete set, so that

$$\int |R\rangle \, \langle R| \, dR = 1. \tag{2.10.7}$$

In the energy basis, the vibrational Hamiltonian $\hat{\mathscr{H}_v}$ is diagonal, and the wavefunctions are written as eigenfunctions of the vibrational Hamiltonian, with eigenvalues E_v,

$$\hat{\mathscr{H}_v} \, |v\rangle = E_v \, |v\rangle \; . \tag{2.10.8}$$

As with the position-basis eigenvectors $|R\rangle$, the energy-basis eigenvectors $|v\rangle$ also comprise an orthonormal complete set

$$\langle v|v'\rangle = \begin{cases} \delta_{vv'} & \text{for bound states} \\ \delta(E_v - E_{v'}) & \text{for continuum states} \end{cases}$$
$$\sum_v |v\rangle \langle v| = 1. \tag{2.10.9}$$

The S-matrix is first written in the position basis, with $\underline{\underline{\mathcal{S}}}$ being the eigenvalue of some operator $\hat{\mathbf{S}}$

$$\begin{aligned} \hat{\mathbf{S}}|R\rangle &= \underline{\underline{\mathcal{S}}}(R)|R\rangle \\ \left\langle R\left|\hat{\mathbf{S}}\right|R'\right\rangle &= \underline{\underline{\mathcal{S}}}(R)\delta(R-R'). \end{aligned} \tag{2.10.10}$$

In an energy basis, the S-matrix is no longer written in terms of R, but rather in terms of v and v',

$$\left\langle v\left|\hat{\mathbf{S}}\right|v'\right\rangle = \mathcal{S}_{vv'} \quad . \tag{2.10.11}$$

To do this, the completeness and orthogonality properties of the wavefunctions are exploited. Beginning with 2.10.11, the completeness of $|R\rangle$ is inserted,

$$\begin{aligned} \mathcal{S}_{vv'} &= \left\langle v\left|\hat{\mathbf{S}}\right|v'\right\rangle \\ &= \left\langle v\left|\hat{\mathbf{S}}\left(\int |R\rangle \langle R|\, dR\right)\right|v'\right\rangle. \end{aligned}$$

The integration over vibrational states is not dependent on R, so the integration order may be reversed

$$\mathcal{S}_{vv'} = \int \left\langle v \left| \left(\hat{\mathbf{S}} \left| R \right\rangle \, \langle R | \right) \right| v' \right\rangle dR.$$

From 2.10.10, then, the term in parentheses may be simplified

$$\begin{aligned} \mathcal{S}_{vv'} &= \int \left\langle v \left| \left(\underline{\underline{\mathcal{S}}}(R) \left| R \right\rangle \, \langle R | \right) \right| v' \right\rangle dR \\ &= \int \left\langle v \left| \left(\left| R \right\rangle \, \underline{\underline{\mathcal{S}}}(R) \, \langle R | \right) \right| v' \right\rangle dR \\ &= \int \langle v | R \rangle \, \underline{\underline{\mathcal{S}}}(R) \, \langle R | v' \rangle \, dR. \end{aligned} \tag{2.10.12}$$

What remains, then, is to find $\langle R | v' \rangle$. Beginning with 2.10.8, a similar procedure to the above may be employed. The completeness of $\{ | R \rangle \}$ is again utilized

$$\begin{aligned} 0 &= \left(\hat{\mathscr{H}}_v - E_v \right) | v \rangle \\ &= \int \left(| R \rangle \, \langle R | \, dR \right) \left(\hat{\mathscr{H}}_v - E_v \right) | v \rangle \\ &= \int \int \left(| R \rangle \, \langle R | \, dR \right) \left(\hat{\mathscr{H}}_v - E_v \right) \left(| R' \rangle \, \langle R' | \, dR' \right) | v \rangle \, . \end{aligned}$$

Once again, the integration order may be reversed, giving

$$0 = \int \int | R \rangle \left[\langle R | \left(\hat{\mathscr{H}}_v - E_v \right) | R' \rangle \right] \langle R' | v \rangle \, dR \cdot dR'.$$

The term in the square brackets is nothing more than a Dirac delta

$$0 = \int \int | R \rangle \left[\left(\mathscr{H}(R) - E_v \right) \delta(R - R') \right] \langle R' | v \rangle \, dR \cdot dR',$$

leaving

$$0 = \int |R\rangle \, (\mathscr{H}(R) - E_v) \, \langle R|v\rangle \, dR. \tag{2.10.13}$$

The set of functions $|R\rangle$ is, as previously stated, orthonormal. As such, the only way for the integral in 2.10.13 to vanish is for the coefficient of $|R\rangle$ to vanish, i.e.,

$$(\mathscr{H}(R) - E_v) \, \langle R|v\rangle = 0,$$

which reveals the quantity $\langle R|v\rangle$ to be none other than the eigenfunctions of the vibrational Hamiltonian, expressed as functions of R

$$\begin{aligned} 0 &= (\mathscr{H}(R) - E_v) \, \langle R|v\rangle \\ &= (\mathscr{H}(R) - E_v) \, \chi_v(R). \end{aligned} \tag{2.10.14}$$

Finally, the S-matrix may be expressed in the energy basis. Combining 2.10.12 and 2.10.14, the transformed S-matrix $\mathcal{S}_{vv'}$ is

$$\mathcal{S}_{vv'} = \int \chi_v^*(R) S_{ij}(R) \chi_{v'}(R) dR. \tag{2.10.15}$$

The same procedure is followed for transforming the d-matrix. Unlike the S-matrix, the d-matrix links an initial N-electron molecular state to a final $(N-1)$-electron ionic state. As with the S-matrix, the d-matrix is first written in the position basis, with $\vec{d}$ being the eigenvalue of some operator $\hat{\mathbf{d}}$, in a way similar to that of 2.10.10

$$\begin{aligned} \hat{\mathbf{d}} \, |R\rangle &= \vec{d}(R) \, |R\rangle \\ \left\langle R \left| \hat{\mathbf{d}} \right| R' \right\rangle &= \vec{d}(R) \delta(R - R'). \end{aligned} \tag{2.10.16}$$

In an energy basis, the d-matrix is written in terms of two vibrational states $|v''\rangle$ and $|v'\rangle$, where the first is a vibrational state of the initial neutral molecule and $|v'\rangle$ of the final molecular ion

$$d_{v'}^{(v'')} = \left\langle v'' \left| \hat{\mathbf{d}} \right| v' \right\rangle . \tag{2.10.17}$$

The completeness of $\{|R\rangle\}$ is appropriated,

$$\begin{aligned} d_{v'}^{(v'')} &= \left\langle v'' \left| \hat{\mathbf{d}} \right| v' \right\rangle \\ &= \left\langle v'' \left| \hat{\mathbf{d}} \left(\int |R\rangle \, \langle R| \, dR \right) \right| v' \right\rangle \\ &= \int \left\langle v'' \left| \left(\hat{\mathbf{d}} \, |R\rangle \, \langle R| \right) \right| v' \right\rangle dR \quad , \end{aligned}$$

after which the eigenvalue equation 2.10.16 is used to rewrite the parenthetical term

$$\begin{aligned} d_{v'}^{(v'')} &= \int \left\langle v'' \left| \left(\vec{d}(R) \, |R\rangle \, \langle R| \right) \right| v' \right\rangle dR \\ &= \int \langle v'' \, |R\rangle \, \vec{d}(R) \, \langle R \, |v'\rangle \, dR \quad . \end{aligned}$$

Finally, the vibrational wavefunctions are recognized, giving

$$d_{v'}^{(v'')} = \int \chi_{v''}^{*}(R) \vec{d}(R) \chi_{v'}(R) dR \quad . \tag{2.10.18}$$

Thus the transformations 2.10.4 are enacted through 2.10.5, 2.10.15, and 2.10.18 via the unitary and orthogonal transformation matrix

$$U_v(R) = \chi_v(R).$$

In order to enact the vibrational frame transformation, then, it is necessary to construct the nuclear vibrational wavefunctions.

2.11 Nuclear Motion

Having established electronic wavefunctions and eigenquantum defects under the Born-Oppenheimer approximation, it remains to unfreeze the nuclei. The potential energy is dependent on the separation distance R of the two nitrogen nuclei. In order to enact the vibrational frame transformation, nuclear wavefunctions, as well as their eigenenergies, are needed. By allowing this internuclear separation to vary and calculating the corresponding potential energies, a potential energy curve was constructed for both the SCF and CI cases. These curves were fit with various models, each of which will be subsequently discussed.

2.11.1 The Harmonic Oscillator Potential

While the overall trend is certainly not so kind, near the equilibrium separation R_{eq}, the nuclei experience a potential that is nearly quadratic in shape. The potential near this point may be approximated by a harmonic oscillator potential

$$V(R) = \frac{1}{2}\mu\omega\left(R - R_{eq}\right)^2 + U_0,$$

where the parameters ω and U_0 are determined from the curve. This gives a one-dimensional Schrödinger equation , in atomic units, for the nuclear wavefunctions $\chi(R)$

$$\left[-\frac{1}{2\mu}\frac{\partial^2}{\partial R^2} + \frac{1}{2}\mu\omega^2\left(R - R_{eq}\right)^2 + U_0\right]\chi(R) = E\chi(R). \tag{2.11.1}$$

The solutions to this potential are well known, but, for posterity's sake, will be quickly discussed here.

The eigenfunctions of the harmonic oscillator potential are

$$\chi_n(\xi) = \frac{1}{\sqrt{2^n n!}} \left(\frac{m\omega}{\pi}\right)^{1/4} H_n(\xi) e^{-\xi^2/2}, \tag{2.11.2}$$

where

$$\xi \equiv \sqrt{m\omega}(R - R_{eq})$$

and $H_n(\xi)$ are the Hermite polynomials. The corresponding energy eigenvalues are

$$E_n = -U_0 + \left(n + \frac{1}{2}\right)\omega. \tag{2.11.3}$$

It bears mentioning, at this point, that the energy levels of the harmonic oscillator are, as indicated by 2.11.3, evenly spaced. The wavefunctions are shown in Figure 2.11.1.

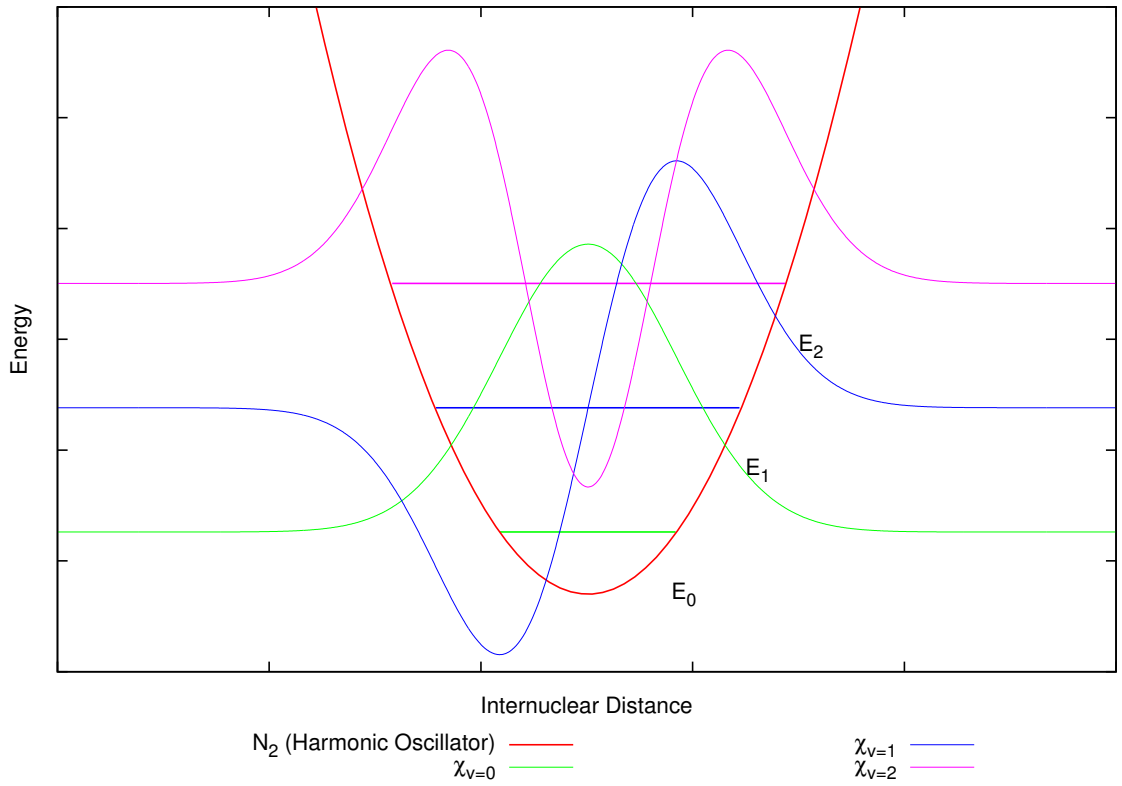

Figure 2.11.1: The eigenfunctions of the harmonic oscillator potential for vibrational numbers $v = 0$, $v = 1$, and $v = 2$. The energy levels are evenly spaced, giving a crude model for the true vibrational energies near $v = 0$. The wavefunctions are color-coded to correspond to their respective energy levels. The vibrational quantum number v is equal to the number of nodes in the wavefunction. Note that, while the $v = 3$ energy level does fall within the displayed range, it is not shown here, in an effort to show a representative but not cluttered plot.

For low-lying energies, that is, very bound states, this approximation is reasonable. For higher-energy vibrational states, leading to classically-allowed regions. Far away from equilibrium, however, this regular energy spacing becomes problematic, and a more appropriate model must be employed.

2.11.2 The Morse Potential

The harmonic oscillator assumes a potential that is even about the equilibrium internuclear distance. Of course, this model must fail, as it does not properly represent the asymptotic behavior of the potential energy at small or large R. To address this asymp-

totic behavior, an anharmonicity is introduced. In 1929, physicist Philip M. Morse proposed an anharmonic function with three adjustable parameters. This potential, which now bears his name, takes the form

$$\begin{aligned} V(R) &= D\left(\left(1-e^{-\alpha(R-Req)/R_{eq}}\right)^2-1\right) \\ &= D\left(e^{-2\alpha(R-Req)/R_{eq}}-2e^{-\alpha(R-Req)/R_{eq}}\right), \end{aligned} \tag{2.11.4}$$

where R_{eq} is the equilibrium internuclear distance or bond length, D is the well depth, and α is associated with the well's concavity. The second form of the potential in 2.11.4 is rather more transparent, with the first term dictating the small-R behavior, and the second, the large-R behavior. Aside from its accuracy, perhaps the greatest benefit of the Morse potential is that it may be solved analytically.

The one-dimensional, time-independent Schrödinger equation is, in atomic units,

$$\left(-\frac{1}{2m}\frac{\partial^2}{\partial R^2}+V(R)\right)\chi(R)=E\chi(R), \tag{2.11.5}$$

where $\chi(R)$ are the radial wavefunctions. It is understood that the mass in this equation is the reduced mass of the nuclei, i.e.,

$$\begin{aligned} m &= \frac{M_N^{(1)}\cdot M_N^{(2)}}{M_N^{(1)}+M_N^{(2)}} \\ &= \frac{M_N\cdot M_N}{M_N+M_N} \text{ (for homonuclear molecules)} \\ &= \frac{M_N}{2}, \end{aligned} \tag{2.11.6}$$

and the choice is made to use m instead of the typical convention of μ, as μ will herein be reserved for eigenquantum defects. As stated previously, the Morse potential may be solved analytically, and this is done in Appendix D. The normalized discrete spectrum

wavefunctions are

$$\chi_n(y) = \sqrt{\frac{n!\,(2\lambda)!}{\Gamma\left(2\lambda+n+1\right)}} \cdot y^{\lambda} e^{-y/2} L_n^{2\lambda}(y), \tag{2.11.7}$$

with

$$\begin{aligned}
\gamma^2 &\equiv 2mR_{eq}^2 D \\
\beta^2 &\equiv -2mR_{eq}^2 E \\
\lambda &\equiv \frac{\beta}{\alpha} \\
y &\equiv \left(\frac{2\gamma}{\alpha}\right) e^{-\alpha(R-R_{eq})/R_{eq}} \\
-n &\equiv \lambda + \frac{1}{2} - \frac{\gamma}{\alpha}.
\end{aligned}$$

These wavefunctions are shown in Figure 2.11.2. The Morse potential does, of course, have continuum solutions, as well. However, in this study, only the lowest few vibrational states of the Morse potential are utilized, so a discussion of the continuum states is excluded here.

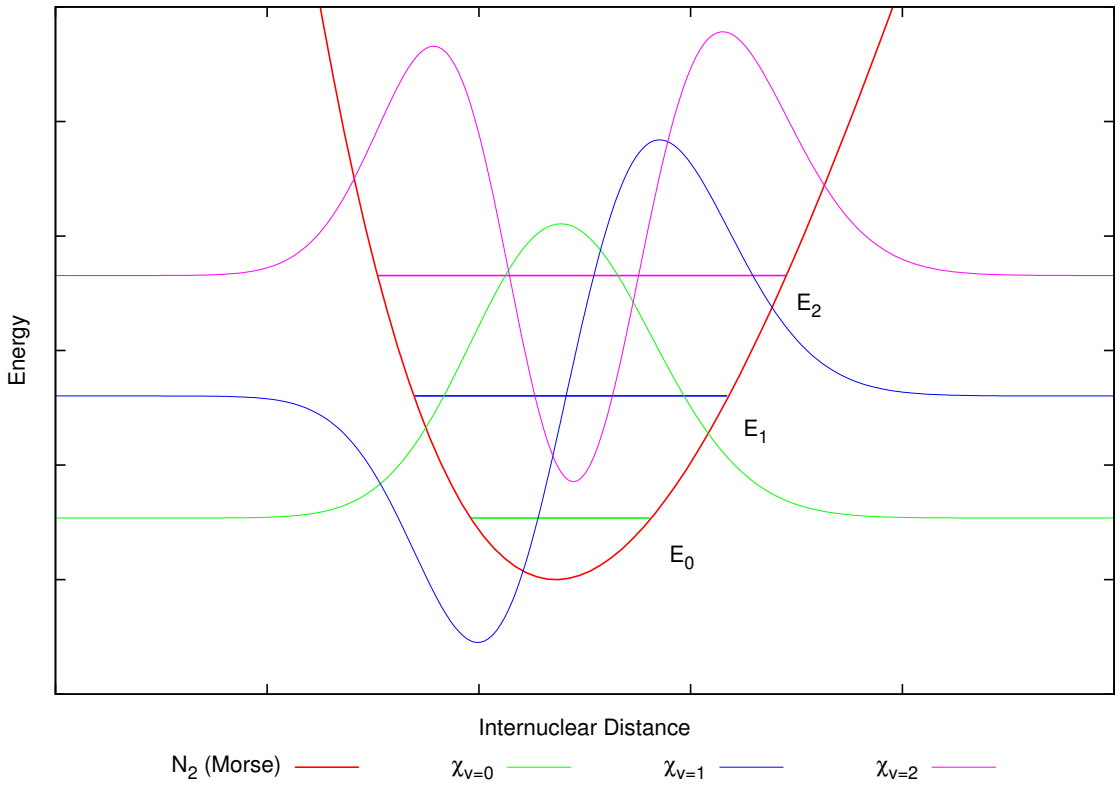

Figure 2.11.2: The eigenfunctions of the Morse potential for vibrational numbers $v = 0$, $v = 1$, and $v = 2$. Note that the energy levels are not evenly spaced, but rather become more dense with increasing v. The wavefunctions are color-coded to correspond to their respective energy levels. Like the harmonic oscillator, the vibrational number is equal to the number of nodes in the wavefunction.

2.12 Further Energy Splittings

Beside vibrational motion, the nuclei may also undergo rotational motion about their collective center of mass. This, of course, comes with its own kinetic energy term $\hat{\mathbf{T}}_{rot}$,

so that the Hamiltonian, still in atomic units, becomes

$$\hat{\mathscr{H}} = \underbrace{\left[-\frac{1}{2}\sum_{k=1}^{2}\frac{1}{M_k}\nabla_k^2\right]}_{\hat{\mathbf{T}}_{nuc}} + \underbrace{\left[-\frac{1}{2}\sum_{i=1}^{N}\nabla_i^2\right] + \left[\frac{Z_1 Z_2}{R} + \sum_i\sum_j \frac{1}{r_{ij}} - \sum_i\left(\frac{1}{r_{i1}} + \frac{1}{r_{i2}}\right)\right]}_{\hat{\mathscr{H}}_0}, \tag{2.12.1}$$

wherein the individual kinetic energy contributions from vibration are indicated with $\hat{\mathbf{T}}_{vib}$, and the frozen-nuclei Hamiltonian is denoted $\hat{\mathscr{H}}_0$.

The vibrational energy may be approximated to a first order with harmonic oscillator energies, so that

$$\begin{aligned} E_{vib} &\approx \left(n + \frac{1}{2}\right)\hbar\omega \\ &\approx \left(n + \frac{1}{2}\right)\hbar\sqrt{\frac{k}{M}} \\ &\propto \frac{1}{\sqrt{M}}, \end{aligned} \tag{2.12.2}$$

where M is the reduced mass of the nuclei. This vibrational energy splits the electronic energy levels, as seen in Figures 2.11.1 and 2.11.2, by a term that behaves as $1/\sqrt{M}$. By comparison, the rotational energies may be approximated to a first order with rigid rotor energy levels

$$\begin{aligned} E_{rot} &\approx \frac{1}{2}I\omega^2 \\ &\approx \frac{J^2}{2I}, \end{aligned} \tag{2.12.3}$$

where I is the rotational moment of inertia

$$\begin{aligned} I &= \sum_{i=1} 2\left[M_i R_i^2\right] \\ &= MR^2, \end{aligned}$$

so that 2.12.3 becomes

$$\begin{aligned} E_{rot} &\approx \frac{J^2}{2MR^2} \\ &\propto \frac{1}{M}. \end{aligned} \tag{2.12.4}$$

Thus the rotational energy levels split the electronic energy levels by a term that behaves as $1/M$, or, perhaps more relevantly, split the *vibrational* levels by a factor of $1/\sqrt{M}$. The relative scaling of these energy splittings is most easily seen graphically, as in Figure 2.12.1.

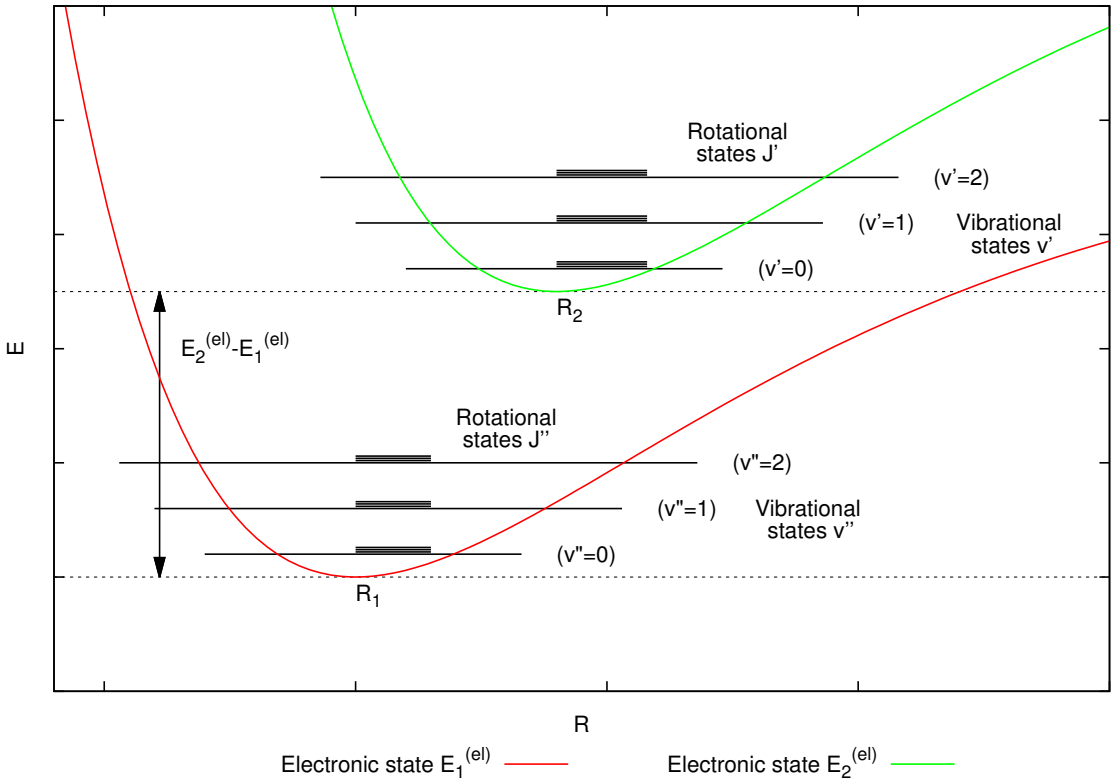

Figure 2.12.1: Relative energy splittings. Plotted are two electronic levels, perhaps pertaining to the N_2^+X and N_2^+A states, and having energies $E_1^{(\mathrm{el})}$ and $E_2^{(\mathrm{el})}$. The vibrational energy levels, labelled with vibrational quantum numbers v' and v'', split the electronic levels by $1/\sqrt{M}$. The rotational levels, labelled with J'' and J', split the vibrational levels by a further $1/\sqrt{M}$. These rotational levels are shown by the shorter lines in the center of each vibrational level. The energy splittings introduced by the rotational levels are clearly dwarfed by those introduced by the vibrational levels.

This uncoupling of vibration and rotation is not entirely accurate, either. As the molecule vibrates, its rotational moment of inertia I changes. Also, as the molecule rotates, it is distorted by centrifugal effects, thereby increasing its rotational moment of inertia. The complexity of the interaction between rotation and vibration, along with the relative scale of energy splittings introduced by the two, make it judicious to neglect rotational effects and focus strictly on vibrational motion of the nuclei.

3

Current Work

The overall purpose of this study is to theoretically treat the photoionization of the homonuclear diatomic molecule N_2. This is divided among three main implements: the UKRmol suite of molecular R-matrix codes, multichannel quantum defect theory (MQDT), and a vibrational frame transformation. Within the Born-Oppenheimer approximation, the nuclei of the parent molecule are fixed, as the electron, in the inner region, is very fast in the time scale of the nuclei. The molecular R-matrix utilizes said approximation, and is used to obtain information such as the reactance matrix $\underline{\underline{\mathbf{K}}}$ and dipole matrix $\underline{\mathbf{d}}$. The eigenquantum defects μ are extracted and transformed by way of a vibrational frame transformation. Finally, the energetically unavailable channels are closed, giving a vibrationally-resolved photoionization cross section.

3.1 Configuration Models

The molecular R-matrix approach[20,87,88,89,8] stems from the atomic R-matrix method, which owes its inception to Wigner and Eisenbud, who formulated a method to treat nuclear phenomena[20]. The underlying premise of their method was to split configuration space into two regions: an inner region, in which short-range interactions have strong and significant effects, and an outer region, in which short-range interactions are negligible in lieu of the dominance of long-range interactions[8]. Through much evolution, the R-matrix methodology was adapted for molecules, although packages for photoionization were not yet available. However, utilizing an existing photoionization model from Motomichi Tashiro[9], the photoionization of molecular nitrogen (N_2) was able to be studied. Tashiro considered two different approximations for the N_2 wavefunction. The first is a single-channel Hartree-Fock, or self-consistent field (SCF), model, in which the electron is treated as if subjected to the mean field of all the other particles. The second is a multichannel configuration interaction (CI) model, which employs a variational approach to optimize the wavefunction as a linear combination of configuration state functions. In addition to these, and with the invaluable help of Connor Ballance[101], the current study has involved a range of models that are variations on the two schemes put forth by Tashiro[9], altering the number of electronic configurations in the configuration-interaction model, among other modifications.

For these models, the fixed nuclei approximation was used with an initial equilibrium nuclear separation of 2.068 bohr, or 1.094 $\mathring{A}$, in accordance with the work of Jacek Kobus[102]. It should be mentioned that NIST offers a slightly larger bond length of 2.075 bohr, or 1.098 $\mathring{A}$, but this small difference will not change the overall physics of the molecule, nor is this work exhaustive. The nuclear separation was subsequently varied over a range of $1.000 - 9.000$ bohr $(0.529 - 4.763$ $\mathring{A})$.

T.H. Dunning's[103] cc-pVTZ (correlation-consistent polarized valence triple-zeta) basis set was used to describe molecular orbitals in both of these models. This basis set includes polarization functions, and have been optimized for computational efficiency. It uses double substitutions from the Hartree-Fock determinant, and includes triple (thus the 'T') excitations. This basis set, along with its variants (cc-pVNZ), are the best current post-Hartree-Fock calculations.

The CI model includes about 80 electronic N_2^+ configurations

$$\Phi_q = \sum C_{qk}\phi_k \quad .$$

Full valence complete active space (CAS), which treats closed-shell, or inactive, orbital space as doubly-occupied in the Slater determinants, was used to construct the configuration state functions for N_2^+. To represent the scattering electron, diffuse Gaussians up to $l = 5$ were included, with varying numbers of functions for each l value. The radius of the R-matrix "box" was chosen as 10 bohr, or $5.292\ \mathring{A}$.[9]

The specific problem at hand is for a photon incident on N_2 is

$$h\nu + N_2\left(1\sigma_g^2 1\sigma_u^2 2\sigma_g^2 2\sigma_u^2 2\pi_u^4 3\sigma_g^2\right) \rightarrow \begin{cases} \mathrm{X}\ \left(3\sigma_g\right)^{-1} + e^- \\ \mathrm{A}^{\pm}\ \left(2\pi_u\right)^{-1} + e^- \\ \mathrm{B}\ \left(2\sigma_u\right)^{-1} + e^- \\ \ldots \end{cases}$$

The photon interacts with the neutral nitrogen molecule, photoionizing one electron and leaving the N_2^+ ion in one of many configurations. Table 3.1 lists several of the most

prominent N_2^+ states explicitly. The SCF model considers the X $\left(^2\Sigma_g^+\right)$ state alone. For

N_2^+ State	Main Configuration
X $^2\Sigma_g^+$	$(3\sigma_g)^{-1}$
A $^2\Pi_u$	$(1\pi_u)^{-1}$
B $^2\Sigma_u^+$	$(2\sigma_u)^{-1}$
D $^2\Pi_g$	$(3\sigma_g)^{-2}(1\pi_g)^{+1}$
C $^2\Sigma_u^+$	$(3\sigma_g)^{-1}(1\pi_u)^{-1}(1\pi_g)^{+1}$
2 $^2\Pi_g$	$(1\pi_u)^{-2}(1\pi_g)^{+1}$
1 $^2\Sigma_u^-$	$(3\sigma_g)^{-1}(1\pi_u)^{-1}(1\pi_g)^{+1}$
1 $^2\Delta_u$	$(3\sigma_g)^{-1}(1\pi_u)^{-1}(1\pi_g)^{+1}$
2 $^2\Sigma_g^+$	$(2\sigma_u)^{-1}(1\pi_u)^{-1}(1\pi_g)^{+1}$

Table 3.1: Listed are some of the main configurations of the N_2^+ states available in a configuration interaction model. The states used in this study's configuration interaction appear above the horizontal line.

this study, only the X $\left(^2\Sigma_g^+\right)$ and A $(^2\Pi_u)$ states are considered in the configuration interaction model. The individual channels used are detailed in Table 3.2.

Total Symmetry	Target State	l	Λ
Σ_u	X	p	σ
Σ_u	X	f	σ
Σ_u	X	f	δ^+
Σ_u	A_+	d	π^+
Σ_u	A_-	d	π^-
Π_u^+	X	p	π^+
Π_u^+	X	f	π^+
Π_u^+	X	f	δ^+
Π_u^+	A_+	s	σ^+
Π_u^+	A_+	d	σ^+
Π_u^+	A_+	d	δ^+
Π_u^+	A_-	d	δ^-
Π_u^-	X	p	π^-
Π_u^-	X	f	π^-
Π_u^-	X	f	δ^-
Π_u^-	A_+	d	δ^-
Π_u^-	A_-	s	σ^+
Π_u^-	A_-	d	σ^+
Π_u^-	A_-	d	δ^+

Table 3.2: Listed are the channels included in the N_2^+ X and N_2^+ A states. The topmost block of channels comprises the Z dipole, the middle block comprises the X dipole, and the bottom-most block comprises the Y dipole.

3.2 Fixed Nuclei Calculations

As stated in Section 2.4, the Born-Oppenheimer approximation asserts that, when operating under certain assumptions, the total molecular wavefunction may be separated, as indicated in equation 2.4.2, into an electronic and a nuclear component, i.e.,

$$\Psi_s(\vec{R};\vec{r}_1,\vec{r}_2,\ldots,\vec{r}_N) = F_s\left(\vec{R}\right)\Phi_q\left(\vec{R};\vec{r}_1,\vec{r}_2,\ldots,\vec{r}_N\right).$$

This then allows each portion of the total wavefunction to be solved individually.

3.2.1 Photoionization Cross Sections

Under the fixed nuclei construct, photoionization cross sections were calculated for the SCF and CI models. The SCF cross section, as expected, is well-behaved and smooth, exhibiting a peak value of 10.59 Mb at a photon energy of 31.14 eV. The photoionization cross section for the CI model, on the other hand, shows a very resonance-rich structure at photon energies in the region between the X $\left({}^2\Sigma_g^+\right)$ and A $\left({}^2\Pi_u\right)$ states of N_2^+. The threshold energy for the A $\left({}^2\Pi_u\right)$ state of N_2^+ occurs at 15.91 eV, as seen in Figure 3.2.1. In the near-threshold region, the SCF treatment coincides well with that of Tashiro, and, even at the two-state level, the broad-range cross section agrees reasonably well with the work of Plummer, et al.[104] The additional features near the photon energy of 25 eV reveal a series of resonances leading up to the B $\left({}^2\Sigma_u^+\right)$ state of the N_2^+ ion.

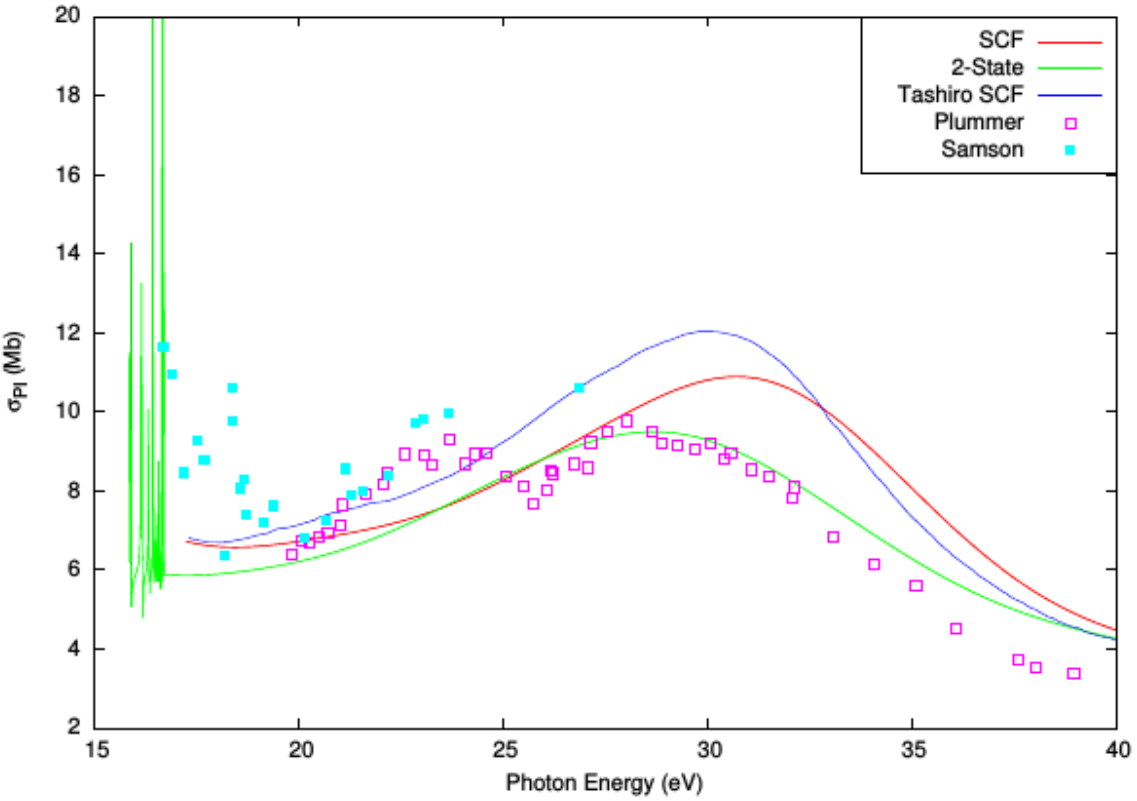

Figure 3.2.1: N_2 Photoionization Cross Section. Using an SCF and a 2-state model, the photoionization cross sections were plotted against photon energy. The cross section is smooth and well-behaved, reaching a peak value of nearly 11 Mb at a photon energy of about 31 eV.

Photoionization cross sections were first computed over a broad photon energy range to study the energy of the strong, broad shape resonance that affects the near-threshold energy dependence in scattering quantities. As also seen in Figure 3.2.2, the cross section features a Rydberg series of resonances building up to the threshold of the A ($^2\Pi$) state of the N_2^+ ion. The Rydberg manifolds n seen in Figure 3.2.2 are comprised of three prominent resonances, corresponding, from left to right, to symmetries A$n(sd)_+\sigma$, A$nd\delta$, and A$n(sd)_-\sigma$, where

$$(sd)_\pm = \frac{s \pm d}{\sqrt{2}}$$

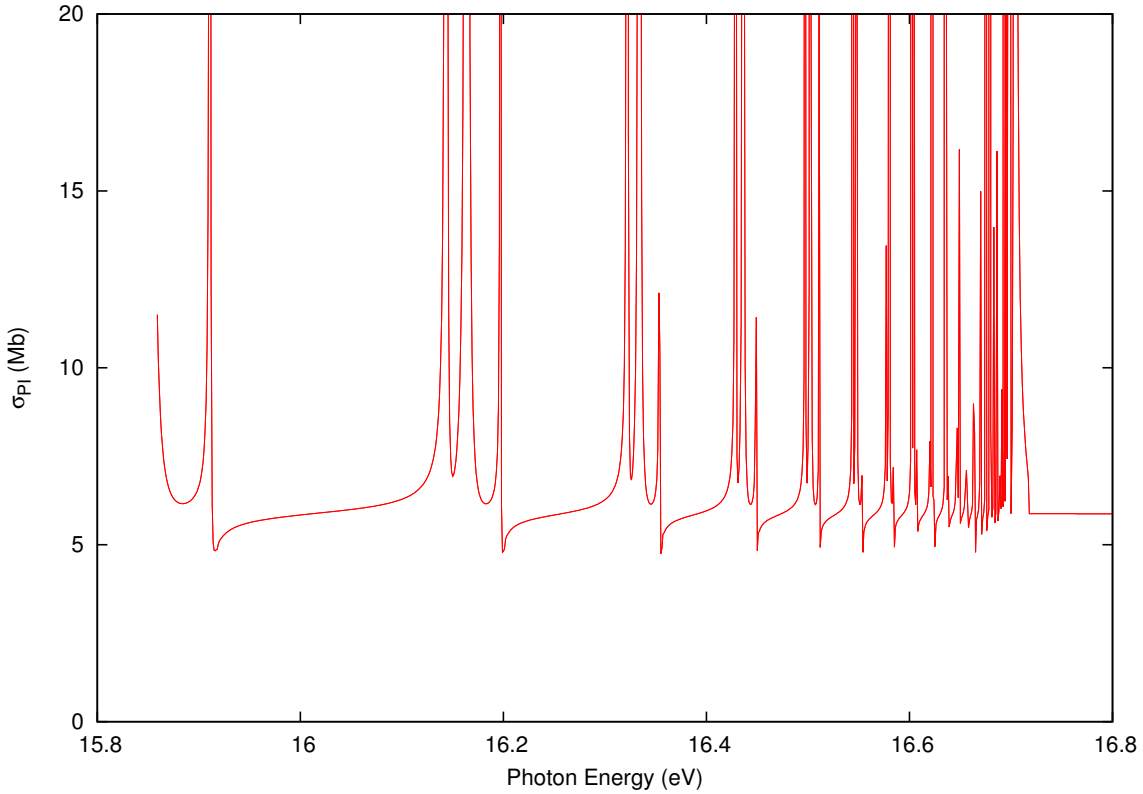

Figure 3.2.2: N_2 Photoionization Cross Section. Between the thresholds of the $X\left({}^2\Sigma_g^+\right)$ and $A\left({}^2\Pi_u\right)$ states of the N_2^+ ion, the photoionization cross section builds up to a Rydberg series of resonances. Each Rydberg manifold n is comprised of three prominent resonances: from left to right, $An(sd)_+\sigma$, $And\delta$, and $An(sd)_-\sigma$. Pictured is the cross section for the 2-state model in this study.

3.2.2 Eigenquantum Defects

Further, an unphysical K-matrix was constructed and extracted from the R-matrix suite of codes, and plotted against energy. The SCF model, which uses one target state and two channels (X $p$and X f), is smooth, varying rather slowly with energy. The low-energy limits approach 0.57 and 0.66, respectively, which compare reasonably well with other works, as seen in Figure 3.2.3, and numerically summarized in Table 3.3.

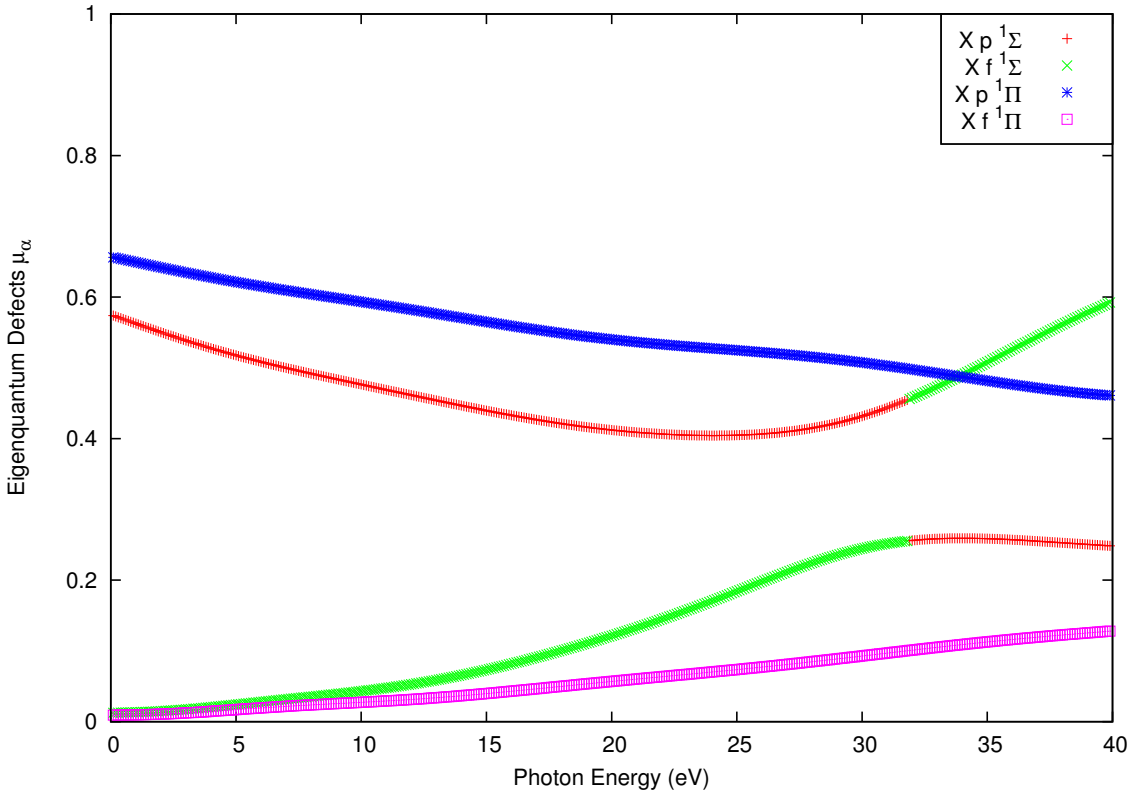

Figure 3.2.3: Eigenquantum defects for the N_2^+ SCF representation. Using a self-consistent field model, the eigenquantum defects were plotted against energy. The low-energy limits are 0.57 for the X $p\left(^1\Sigma_u^+\right)$ symmetry, and 0.66 for the X $p\left(^1\Sigma_u^+\right)$ symmetry.

The eigenquantum defects were also plotted for the CI model, in which, again, only the X $\left(^2\Sigma_g^+\right)$ and A $\left(^2\Pi_u\right)$ states of the N_2^+ ion were considered. Noticeable improvement comes with the 2-state, 4-channel, configuration interaction model. This CI model gives low-energy eigenquantum defects of 0.576 and 0.660 for the X $p\left(^1\Sigma_u^+\right)$ and X $p\left(^1\Pi_u\right)$ symmetries, respectively. These results are depicted in Figure 3.2.4, and numerically summarized in Table 3.3. While the eigenquantum defects are rather well-behaved across the broad energy region, they are much more so in the region of interest, i.e., the photon energy range between the X $\left(^2\Sigma_g^+\right)$ and A $\left(^2\Pi_u\right)$ thresholds. Between these thresholds, the eigenquantum defects show very little energy dependence, as seen in Figure 3.2.5.

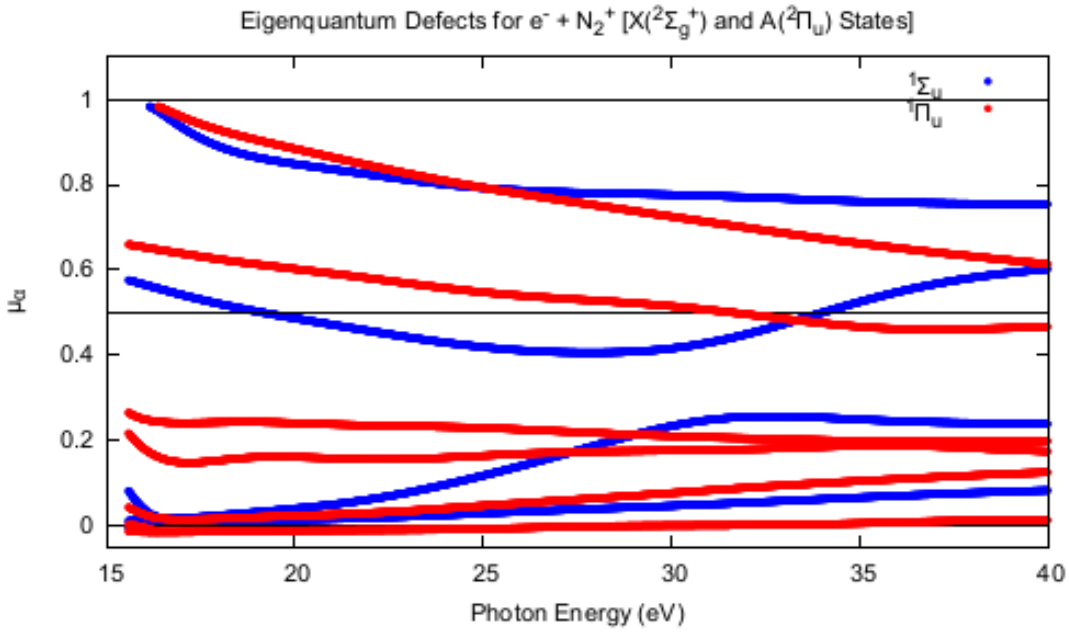

Figure 3.2.4: N_2 eigenquantum defects for the $^1\Sigma$ and $^1\Pi$ symmetries across a broad energy range. These are quite well-behaved, even across such a large range.

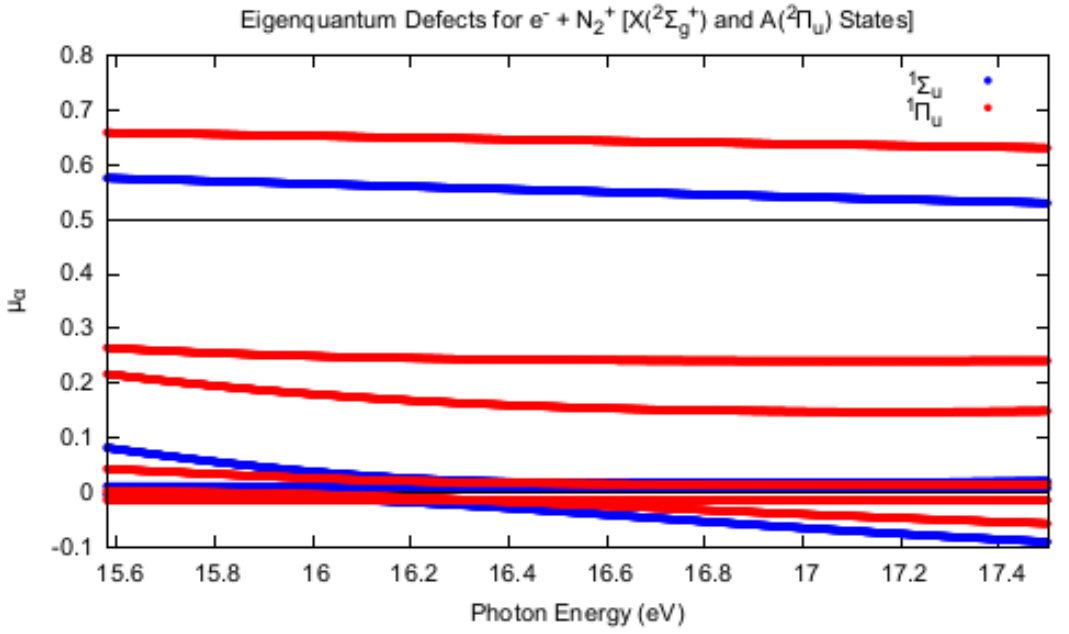

Figure 3.2.5: N_2 eigenquantum defects for the $^1\Sigma$ and $^1\Pi$ symmetries between the X $\left(^2\Sigma_g^+\right)$ and A $\left(^2\Pi_u\right)$ thresholds. In this region of interest, the eigenquantum defects exhibit almost no dependence on photon energy.

Work	$X\,p\,(^1\Sigma_u^+)$	$X\,p\,(^1\Pi_u)$
Huber and Jungen 1990[17]	0.608	0.683
Jungen, et al. 2003[18]	0.594	0.672
SCF 2 channel (Xp, Xf)	0.574	0.656
2-state (X, A)	0.576	0.660

Table 3.3: Eigenquantum defects for $k^2 \to 0$ for $\left(e^- + N_2^+\right)$ scattering. The low-energy eigenquantum defects calculated from the SCF model compare well to the empirical eigenquantum defects of Huber and Jungen[17], and Jungen, et al.[18]. Those of the 2-state model show slightly better agreement with the empirical values.

3.3 Varied Internuclear Distance

With the fixed-nucleus, Born-Oppenheimer calculations completed, it remained to "unfreeze" the nuclei. This was done by enacting a vibrational frame transformation, leading to a vibrationally-resolved photoionization cross section.

3.3.1 Potential Energy Curves

First, the internuclear distance was varied over a range of $1.000 - 9.000$ bohr $(0.529 - 4.763\ \mathring{A})$. Potential energy curves were constructed for both the SCF and 2-state models, and were fit, first with a harmonic oscillator potential, and later with a Morse potential.

The SCF model shows an equilibrium internuclear separation of 2.016 bohr $(1.066\ \mathring{A})$, which is near the expected value of 2.074 bohr $(1.098\ \mathring{A})$. This produced a potential energy of -108.987 a.u. for the neutral N_2 molecule. For the N_2^+ ion, the SCF treatment gave a minimum energy of -108.352 a.u. at an internuclear separation of 2.040 bohr $(1.079\ \mathring{A})$. The resulting first ionization energy for the SCF model, then, was 0.635 a.u. (17.280 eV), which compares with reasonable accuracy to the first ionization energy of 15.581 ± 0.008 eV provided by NIST[105]. These curves can be seen in Figure 3.3.1. The asymptotic energies are indicated therein with dashed lines, and appear at -107.866 a.u.

$(-2935$ eV) and -107.555 a.u. $(-2927$ eV) for the N_2 and N_2^+ curves, respectively. The 2-state model shows potential curves for the X $\left(^2\Sigma_g^+\right)$ and A $\left(^2\Pi_u\right)$ states of the N_2^+ ion.

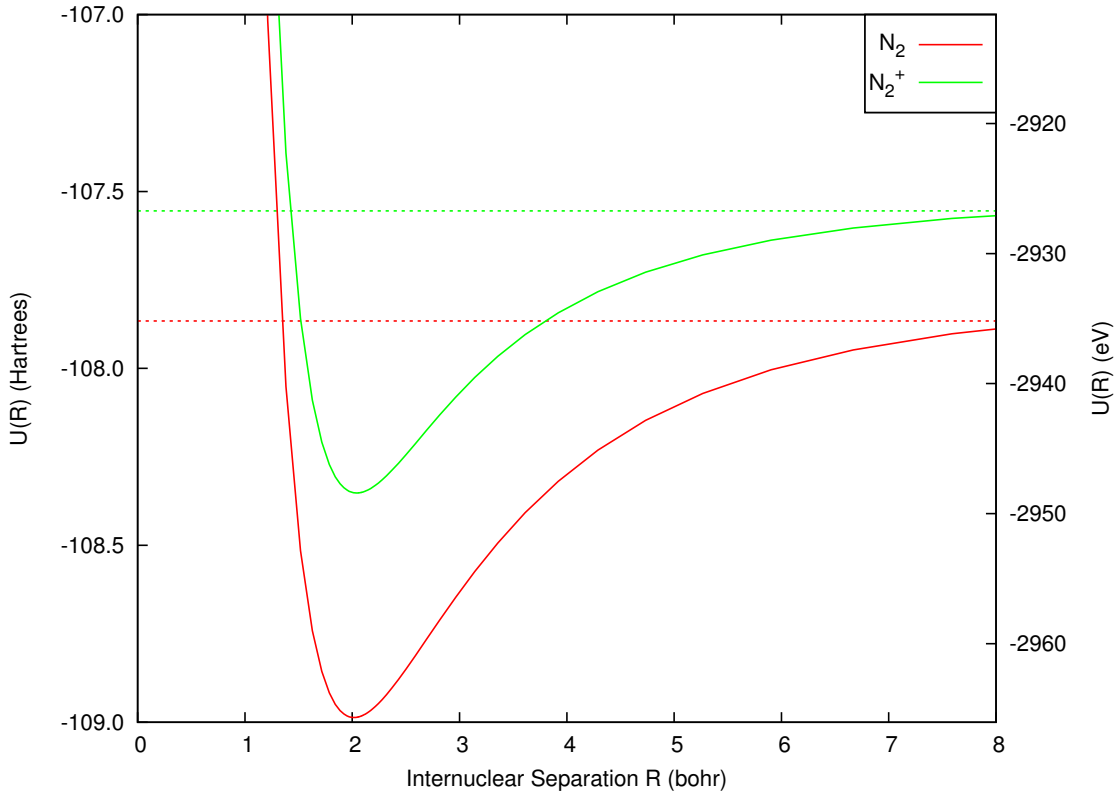

Figure 3.3.1: Potential energy curves for the SCF model. Using an SCF model, a plot of potential energy vs. internuclear separation was constructed for N_2 and N_2^+. The asymptotic energies are indicated with dashed lines, and the expected equilibrium internuclear separation is 2.068 bohr.

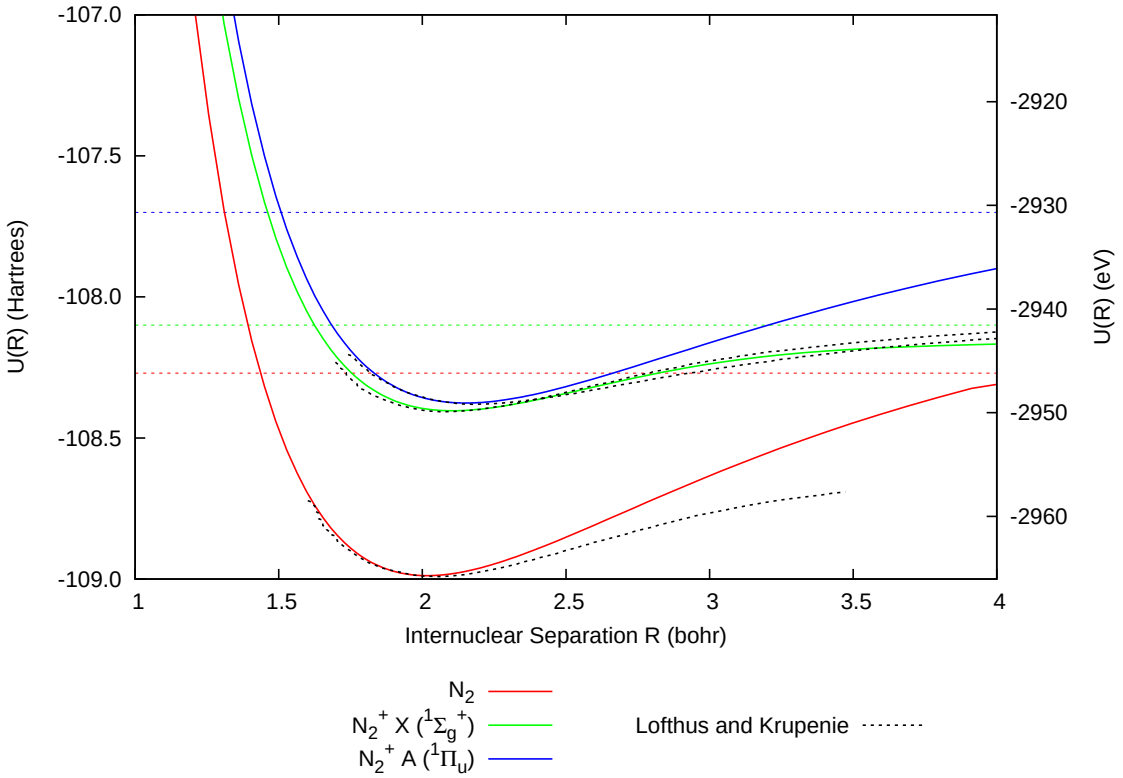

Figure 3.3.2: Potential energy curves for the 2-state model. Using a 2-state model, a plot of potential energy vs. internuclear separation was constructed for N_2 and the two N_2^+ states. The asymptotic energies are indicated with dashed lines, and the expected equilibrium internuclear separation is 2.068 bohr. The experimental curves of Lofthus and Krupenie[15] are shown in black.

3.3.2 Nuclear Wavefunctions

Having constructed potential energy curves, the nuclear wavefunctions were found. To do this, the potential curves were fit with functions. With the discrepancies between the curves produced by this study, and those found in the literature, a choice was made to use experimental curves[15,16] to construct the nuclear wavefunctions. As these wavefunctions would be carried through the vibrational frame transformation, it was prudent to use the established potential curves, so as to minimize additional discrepancies in the vibrationally-resolved results. For internuclear distances near the equilibrium separation, the potentials were fitted with harmonic oscillator potentials. As discussed in Section 2.11.1, the harmonic oscillator allows two fitting parameters, and produces evenly-spaced energy levels. For the both the SCF and 2-state models, the harmonic oscillator fit the potential curves with reasonable accuracy near the equilibrium internuclear separation. These fits, along with their corresponding wavefunctions, are shown in Figure 3.3.3.

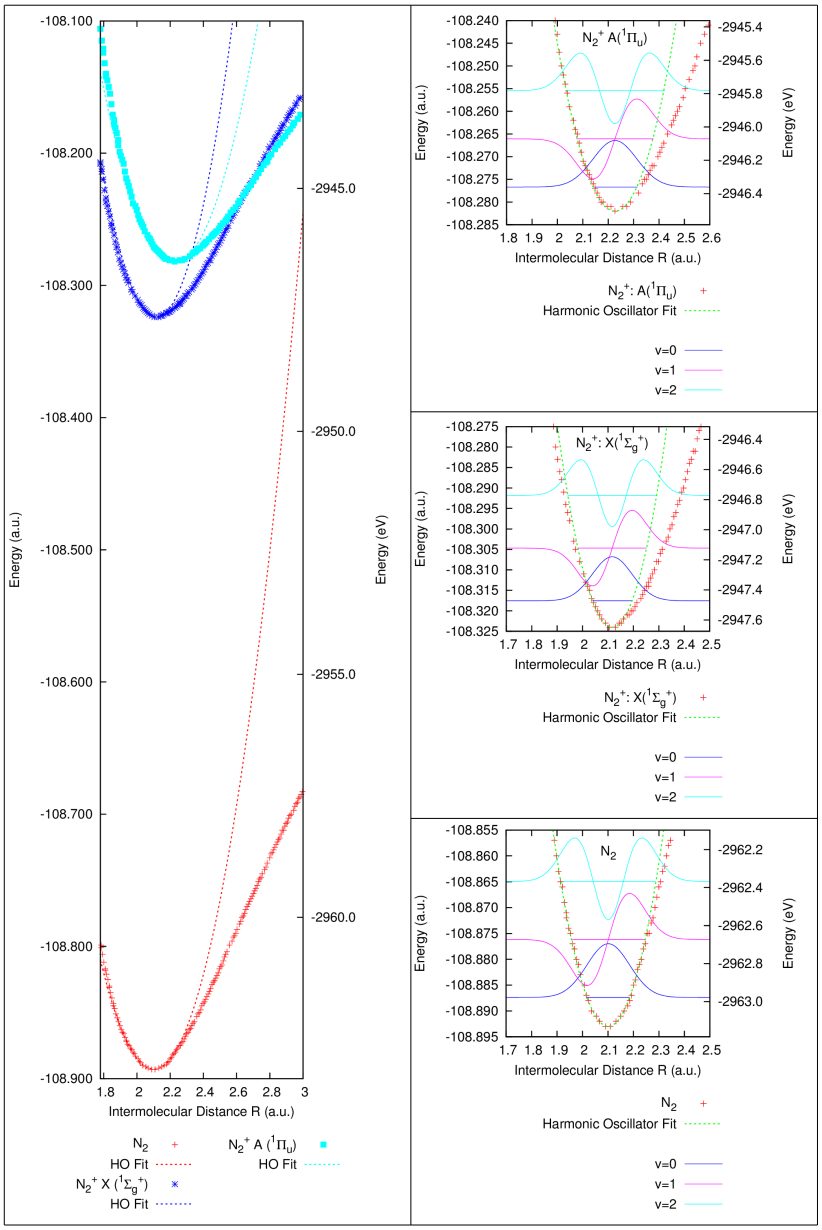

Figure 3.3.3: Harmonic oscillator fits for the 2-state model. Left: A broad-scale view of the three potentials, shown for scale. The experimental curves[15,16] are shown with points, while those constructed in this study are dashed. Right, from top to bottom: The harmonic oscillator fit for the A $\left(^2\Pi_u\right)$ and X $\left(^2\Sigma_g^+\right)$ states of the N_2^+ ion[15], and the corresponding curves for the neutral N_2 molecule[15,16]. The energy levels are evenly spaced, with a separation of 0.01061 a.u. (0.289 eV), 0.01287 a.u. (0.350 eV), and 0.01122 a.u. (0.305 eV), respectively. The wavefunctions are scaled down by a factor of 250, so that they may be superimposed on the curves.

To improve on these fits, the Morse potential was employed. While the harmonic oscillator potential exhibits evenly-spaced energy levels, the Morse potential, as discussed in Section 2.11.2, does not. The lowest energy state of the Morse oscillator nearly coincides with that of the harmonic oscillator, but subsequent states are increasingly more densely packed, as indicated by equation D.1.19 and shown in Figure 3.3.4. Following the treatment in Section 2.11.2, the nuclear vibrational wavefunctions are determined for the Morse oscillator fit, and will be carried into the frame transformation. While the near-equilibrium potential curves are similar for the harmonic oscillator and Morse potentials, the corresponding energy levels differ noticeably, as can be seen in Figure 3.3.5.

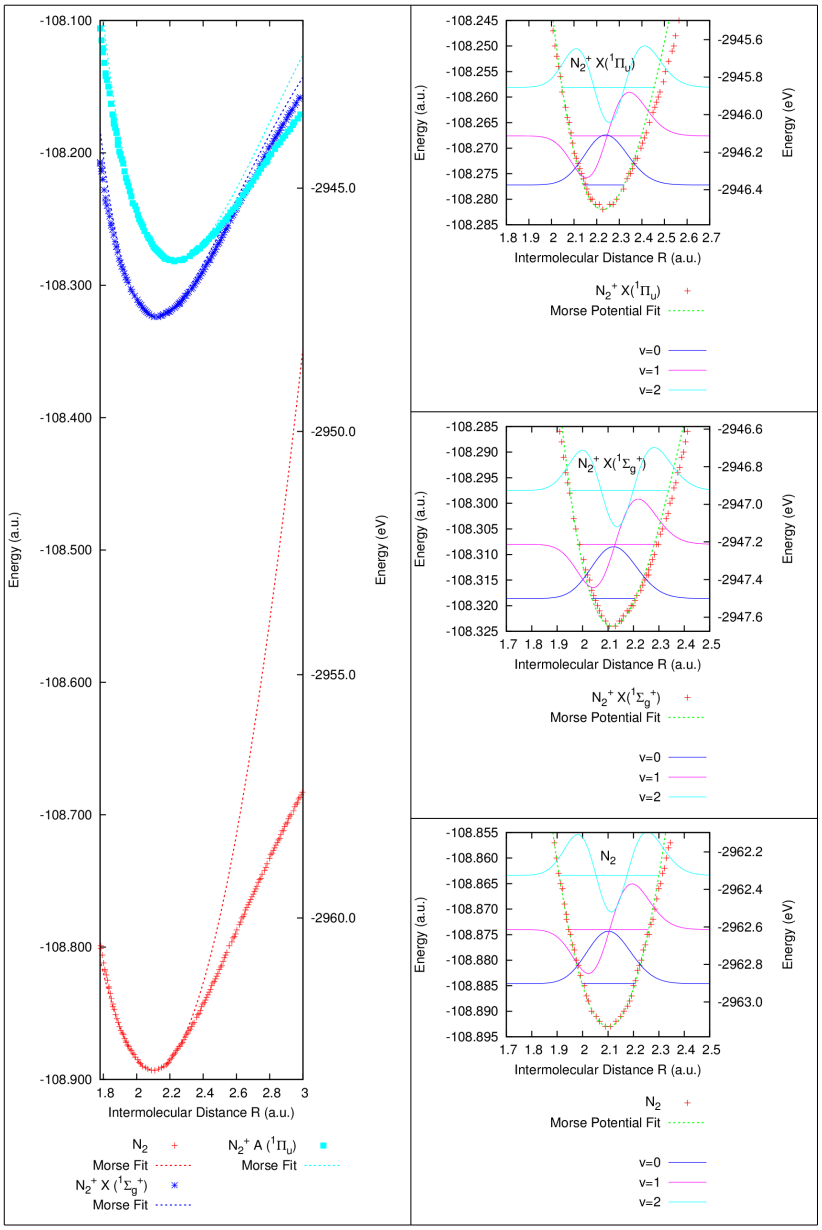

Figure 3.3.4: Morse potential fits for the 2-state model. Left: A broad-scale view of the three potentials, shown for scale. The experimental curves[15,16] are shown with points, while those constructed in this study are dashed. Right, from top to bottom: The Morse potential fit for the A $\left(^2\Pi_u\right)$ and X $\left(^2\Sigma_g^+\right)$ states of the N_2^+ ion[15], and the corresponding curves for the neutral N_2 molecule[15,16]. The energy levels are not evenly spaced, becoming more densely packed with increasing vibrational number v. The wavefunctions are scaled down by a factor of 250, so that they may be superimposed on the curves.

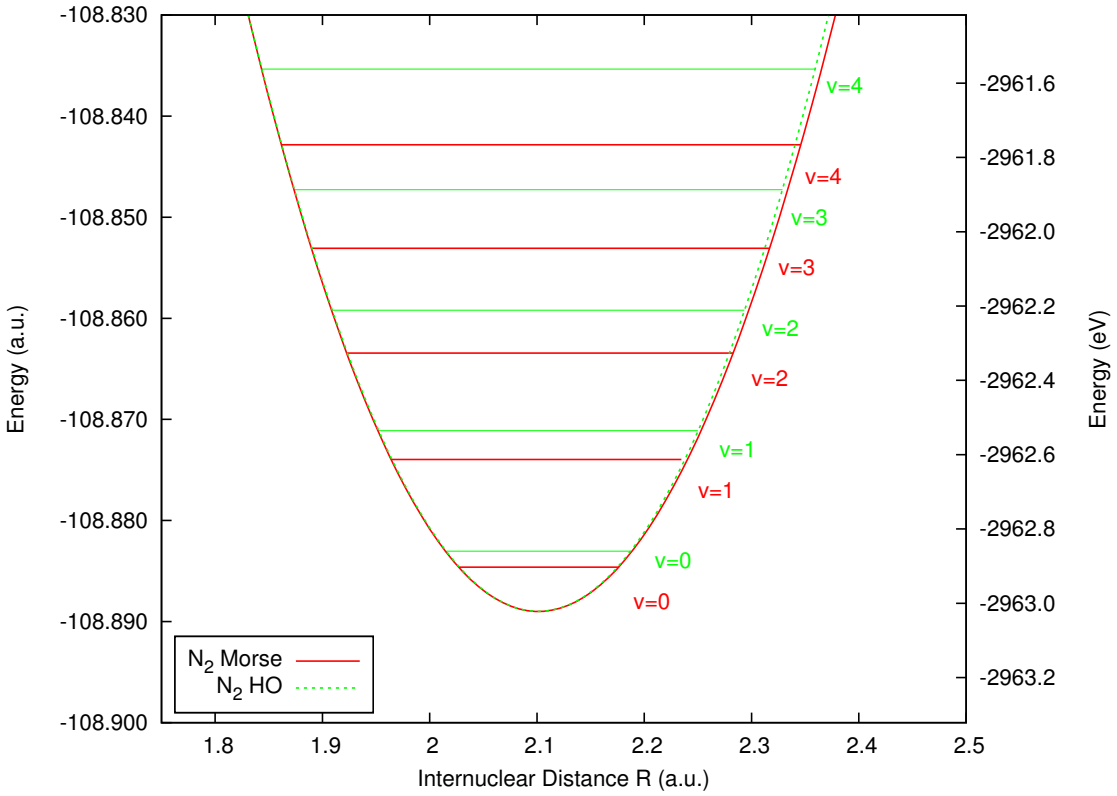

Figure 3.3.5: The Morse potential vs. the harmonic oscillator potential in the 2-state model.While the harmonic oscillator fits the potential well for the lower vibrational levels, the discrepancy in the fit begins to show even by the $v = 4$ level. The asymmetry of the nuclear potential renders the harmonic oscillator potential incapable of matching the nuclear potential curve very well beyond the first few energy levels, and the Morse potential is the more prudent choice. The energy levels of both the harmonic oscillator and the Morse potential are shown in the figure. Note that the spacing between consecutive Morse energy levels decreases with increasing vibrational number v, where those of the harmonic oscillator remain evenly spaced.

3.3.3 Scattering Matrices

In order to perform a frame transformation, it is necessary to obtain dipole and scattering matrices as functions of both photon energy E and internuclear separation R, as discussed in Section 2.10. The UKRMol suite of codes does not ordinarily output unphysical dipole and scattering matrices, but rather closes all energetically unavailable channels. In this work, the closing of these channels has been circumvented, and unphysical dipole and scattering matrices produced. The first matrix element in the Σ_u symmetry $S_{11}(R, E)$ is plotted separately as a representative sample in Figure 3.3.6, after which representative matrix elements are plotted together in Figures 3.3.7-3.3.9.

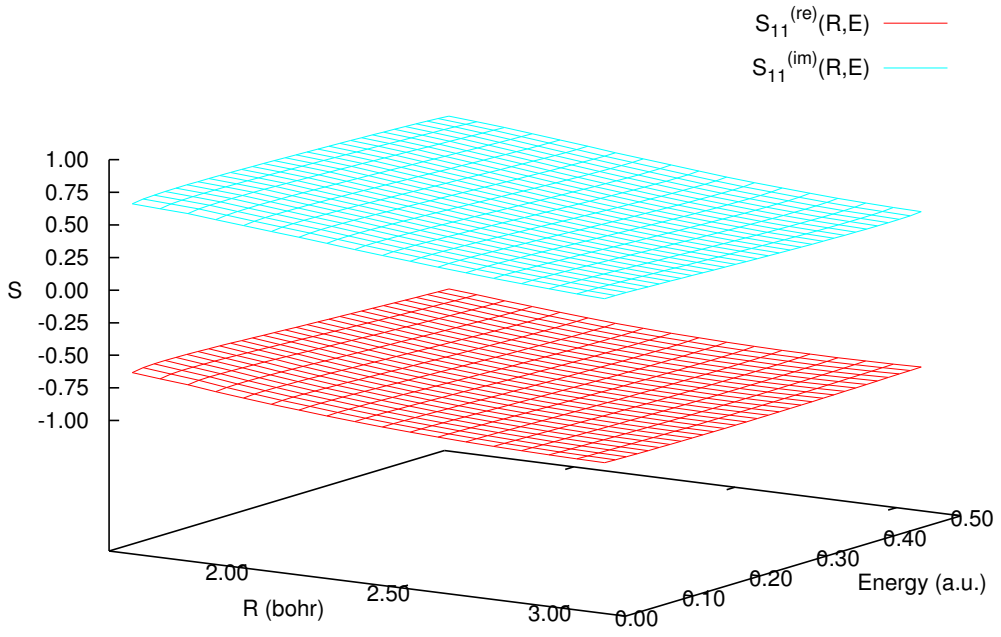

Figure 3.3.6: S_{11}. The real and imaginary parts of the first S-matrix element S_{11} are shown in red and blue, respectively. These vary slowly in both R and E.

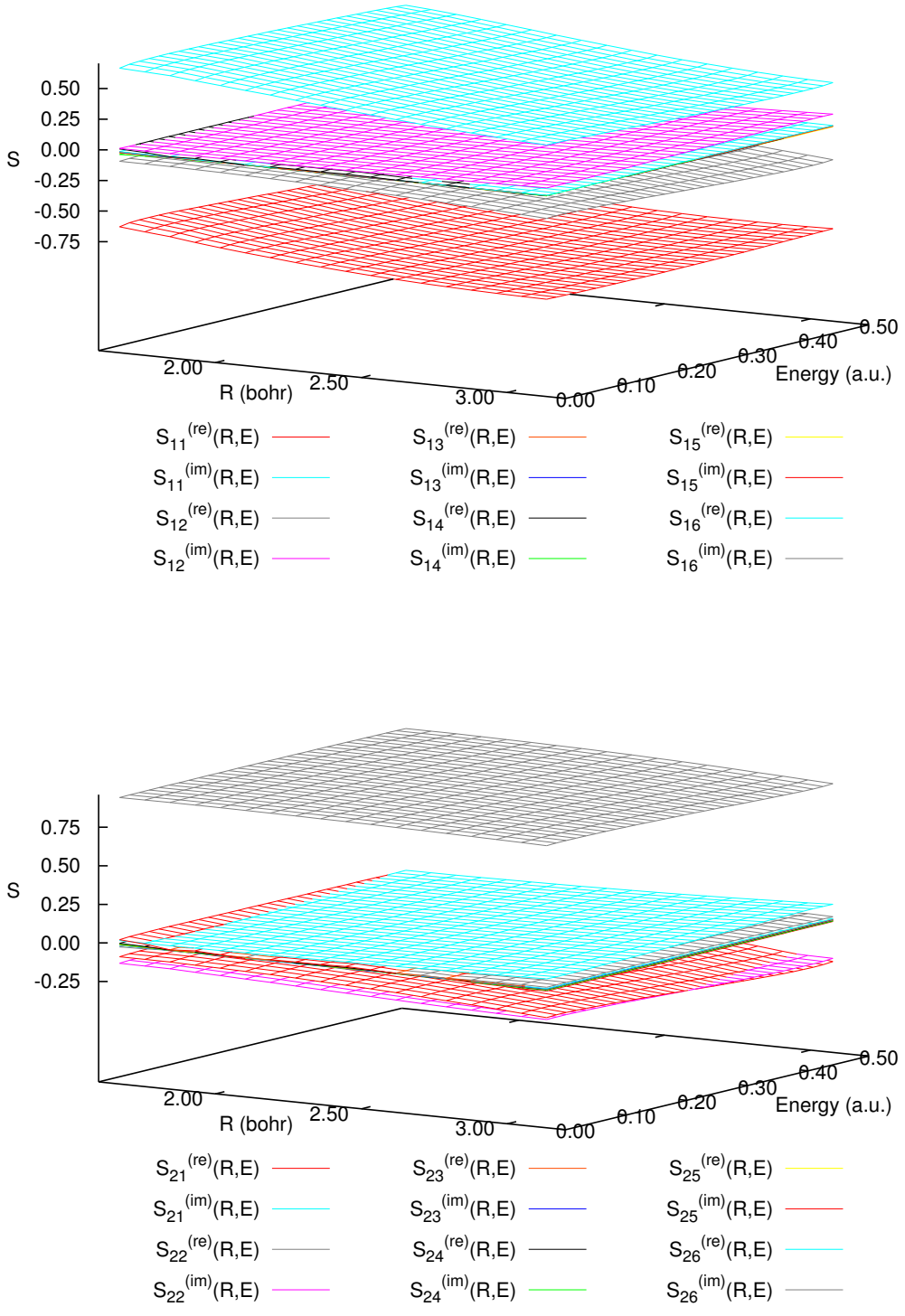

Figure 3.3.7: The first two rows of the S-matrix. The real and imaginary parts of the first two rows of S-matrix elements are shown, plotted against internuclear separation R and photon energy E. For both the first row (above) and second row (below), the S-matrix elements are very smooth in both of these variables.

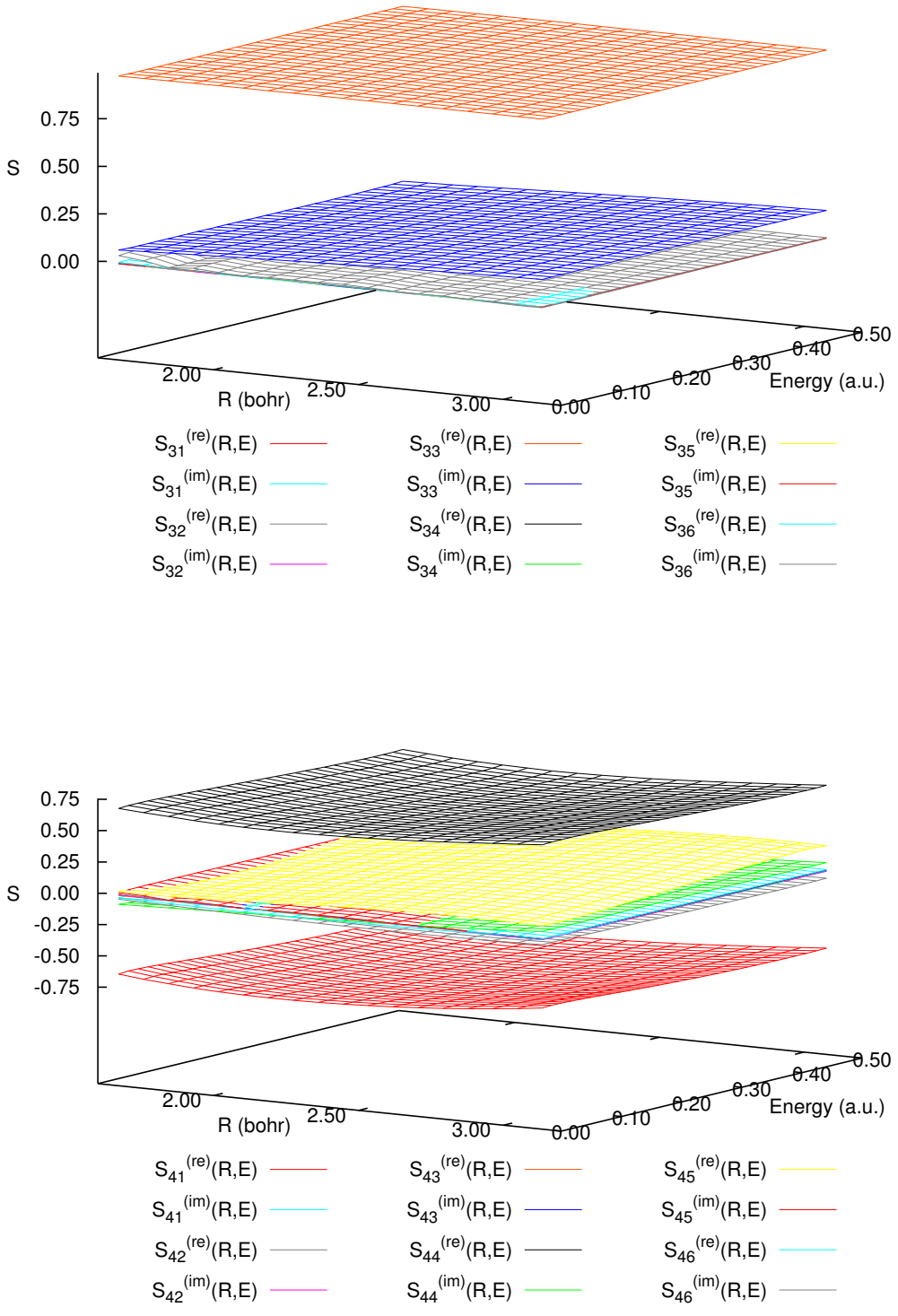

Figure 3.3.8: The second two rows of the S-matrix. The real and imaginary parts of the second two rows of S-matrix elements are shown, plotted against internuclear separation R and photon energy E. For both the third row (above) and fourth row (below), the S-matrix elements are very smooth in both of these variables.

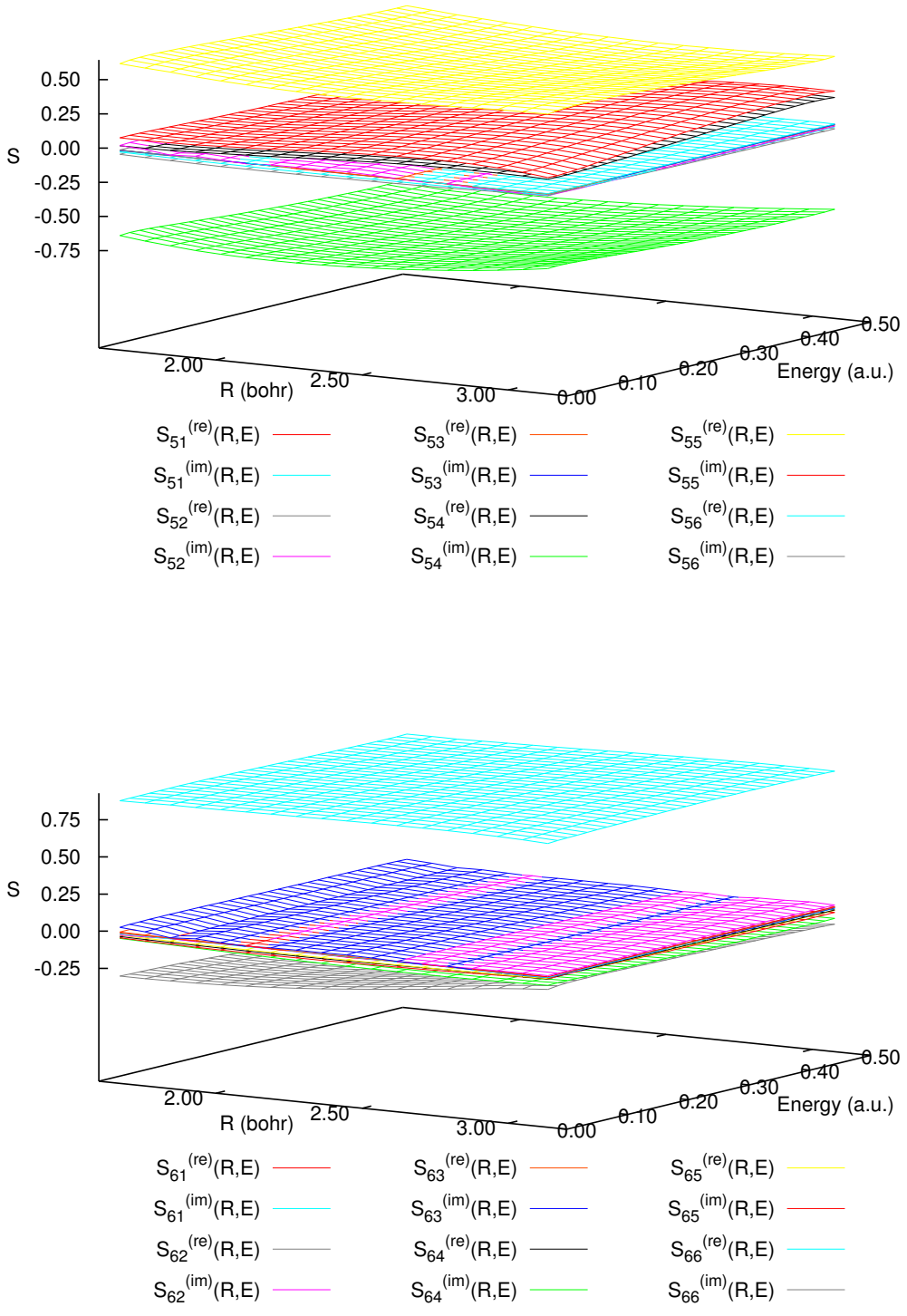

Figure 3.3.9: The last two rows of the S-matrix. The real and imaginary parts of the last two rows of S-matrix elements are shown, plotted against internuclear separation R and photon energy E. For both the fifth row (above) and sixth row (below), the S-matrix elements are very smooth in both of these variables.

These scattering matrices are, indeed, rather featureless, as are the scattering matrices for the remaining symmetries. By virtue of the Franck-Condon principle, the relevant range for the internuclear separation is the region in which the initial vibrational wavefunction is nonzero, which is from 1.8 to 2.4 bohr. While some features do begin to appear in the imaginary portions of S_{54} and S_{55} (see Figure 3.3.9), these features exist at internuclear separations greater than 3 bohr, which is large enough to be outside the region of interest.

3.4 Closing the Channels

Once the nuclear wavefunctions had been obtained, they could be used to enact the vibrational frame transformation, as outlined in Section 2.10. However, the untransformed K-matrix varies drastically with energy. This is problematic for a frame transformation, which requires quantities that vary slowly with energy. The MQDT approach avoids this.[106,72] Rather than immediately eliminate closed channels, an unphysical outer region wavefunction is found

$$\overrightarrow{F}^{(u)} = \begin{pmatrix} \underline{\underline{\mathbf{S_o}}} & 0 \\ 0 & \underline{\underline{\mathbf{S_c}}} \end{pmatrix} + \begin{pmatrix} \underline{\underline{\mathbf{C_o}}} & 0 \\ 0 & \underline{\underline{\mathbf{C_c}}} \end{pmatrix} \begin{pmatrix} \underline{\underline{\mathbf{K_{oo}}}} & \underline{\underline{\mathbf{K_{oc}}}} \\ \underline{\underline{\mathbf{K_{co}}}} & \underline{\underline{\mathbf{K_{cc}}}} \end{pmatrix}, \tag{3.4.1}$$

where the superscript (u) is used to denote an unphysical quantity. Here, the closed functions behave asymptotically as linear combinations of exponentially increasing and decaying *analytical* functions

$$\begin{aligned} \underline{\underline{\mathbf{S_c}}} &\to De^{-kr}\cos\beta + D^{-1}e^{+kr}\sin\beta \\ \underline{\underline{\mathbf{C_c}}} &\to -De^{-kr}\sin\beta + D^{-1}e^{+kr}\cos\beta, \end{aligned} \tag{3.4.2}$$

in which D is the rescaling parameter discussed by Greene, Rau, and Fano[11]. As these are outer region functions, they are subject to the long-range Coulomb potential, and, as such, the parameter β is related to the effective quantum number ν as

$$\beta = \pi(\nu - \ell) \quad , \tag{3.4.3}$$

with

$$E = E_i - \frac{Z^2}{2\nu_i^2} \quad . \tag{3.4.4}$$

Because of the form of the closed functions in Equation 3.4.2, neither $\underline{\underline{\mathbf{S_c}}}$ nor $\underline{\underline{\mathbf{C_c}}}$ independently converges for large r. However, there exists a linear combination of the two for which the asymptotic behavior is exponentially decreasing:

$$\underline{\underline{\mathbf{S_c}}} \cos\beta - \underline{\underline{\mathbf{C_c}}} \sin\beta \rightarrow De^{-kr}. \tag{3.4.5}$$

Unlike the physical K-matrix, the unphysical K-matrix is a smooth function of energy. It is transformed from the R to the v representation via the unitary operation

$$\begin{aligned} \underline{\underline{\mathbf{K}}}^{(u)} &\rightarrow \hat{\mathbf{U}}^{\dagger}_{(vib)} \underline{\underline{\mathbf{K}}}^{(u)} \hat{\mathbf{U}}_{(vib)} \\ \vec{d} &\rightarrow \hat{\mathbf{U}}^{\dagger}_{(vib)} \vec{d}, \end{aligned} \tag{3.4.6}$$

after which the eigenquantum defects may be extracted:

$$\underline{\underline{\mathbf{K}}}^{(u)} = \hat{\mathbf{U}}^{\dagger} \tan\pi\mu \hat{\mathbf{U}}. \tag{3.4.7}$$

The details of this transformation, as well as the meaning of the unitary transformation matrix $\hat{\mathbf{U}}_{(vib)}$ are discussed in Section 2.10.

The unphysical K and d-matrices are thus fed into the frame transformation, after which the closed channels are eliminated:

$$\begin{aligned}\overrightarrow{\underline{F}}^{(p)} &= \left[\overrightarrow{\underline{F}}^{(u)}\right]\begin{pmatrix}\mathbb{1}_{oo}\\ \mu_{co}\end{pmatrix}\\ &= \left[\begin{pmatrix}\underline{\underline{\mathbf{S_o}}} & 0\\ 0 & \underline{\underline{\mathbf{S_c}}}\end{pmatrix}+\begin{pmatrix}\underline{\underline{\mathbf{C_o}}} & 0\\ 0 & \underline{\underline{\mathbf{C_c}}}\end{pmatrix}\begin{pmatrix}\underline{\underline{\mathbf{K_{oo}}}} & \underline{\underline{\mathbf{K_{oc}}}}\\ \underline{\underline{\mathbf{K_{co}}}} & \underline{\underline{\mathbf{K_{cc}}}}\end{pmatrix}\right]\begin{pmatrix}\mathbb{1}_{oo}\\ \mu_{co}\end{pmatrix} \quad , \end{aligned} \tag{3.4.8}$$

requiring

$$\mu_{co} = -\left(\underline{\underline{\mathbf{K_{cc}}}} + \tan\beta\right)^{-1}\underline{\underline{\mathbf{K_{co}}}} \quad . \tag{3.4.9}$$

By comparing 3.4.1 and 3.4.8, the physical K-matrix $\underline{\underline{\mathbf{K_{oo}}}}^{(phys)}$ is found as

$$\underline{\underline{\mathbf{K_{oo}}}}^{(p)} = \underline{\underline{\mathbf{K_{oo}}}} + \underline{\underline{\mathbf{K_{oc}}}}\,\mu_{co} \quad ,$$

and, by inserting 3.4.9,

$$\underline{\underline{\mathbf{K_{oo}}}}^{(phys)} = \underline{\underline{\mathbf{K_{oo}}}} - \underline{\underline{\mathbf{K_{oc}}}}\left(\underline{\underline{\mathbf{K_{cc}}}} + \tan\beta\right)^{-1}\underline{\underline{\mathbf{K_{co}}}}. \tag{3.4.10}$$

3.5 Photoionization Cross Section

Ultimately, the photoionization cross section is computed from the dipole matrices thus

$$\sigma_{PI}(E) = \frac{4\pi^2\alpha\omega}{3}\,\overrightarrow{d_o}^{\dagger(phys)}\,\overrightarrow{d_o}^{(phys)} \quad , \tag{3.5.1}$$

where ω is the energy of the ionizing radiationin atomic units, and α is the fine structure constant. The frame transformation may be applied to the reactance matrix $\underline{\underline{\mathbf{K}}}$, after

which the scattering matrix may be constructed as

$$\underline{\underline{\mathbf{S}}}^{\dagger} = \left(\underline{\underline{\mathbb{1}}} - i\underline{\underline{\mathbf{K}}}\right)\left(\underline{\underline{\mathbb{1}}} + i\underline{\underline{\mathbf{K}}}\right)^{-1}, \tag{3.5.2}$$

whereafter the physical scattering and dipole matrices are found

$$\begin{aligned} \underline{\underline{\mathbf{S_{oo}}}}^{\dagger(phys)} &= \underline{\underline{\mathbf{S_{oo}}}}^{\dagger} - \underline{\underline{\mathbf{S_{oc}}}}^{\dagger}\left(\underline{\underline{\mathbf{S_{cc}}}}^{\dagger} - e^{+2i\pi\nu}\right)^{-1}\underline{\underline{\mathbf{S_{co}}}}^{\dagger} \\ \vec{d}_o^{\,\dagger(phys)} &= \vec{d}_o^{\,\dagger} - \vec{d}_c^{\,\dagger}\left(\underline{\underline{\mathbf{S_{cc}}}}^{\dagger} - e^{+2i\pi\nu}\right)^{-1}\underline{\underline{\mathbf{S_{co}}}}^{\dagger}. \end{aligned} \tag{3.5.3}$$

In performing these calculations, however, it was found that the eigenquantum defects passed through $1/2$. Consequently, the reactance matrix $\underline{\underline{\mathbf{K}}} = \tan\pi\mu$ exhibited a pole at this point. This led to a complication in the computation of the scattering matrix via 3.5.2. Rather than transform the reactance matrix, then, the eigenquantum defects themselves were transformed using

$$Ue^{i2\pi\mu}U^{\dagger}.$$

The photoionization cross sections were computed and compared to unpublished SOLEIL synchrotron photoabsorption data from Heays, et al.[14] and to empirical photoionization data from O'Keeffe, et al.[13], as seen in Figure 3.5.1.

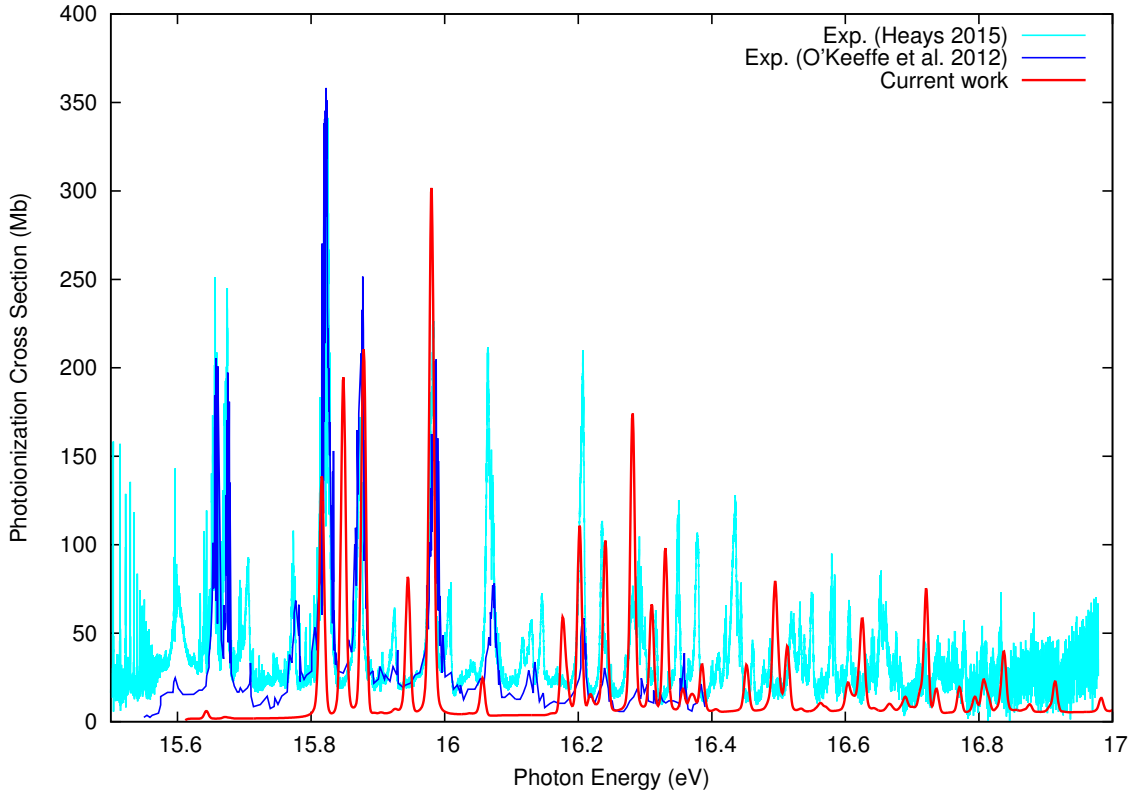

Figure 3.5.1: Vibrationally-resolved photoionization cross sections. Experimental photoioinization data from O'Keeffe, et al.[13] is shown in blue, and recent SOLEIL synchrotron photoabsorption data from Heays, et al[14] is shown in cyan. The pair of signals near 15.65 eV are produced by a low-lying N_2^+ B resonance, and are therefore absent from this current work.

As this study considered only photoionization, there are peaks present in the Heays[14] total photoabsorption data that are necessarily absent in this theoretical work, but the Heays[14] data is included to show consistency with the work of O'Keeffe, et al.[13] The set of strong peaks present in the experimental data near 15.65 eV are produced by a low-lying N_2^+ B resonance, and, because the current work considers only the N_2^+ X and N_2^+ A states, is absent in this theoretical cross section. The calculated vibrationally-resolved results show some similarities to the experimental work at photon energies near threshold, but there are certainly discrepancies between the two.

4

Conclusion

This work sought to theoretically treat the photoionization of molecular nitrogen by combining the R-matrix method, multichannel quantum defect theory, and a vibrational frame transformation. This began with an existing configuration interaction model consisting of 160 states of the N_2^+ ion. Tashiro's 160-state model[9] included many states that were problematic. First, the model was too computationally demanding for the available resources, as well as being altogether too large to be practical for the purposes of this study. More importantly, the eigenquantum defects did not exhibit smooth energy behavior, so that $\frac{d\mu}{dE}$ was quite erratic and inappropriate for use in a frame transformation.

The 160-state model was reduced first to a model that included only single-electron excitations, which reduced the model to only four states: the N_2^+ X state, two degenerate N_2^+ A states, and the N_2^+ B state listed in Table 3.1. As seen in Figure 3.2.1, the resonances belonging to the N_2^+ B state introduces a discernable signal in the broad-range

photoionization cross section, but these do not fall in the near-threshold region which was the focus of this study. Upon inspection of the eigenquantum defects μ_α, the 160-state values were not well behaved. After reducing the model to states involving single electron promotions, i.e., the 4-state model, problems still persisted in the eigenquantum defects. The model was therefore further reduced by removing the N_2^+ B state, leaving only the N_2^+ X state and the two degenerate N_2^+ A states (N_2^+ A_+ and N_2^+ A_-), but again, the eigenquantum defects were ill-behaved. Finally, by removing the second N_2^+ A state (N_2^+ A_-) and double-counting the first, the eigenquantum defects were smooth and well-behaved.

The N_2^+ A states brought about a different set of difficulties. These N_2^+ A states are the result of removing an electron from the $1\pi_u$ orbital, of which there are two, both perpendicular to the internuclear axis, so that one is oriented along the x-axis (N_2^+ A_+), and the other along the y-axis (N_2^+ A_-). Since the inclusion of both N_2^+ A states yielded erratic eigenquantum defect variations with energy, and the inclusion of only the N_2^+ A^+ state yielded smooth eigenquantum defects, an approximation of energetic degeneracy of the two N_2^+ A states was made. Rather than include both N_2^+ A states, then, the N_2^+ A^- state was excluded and the N_2^+ A^+ state was included twice. This approach, however, may not have been valid, as the symmetries of these energetically degenerate states are not the same. It is entirely possible that simply double-counting one of these states was not sufficient to account for all effects, and that the resulting quantities differed from those that would have been obtained by treating the two N_2^+ A states separately. In addition to the 2-state configuration interaction model, a single-state, self-consistent field model was also considered, in which the N_2^+ X state was the only state considered. This model, of course, showed no resonances beyond the N_2^+X threshold, but did allow for certain other quantities to be inspected, such as the strong, broad $\sigma \rightarrow p$ shape resonance similar to that found in the model study of Appendix C.

With the nuclei frozen, the eigenquantum defects were extracted for both the single-state and two-state models. The single-state model eigenquantum defects compared well to empirical results from Jungen, et al.,[18] as summarized in Table 3.3. The low-energy limit values for the two-state model, which consists of only one more state than the single-state model, showed slight improvement over those for the single-state model. Further, photoionization cross sections were constructed under the frozen nuclei approximation, so as to first serve as a sort of confirmation of initial calculations, and more importantly, to serve as input to the frame transformation. The photoionization cross section for the single-state model was, as expected, smooth and well-behaved, showing no resonance series over a broad energy range. The additional N_2^+ A electronic state of the N_2^+ molecular ion used in the two-state model led to Rydberg series of resonances in the photoionization cross section visible in the near-threshold reason, as was expected, and produced no further resonances in the broad energy range. In fact, other than an apparent resonance series belonging to the N_2^+B state (and possibly to other higher electronic states that were also absent in the model used in this study), the broad-range photoionization cross section for the two-state model was reasonably consistent with experimental results.

By "unfreezing" the nuclei, potential energy curves were constructed under the single-state and two-state models for the neutral N_2 molecule and the X state of the molecular ion, as well as the A state in the case of the two-state model. These curves were in moderate agreement with experimentally-produced curves near equilibrium internuclear separations, though the asymptotic behavior was less consistent. As only the near-equilibrium internuclear separations ($R \approx R_{eq}$) were necessary for the vibrational frame transformation, it was decided that the experimental curves would be used. These curves were fit with a Morse potential, and vibrational eigenenergies and wavefunctions constructed.

The UKRmol suite of codes ordinarily closes all energetically unavailable channels immediately, producing strong features in scattering quantities, so that they are not amenable to a frame transformation, which relies on smooth scattering quantities. In this study, the *unphysical*, smooth reactance, dipole, and scattering matrices were extracted prior to channel closure. The reactance matrix showed pole behavior, so that an S-matrix normalization was more appropriate than K-matrix normalization. Rather than doing this, however, it may have been beneficial to transform the quantum defect matrix, rather than the S-matrix, thereby guaranteeing the unitarity of the latter. The scattering and dipole matrices were calculated for varying internuclear separations, and their R-dependence was shown to be smooth.

Finally, the smooth, unphysical scattering and dipole matrices were employed into a vibrational frame transformation. The resulting vibrationally-resolved scattering and dipole matrices were then closed, eliminating energetically unphysical channels, and photoionization cross sections were constructed. These vibrationally-resolved photoionization cross sections were compared to experimental results, as shown in Figure 3.5.1. The calculated results were not in very good agreement with experiment, indicating shortcomings in the representations used in the approach used. Several factors could have contributed to this, one of which was the previously-discussed issue with the handling of the degenerate N_2^+ A states. The zero-energy eigenquantum defects in the N_2^+ A channels do not agree with those of Jungen, et al.[18], further suggesting that there were errors introduced in the N_2^+ A states.

Another potential source of error arose from the close-coupling representation of the photoelectron. As discussed in Section 2.5.1, there is a certain amount of Hilbert space lost due to orthogonalization of a discretized representation of the continuum. To re-

cover this space, a number of L^2 configurations were added. A problem arises, though, when more of these L^2 states are added than necessary. If the L^2 states are overly complete, this can lead to series of pseudoresonances that add artificial features to a cross section. Because the two-state model used had been whittled down from 160 states to two states, there were certain to be L^2 states present in excess, resulting in extraneous false signals.

There were discrepancies between calculated and experimental cross sections in the near-threshold region, and more work is necessary to achieve a more respectable result. However, the agreement between calculations and experiment in the broad-range photoionization cross sections and low-energy eigenquantum defects under the frozen nuclei approximation was more than satisfactory. The further agreement between the calculated and experimental potential energy curves for the neutral N_2 molecule and the two states of the N_2^+ ion near equilibrium was encouraging. The asymptotic behavior of the calculated potential energy curves differed from experiment, suggesting that inappropriate approximations in the representations of the N_2^+ molecular ion were made for larger internuclear separation R.

All this said, there is much to be shown for this study. First, this was new territory in that it was the first theoretical molecular photoionization work done by the Western Michigan University Atomic and Molecular physics group. As such, this may be utilized as groundwork for future endeavours at WMU. Second, there have long been difficulties in classifying the spectrum of N_2, and this work addresses the broad-range behavior well, but also picks up on signals produced by the vibrational levels of the lowest two electronic states of the N_2^+ ion. Further work in expanding the two-state model back to three states, i.e., counting the two degenerate N_2^+A states separately, and then four states, i.e., reintroducing the N_2^+B state, could build on this two-state model, allowing

for a more highly-resolved and inclusive theoretical result.

A

Coulomb Functions

The differential equation governing the radial portion of the electronic wavefunction is, from 2.1.12,

$$\left[\frac{\partial^2}{\partial r^2} + 2E + \frac{2Z}{r} - \frac{l(l+1)}{2r^2} - \frac{Z}{r}\right] u(r) = 0.$$

Introducing the scaled quantities

$$\rho \equiv \sqrt{2E}r$$
$$\eta \equiv \frac{Z}{\sqrt{2E}}$$

allows 2.1.12 to be rewritten

$$\left[\frac{\partial^2}{\partial \rho^2} + 1 + \frac{2\eta}{\rho} - \frac{l(l+1)}{\rho^2}\right] u(\rho) = 0. \tag{A.1.1}$$

The regular solution to this differential equation is given by Abramowitz and Stegun[82], and the derivation thereof is the subject of Appendix B:

$$S_l(\eta, \rho) = A_l(\eta)\rho^{l+1}e^{-i\rho}{}_1F_1(l+1-i\eta, 2l+2, 2i\rho), \tag{A.1.2}$$

with

$$A_l(\eta) = \frac{2^l e^{-\pi\eta/2}\,|\Gamma(l+1+i\eta)|}{\Gamma(2l+2)} \tag{A.1.3}$$

and ${}_1F_1$ is the confluent hypergeometric function of the first kind. The confluent hypergeometric function of the second kind, of course, provides a second solution to this differential equation, and the two confluent hypergeometric functions are linearly independent of one another. However, these solutions include several factors other than just the confluent hypergeometric functions, and therefore, the solutions differing only in this term are not linearly independent for all l. Consequently, a third solution must be constructed with which $S_l(\eta,\rho)$ is linearly independent. The irregular Coulomb function is

$$C_l(\eta,\rho) = \frac{2\eta}{A_0^2(\eta)} S_l(\eta,\rho)\left[\ln(2\rho) + \frac{q_l(\eta)}{p_l(\eta)}\right] + \theta_l(\eta,\rho), \tag{A.1.4}$$

with

$$\theta_l(\eta,\rho) = \frac{1}{A_l(\eta)}\frac{1}{2l+1}\rho^{-l}\sum_{k=-l}^{\infty}\left[a_k^l(\eta)\rho^{k+l}\right].$$

The factors $a_k^l(\eta)$ are painstakingly defined by Abramowitz and Stegun[82], and reproducing them here would be more tedious than beneficial. Suffice it to say that the Coulomb function of the first kind $S_l(\eta,\rho)$ is regular at the origin, and the linearly independent Coulomb function of the second kind $C_l(\eta,\rho)$ is irregular at the origin. It has been formally demonstrated by Mukhamedzhanov and Akin[107] that the Coulomb functions constitute a complete set, and, as defined above, these functions have a Wronskian

$$W(S_l, C_l) = 1,$$

thus verifying their linear independence.

B

Coulomb Functions: A Derivation

Alongside the discussion in Section 2.1 and Appendix A, the following will serve as a more complete derivation of the Coulomb functions. The derivation of these functions is often touched upon in quantum mechanics textbooks, but is presented here in more detail.

B.1.1 The Azimuthal Wavefunction

With no preferred orientation in space, the z-axis is free to be chosen so that the eigenfunctions of the Hamiltonian $\hat{\mathscr{H}}$ are simultaneously eigenfunctions of the square of the angular momentum L^2, with quantum numbers l, and z-component of angular momentum L_z, with quantum numbers m, that is,

$$|\psi\rangle \propto \mathscr{Y}_{l,m}$$

The z-component of angular momentum yields a trivial eigenvalue equation

$$\begin{aligned} L_z \mathscr{Y}(\theta,\phi) &= -i\frac{\partial}{\partial\phi}\mathscr{Y}(\theta,\phi) \\ &= m\mathscr{Y}(\theta,\phi) \end{aligned}$$

so that

$$\frac{\partial}{\partial\phi}\mathscr{Y}(\theta,\phi) = i\cdot m\mathscr{Y}(\theta,\phi)$$

and

$$\mathscr{Y}(\theta, \phi) = \Theta(\theta) \cdot e^{i \cdot m\phi} \tag{B.1.1}$$

Thus the entirety of the azimuthal dependence of the wavfunction is contained in a simple exponential term $e^{i \cdot m\phi}$. The restriction that these angular functions must be single valued in both θ and ϕ

$$e^{i \cdot m(\phi + 2\pi)} = e^{i \cdot m\phi}$$

requires that m is an integer

$$m = \left\{ \mathbb{Z}^{\pm}, 0 \right\}.$$

With the azimuthal dependence established, it remains to discuss the polar angle θ.

B.1.2 Eigenvalues

In order to approach the polar angle portion of the wavefunction, it is helpful to first study the eigenvalue equations for the angular momentum. In a method similar to the raising and lowering operators of the quantum oscillator, one can define a raising and lowering operator for angular momentum:

$$L_{\pm} \equiv L_x \pm i \cdot L_y. \tag{B.1.2}$$

Since L^2 commutes with any one component of $\vec{L}$, it is clear that L^2 will also commute with these raising and lowering operators:

$$\left[L^2, L_{\pm} \right] = 0. \tag{B.1.3}$$

The components of the angular momentum have commutation relations with one another, still in atomic units, of

$$[L_i, L_j] = i \cdot \epsilon_{ijk} L_k \tag{B.1.4}$$

where ϵ_{ijk} is the Levi-Civita tensor

$$\epsilon_{ijk} \equiv \hat{x}_i \cdot (\hat{x}_j \times \hat{x}_k).$$

This commutation relation is used to find the eigenvalues of the L^2 operator. First, without loss of generality, the eigenvalue equation for L^2 can be written as

$$L^2\mathscr{Y}_{l,m} = f(l,m)\mathscr{Y}_{l,m},$$

where $f(l,m)$ is an unknown but dimensionless function of l and m. To find the identity of this function, it is helpful to utilize the raising and lowering operators for angular momentum B.1.2. The raising and lowering operators are Hermitian conjugates of one another:

$$(L_\pm)^\dagger = L_\mp,$$

and so their product is real

$$\begin{aligned} L_\pm L_\mp &= (L_x \pm i \cdot L_y)(L_x \mp i \cdot L_y) \\ &= L_x^2 + L_y^2 \mp i \cdot (L_x L_y - L_y L_x) \\ &= \left(L^2 - L_z^2\right) \mp i \cdot [L_x, L_y] \\ &= L^2 - L_z^2 \mp i \cdot (i \cdot L_z) \\ &= L^2 - L_z^2 \pm L_z. \end{aligned} \tag{B.1.5}$$

This allows the square of the angular momentum L^2 to be written in terms of the ladder operators and the angular momentum's z-component:

$$L^2 = L_\pm L_\mp + L_z^2 \mp L_z. \tag{B.1.6}$$

Applying the bottom signs in B.1.6 to the angular wavefunction $\mathscr{Y}_{l,m}$ gives

$$L^2\mathscr{Y}_{l,m} = \left(L_- L_+ + L_z^2 + L_z\right)\mathscr{Y}_{l,m}. \tag{B.1.7}$$

Applying the raising operator to a state $\mathscr{Y}_{l,m}$ generates a new function with an eigenvalue that has increased by 1. This means that the new eigenfunction has a larger z-component of angular momentum, while its *total* angular momentum remains the same. Consequently, there exists some upper limit to the number of times the raising operator may be applied to a state. Beyond this point, additional application of the raising operator yields a zero result:

$$L_+\mathscr{Y}_{l,m_{(max)}} = 0.$$

Each $\mathscr{Y}_{l,m}$ is an eigenstate of L^2 and L_z with eigenvalues, still in atomic units, of $f(l,m)$ and $m_{(max)}$, respectively. After the raising operator has been applied the maximum number of times, the z-component of angular momentum is equal to the total momentum, i.e., $L_z = |\vec{L}|$, so the L_z eigenvalue of this topmost state is $m_{(max)} = l$, that is,

$$L_z \mathscr{Y}_{l,m_{(max)}} = l \cdot \mathscr{Y}_{l,m_{(max)}}$$

Now, with B.1.6, an eigenvalue can be found for the L^2 operator acting on $\mathscr{Y}_{l,l}$:

$$\begin{aligned} L^2 \mathscr{Y}_{l,l} &= \left(L_- L_+ + L_z^2 + L_z\right) \mathscr{Y}_{l,l} \\ &= L_- \left(L_+ \mathscr{Y}_{l,l}\right) + L_z^2 \mathscr{Y}_{l,l} + L_z \mathscr{Y}_{l,l} \\ &= L_- \left(0\right) + l^2 \mathscr{Y}_{l,l} + l \mathscr{Y}_{l,l} \\ &= \left(l^2 + l\right) \mathscr{Y}_{l,l} \\ &= l\left(l+1\right) \mathscr{Y}_{l,l} \end{aligned} \tag{B.1.8}$$

The same process is conducted with the lowering operator, recognizing that there exists a maximum number of times that the lowering operator can be applied before yielding a zero result:

$$L_- \mathscr{Y}_{l,m_{(min)}} = 0. \tag{B.1.9}$$

This gives an L_z eigenvalue of $m_{(min)}$, i.e.,

$$L_z \mathscr{Y}_{l,m_{(min)}} = m_{(min)} \mathscr{Y}_{l,m_{(min)}}. \tag{B.1.10}$$

The total angular momentum is unaffected by the raising and lowering operators, so the eigenvalue of L^2 remains the same:

$$L^2 \mathscr{Y}_{l,m_{(min)}} = l\left(l+1\right) \mathscr{Y}_{l,m_{(min)}}. \tag{B.1.11}$$

Combining equations B.1.9, B.1.10, and B.1.11 in a manner similar to B.1.8 gives an eigenvalue equation for L^2. This time, however, the top signs in B.1.6 are used:

$$\begin{aligned} L^2 \mathscr{Y}_{l,m_{(min)}} &= \left(L_+ L_- + L_z^2 - L_z\right) \mathscr{Y}_{l,m_{(min)}} \\ &= L_+ \left(L_- \mathscr{Y}_{l,m_{(min)}}\right) + L_z^2 \mathscr{Y}_{l,m_{(min)}} - L_z \mathscr{Y}_{l,m_{(min)}} \\ &= L_+ \left(0\right) + m_{(min)}^2 \mathscr{Y}_{l,m_{(min)}} - m_{(min)} \mathscr{Y}_{l,m_{(min)}} \\ &= m_{(min)} \left(m_{(min)} - 1\right). \end{aligned} \tag{B.1.12}$$

Because the total angular momentum, and thus the square thereof, is unaffected by the raising and lowering operators, its eigenvalue must be the same for $\mathscr{Y}_{l,m_{(min)}}$ and $\mathscr{Y}_{l,m_{(max)}}$, so that B.1.12 and B.1.8 may be equated:

$$m_{(min)}\left(m_{(min)}-1\right)=l\left(l+1\right),$$

which has solutions

$$\begin{aligned} m_{(min)} &= -l \\ m_{(min)} &= l+1. \end{aligned}$$

The second solution is illogical, as it would mean that $m_{(min)} > m_{(max)}$, leaving only the first solution. This identifies the minimum value of the z-component of angular momentum as $-l$, thus establishing the constraints on m:

$$m \in \left\{\mathbb{Z}^{\pm}, 0 :\ -l \leq m \leq l\right\} \tag{B.1.13}$$

Having developed the angular momentum eigenvalues, it is now appropriate to find the eigenfunctions $\mathscr{Y}_{l,m}$.

B.1.3 The Polar Wavefunction

First, recall that the angular portion of the wavefunction takes the form shown in equation B.1.1:

$$\mathscr{Y}_{l,m}(\theta,\phi)=\Theta_{l,m}(\theta)\cdot e^{i\cdot m\phi}.$$

To find the polar angle dependence of the wavefunction, the raising and lowering operators are heavily utilized. In the previous section, the raising lowerator was applied to the topmost state, giving

$$L_{+}\mathscr{Y}_{l,l}=0. \tag{B.1.14}$$

Recalling the definition of the raising and lowering operators (B.1.2), along with that of the angular momentum itself (2.1.4), the ladder operators may be written in differential

form:

$$\begin{aligned}
L_{\pm} &= L_x \pm L_y \\
&= i \cdot \left[\sin\phi \frac{\partial}{\partial\theta} + \cos\phi \cot\theta \frac{\partial}{\partial\phi} \right] \pm i \cdot \left[-i \cdot \cos\phi \frac{\partial}{\partial\theta} + i \cdot \sin\phi \cot\theta \frac{\partial}{\partial\phi} \right] \\
&= \left(i \cdot \sin\phi \pm \cos\phi \right) \frac{\partial}{\partial\theta} + i \cdot \cot\theta \left(\cos\phi \pm i \cdot \sin\phi \right) \frac{\partial}{\partial\phi} \\
&= \pm e^{\pm i\phi} \frac{\partial}{\partial\theta} + i \cdot \cot\theta \cdot e^{\pm i\phi} \frac{\partial}{\partial\phi} \\
&= e^{\pm i\phi} \left(\pm \frac{\partial}{\partial\theta} + i \cdot \cot\theta \frac{\partial}{\partial\phi} \right), \qquad \text{(B.1.15)}
\end{aligned}$$

which allows equation B.1.14 to be rewritten:

$$L_+ \mathscr{Y}_{l,l} = e^{i\phi} \left(\frac{\partial}{\partial\theta} + i \cdot \cot\theta \frac{\partial}{\partial\phi} \right) \mathscr{Y}_{l,l}. \qquad \text{(B.1.16)}$$

Because the azimuthal contribution is a complex exponential, a derivative of $\mathscr{Y}_{l,l}$ with respect to ϕ will introduce another imaginary unit. Consider the real portion of B.1.16:

$$\begin{aligned}
\mathbb{R}e \left\{ L_+ \mathscr{Y}_{l,l} \right\} &= \mathbb{R}e \left\{ e^{i\phi} \left(\frac{\partial}{\partial\theta} + i \cdot \cot\theta \frac{\partial}{\partial\phi} \right) \left(e^{i \cdot l\phi} \cdot \Theta_{l,l}(\theta) \right) \right\} \\
&= \mathbb{R}e \left\{ e^{i\phi} \left[e^{i \cdot l\phi} \frac{\partial}{\partial\theta} \left(\Theta_{l,l}(\theta) \right) - l \cdot \cot\theta \cdot \Theta_{l,l}(\theta) \cdot e^{i \cdot l\phi} \right] \right\} \\
&= \mathbb{R}e \left\{ e^{i\phi} e^{i \cdot l\phi} \left[\frac{\partial}{\partial\theta} \left(\Theta_{l,l}(\theta) \right) - l \cdot \cot\theta \cdot \Theta_{l,l}(\theta) \right] \right\}
\end{aligned}$$

The requirement that this expression must vanish sets up a (first order) differential equation for $\Theta_{l,l}(\theta)$:

$$\begin{aligned}
\frac{\partial}{\partial\theta} \left(\Theta_{l,l}(\theta) \right) &= l \cdot \cot\theta \cdot \Theta_{l,l}(\theta) \\
\Theta_{l,l}(\theta) &= A_{l,m} \cdot \sin^l\theta, \qquad \text{(B.1.17)}
\end{aligned}$$

where $A_{l,m}$ is a normalization constant that will be determined later. Having found the functional form of the polar angle dependence for the topmost state $\mathscr{Y}_{(l,m=l)}$, the lowering operator may now be applied repeatedly to find the θ dependence of any other

angular momentum state:

$$\begin{aligned}\Theta_{(l,l-1)}(\theta) &= L_{-}\Theta_{l,l}(\theta)\\ \Theta_{l,m}(\theta) &= (L_{-})^{l-m}\,\Theta_{l,l}(\theta)\end{aligned}$$

In differential form, as shown in equation B.1.15, the lowering operator, when acting on the state $\mathscr{Y}_{l,l}$, is expressed as

$$L_{-}\mathscr{Y}_{l,l} = e^{-i\phi}\left(-\frac{\partial}{\partial\theta} + i\cdot\cot\theta\frac{\partial}{\partial\phi}\right)\left(e^{i\cdot l\phi}\cdot\Theta_{l,l}(\theta)\right) \tag{B.1.18}$$

As angular momentum is a real observable, the lowering operator must yield a real result. Once again, differentiating with respect to ϕ introduces another imaginary unit, so that the real portion of B.1.18 is

$$\begin{aligned}\mathbb{R}e\left\{L_{-}\mathscr{Y}_{l,l}\right\} &= \mathbb{R}e\left\{e^{-i\phi}\left(-\frac{\partial}{\partial\theta} + i\cdot\cot\theta\frac{\partial}{\partial\phi}\right)\left(e^{i\cdot l\phi}\cdot\Theta_{l,l}(\theta)\right)\right\}\\ &= \mathbb{R}e\left\{-e^{-i\phi}e^{i\cdot l\phi}\left[\frac{d}{d\theta}\left(\Theta_{l,l}(\theta)\right) + l\cdot\cot\theta\cdot\Theta_{l,l}(\theta)\right]\right\}\\ &= \mathbb{R}e\left\{-e^{i\cdot(l-1)\phi}\left[\frac{d}{d\theta}\left(\Theta_{l,l}(\theta)\right) + l\cdot\cot\theta\cdot\Theta_{l,l}(\theta)\right]\right\},\end{aligned} \tag{B.1.19}$$

where the full derivative replaces the partial derivative when it acts on a function of θ alone. With regards to the azimuthal angle, then, the lowering operator affects no more than the exponential term. The effect of the lowering operator may therefore be written as

$$L_{-}\left(e^{i\cdot m\phi}\cdot f(\theta)\right) = -e^{i\cdot(m-1)\phi}\left[\frac{d}{d\theta} + m\cdot\cot\theta\right]f(\theta). \tag{B.1.20}$$

The form of $f(\theta)$ evolves with each derivative, but some power of $\sin\theta$ emerges, so that $f(\theta) = g(\theta)\sin^m\theta$. Recognizing this allows for a trend to be seen:

$$\begin{aligned}\frac{d}{d\theta}\left(\sin^m\theta\cdot g(\theta)\right) &= m\cdot\sin^{m-1}\theta\cos\theta\cdot g(\theta) + \sin^m\theta\cdot\frac{d}{d\theta}\left(g(\theta)\right)\\ &= \sin^m\theta\left[m\cdot\cot\theta\cdot g(\theta) + \frac{d}{d\theta}\left(g(\theta)\right)\right]\\ &= \sin^m\theta\left(\frac{d}{d\theta} + m\cdot\cot\theta\right)g(\theta). \end{aligned} \tag{B.1.21}$$

Via the chain rule, this differentiation by θ may be otherwise presented

$$\begin{aligned}\frac{d}{d\theta} &= -\sin\theta\frac{d}{d(\cos\theta)}\\ \sin^m\theta\left(\frac{d}{d\theta} + m\cdot\cot\theta\right)g(\theta) &= -\sin\theta\frac{d}{d(\cos\theta)}\left(\sin^m\theta\cdot g(\theta)\right)\\ \left(\frac{d}{d\theta} + m\cdot\cot\theta\right)g(\theta) &= -\left(\frac{1}{\sin^{m-1}\theta}\right)\frac{d}{d(\cos\theta)}\left(\sin^m\theta\cdot g(\theta)\right),\end{aligned}$$

which is inserted into the lowering operator from B.1.20:

$$\begin{aligned}L_-\left(e^{i\cdot m\phi}\cdot f(\theta)\right) &= -e^{i\cdot(m-1)\phi}\left[\frac{d}{d\theta} + m\cdot\cot\theta\right]f(\theta)\\ &= e^{i\cdot(m-1)\phi}\left[\left(\frac{1}{\sin^{m-1}\theta}\right)\frac{d}{d(\cos\theta)}\left(\sin^m\theta\cdot g(\theta)\right)\right].\end{aligned}$$

This function again has the form of $e^{i\cdot m\phi}\cdot g(\theta)$ seen in B.1.20, meaning that the next iteration of the lowering operator proceeds exactly as the previous, replacing m with $(m-1)$:

$$\begin{aligned}\left(L_-\right)^2\left(e^{i\cdot m\phi}\cdot f(\theta)\right) &= L_-\left[e^{i\cdot(m-1)\phi}\left(\frac{1}{\sin^{m-1}\theta}\right)\frac{d}{d(\cos\theta)}\left(\sin^m\theta\cdot g(\theta)\right)\right]\\ &= e^{i\cdot(m-2)\phi}\left[\left(\frac{1}{\sin^{m-2}\theta}\right)\frac{d}{d(\cos\theta)}\left(\sin^{m-1}\theta\cdot g(\theta)\right)\right].\end{aligned}$$

Recalling that $f(\theta) = g(\theta) \cdot \sin^m \theta$, this relation becomes

$$(L_-)^2 \left(e^{i \cdot m\phi} \cdot f(\theta) \right) = e^{i \cdot (m-2)\phi} \left[\left(\frac{1}{\sin^{m-2} \theta} \right) \left[\frac{d}{d(\cos\theta)} \right]^2 \left(\sin^m \theta \cdot f(\theta) \right) \right], \quad \text{(B.1.22)}$$

where, again, $f(\theta)$ is the topmost angular momentum state, i.e.,

$$f(\theta) = \Theta_{l,l}(\theta).$$

The result is extrapolated to find the generating function for any angular momentum state $\mathscr{Y}_{l,m}$:

$$\mathscr{Y}_{l,m} = (L_-)^{l-m} \mathscr{Y}_{l,l}. \quad \text{(B.1.23)}$$

Now, the effect of the ladder operators can be rather cleverly found by utilizing their Hermitian conjugate relationship from B.1.2.

$$\langle L_\pm \mathscr{Y}_{l,m} | L_\pm \mathscr{Y}_{l,m} \rangle = \langle L_\pm \mathscr{Y}_{l,m} | L_\mp L_\pm \mathscr{Y}_{l,m} \rangle .$$

The product of the ladder operators is rewritten in terms of operators with known eigenvalues via B.1.6

$$\begin{aligned} \langle L_\pm \mathscr{Y}_{l,m} | L_\pm \mathscr{Y}_{l,m} \rangle &= \left\langle \mathscr{Y}_{l,m} \middle| \left(L^2 - L_z^2 \mp L_z \right) \mathscr{Y}_{l,m} \right\rangle \\ &= \left\langle \mathscr{Y}_{l,m} \middle| \left(l(l+1) - m^2 \mp m \right) \mathscr{Y}_{l,m} \right\rangle \\ &= (l \mp m)(l \pm m + 1) \langle \mathscr{Y}_{l,m} | \mathscr{Y}_{l,m} \rangle \end{aligned} \quad \text{(B.1.24)}$$

This means that the effect of the raising and lowering operators on the state $\mathscr{Y}_{l,m}$ is

$$L_\pm \mathscr{Y}_{l,m} = \sqrt{(l \mp m)(l \pm m + 1)}\, \mathscr{Y}_{l,m\pm1}, \quad \text{(B.1.25)}$$

which can be used to find any $\mathscr{Y}_{l,m}$ once one state, such as $\mathscr{Y}_{l,l}$, has been found. From here, then, it remains to repeatedly apply the lowering operator as per equation B.1.23:

$$\begin{aligned} \mathscr{Y}_{l,m} &= (L_-)^{l-m} \mathscr{Y}_{l,l} \\ &= \frac{1}{\sqrt{(l+l)(l-l+1)}} (L_-)^{l-m-1} \mathscr{Y}_{l,l-1} \end{aligned}$$

The result of the second application can stand to be simplified somewhat

$$\begin{aligned}\mathscr{Y}_{l,m} &= \frac{1}{\sqrt{(l+l)(l-l+1)}}\frac{1}{\sqrt{(l+(l-1))(l-(l-1)+1)}}\left(L_-\right)^{l-m-1}\mathscr{Y}_{l,l-2} \\ &= \frac{1}{\sqrt{(l+l)(l-l+1)}}\frac{1}{\sqrt{(2l-1)(2)}}\left(L_-\right)^{l-m-1}\mathscr{Y}_{l,l-1}.\end{aligned}$$

Continuing this trend gives

$$\mathscr{Y}_{l,m} = A_{l,m}\sqrt{\frac{(l+m)!}{(l-m)!}}e^{i\cdot m\phi}\frac{1}{\sin^m\theta}\left[\frac{d}{d(\cos\theta)}\right]^{l-m}\sin^{2l}\theta. \tag{B.1.26}$$

The functional form of the angular wavefunction is thus determined.

B.1.4 Spherical Harmonics

As can be seen in B.1.24 (and B.1.17, for that matter), the above treatment assumes that the state $\mathscr{Y}_{l,l}$ is normalized. It is necessary, then, to find $A_{l,m}$.

$$\left\langle \mathscr{Y}_{l,l} \middle| \mathscr{Y}_{l,l} \right\rangle = \int_{(\phi=0)}^{2\pi}\left[\int_{(\theta=0)}^{\pi}\left(\left|A_{l,l}\right|^2\sin^{2l}\theta\right)\sin\theta d\theta\right]d\phi \tag{B.1.27}$$

As such, the product $\left\langle \mathscr{Y}_{l,l} \middle| \mathscr{Y}_{l,l} \right\rangle$ is independent of m, meaning that B.1.27 becomes

$$\begin{aligned}1 &= \left\langle \mathscr{Y}_{l,l} \middle| \mathscr{Y}_{l,l} \right\rangle \\ &= \left|A_{l,l}\right|^2\left[4^l\left(l!\right)^2\cdot\frac{4\pi}{(2l+1)}\right] \\ A_{l,l} &= \frac{(-1)^l}{l!\,2^l}\sqrt{\frac{(2l+1)}{4\pi}}.\end{aligned}$$

Because the m dependence is entirely in the complex exponential, the value of $A_{l,m}$ is the same for all m, meaning

$$A_{l,m} = \frac{(-1)^l}{l!\,2^l}\sqrt{\frac{(2l+1)}{4\pi}}. \tag{B.1.28}$$

Finally, combining B.1.28 and B.1.26 gives an expression for $\mathscr{Y}_{l,m}$:

$$\mathscr{Y}_{l,m} = \frac{(-1)^l}{l!\,2^l}\sqrt{\frac{(2l+1)(l+m)!}{4\pi(l-m)!}}e^{i\cdot m\phi}\frac{1}{\sin^m\theta}\left[\frac{d}{d(\cos\theta)}\right]^{l-m}\left(\sin^{2l}\theta\right). \tag{B.1.29}$$

This is an appropriate time to address the nature of l, as well. It was established above that the values of m are restricted to integers between $-l$ and l (equation B.1.13). There is an additional constraint that limits l to integer values

$$l \in \{\mathbb{Z}, 0\} \tag{B.1.30}$$

This can be quickly seen by first supposing that l may take half-integer values, and examining the consequences thereof. To be, perhaps, unneccesarily clear that this function is strictly a conjecture, this supposed angular wavefunction will be denoted as $\mathscr{S}_{l,m}$. If l is taken to be $\frac{1}{2}$, then the highest angular momentum state is

$$\begin{aligned}\mathscr{S}_{l,l} &= \mathscr{S}_{1/2,\,1/2}\\ &= A_{1/2}\cdot e^{i\cdot\phi/2}\cdot\sqrt{\sin\theta}.\end{aligned}$$

The lowering operator could be applied only once, but doing so gives, as per B.1.26

$$\begin{aligned}L_-\mathscr{S}_{l,l} &\propto e^{-i\cdot\phi}\left[-\frac{\partial}{\partial\theta}+i\cdot\cot\theta\frac{\partial}{\partial\phi}\right]\left(e^{i\cdot\phi/2}\sqrt{\sin\theta}\right)\\ &\propto e^{i\cdot\phi/2}\cot\theta\sqrt{\sin\theta},\end{aligned}$$

which is undefined for $\theta = 0$. Hence, only integer values are permitted for both l and m.

Having compiled, then, all the necessary pieces, the angular portion of the wavefunction is identified as the so-called spherical harmonics Y_l^m, which are defined

$$Y_l^m(\theta,\phi) \equiv (-1)^m P_l^m(\theta)e^{i\cdot m\phi}, \tag{B.1.31}$$

where P_l^m are the associated Legendre polynomials:

$$P_l^m(\theta) = \frac{(-1)^l}{l!\,2^l}\sqrt{\frac{(2l+1)(l+m)!}{4\pi(l-m)!}}\frac{1}{\sin^m\theta}\left[\frac{d}{d(\cos\theta)}\right]^{l-m}\left(\sin^{2l}\theta\right). \tag{B.1.32}$$

These spherical harmonics are simultaneous eigenfunctions of L^2 and L_z, and they have here been normalized so that

$$\langle Y_{l,m} | Y_{l',m'} \rangle = \delta_{ll'}\delta_{mm'}.$$

As stated previously, the restrictions imposed on m by l are such that m must be an integer between $-l$ and l. Further, the eigenvalues of both the square of the angular momentum operator (L^2) and the z-component of angular momentum (L_z) are known:

$$\begin{aligned} L^2 Y_{lm}(\theta,\phi) &= [l\,(l+1)]\, Y_{lm}(\theta,\phi) \\ L_z Y_{lm}(\theta,\phi) &= m Y_{lm}(\theta,\phi), \end{aligned} \tag{B.1.33}$$

which allows the radial portion of the wavefunction to be addressed.

B.2 The Radial Wavefunction

Of course, bound ($E < 0$) and continuum ($E > 0$) states need to be treated separately. To find the bound state solutions, it is most helpful to look at the asymptotic behavior of the radial wavefunction. For large r, the radial Schrödinger equation becomes

$$\lim_{r\to\infty}\left[\left(-\frac{1}{2}\frac{d^2}{dr^2} + \frac{l(l+1)}{2r^2} - \frac{Z}{r}\right)u(r) = Eu(r)\right]$$

$$-\frac{1}{2}\frac{d^2}{dr^2}u(r) = Eu(r).$$

Introducing a quantity λ such that $\lambda^2 = -2E$ (recall that $E < 0$) yields

$$\left(\frac{d^2}{dr^2} - \lambda^2\right)u(r) = 0,$$

so that in the limit of $r \to \infty$, the radial wavefunction looks like a decaying exponential:

$$\lim_{r\to\infty}\Big[u(r)\Big] \propto e^{-\lambda r}. \tag{B.2.1}$$

In the near limit ($r \to 0$), the wavefunction may be expanded as a polynomial in r

$$\lim_{r\to 0}\Big[u(r)\Big] \propto \begin{cases} r^{l+1} \\ r^{-l} \end{cases}$$

in the general case. It becomes quickly apparent that only the former expansion is valid if the wavefunction is to be finite at the origin. This means that the radial wavefunction takes on the form

$$u(r) = e^{-\lambda r} r^{l+1} f(r), \tag{B.2.2}$$

where $f(r)$ is an as-of-yet undetermined function of r. Inserting this functional form into 2.1.12 gives

$$\left(-\frac{1}{2}\frac{d^2}{dr^2} + \frac{l(l+1)}{2r^2} - \frac{Z}{r} \right) e^{-\lambda r} r^{l+1} f(r) = E e^{-\lambda r} r^{l+1} f(r). \tag{B.2.3}$$

The scaled quantity x is introduced such that $x \equiv 2\lambda r$, which allows B.2.3 to be written

$$\left(-\frac{1}{2} \cdot 4\lambda^2 \frac{d^2}{dx^2} + \frac{l(l+1)2\lambda^2}{x^2} - \frac{2\lambda Z}{x} - \frac{\lambda^2}{2} \right) \left[e^{-x/2} x^{l+1} f(x) \right] = 0.$$

One last set of scaled quantities comes into play

$$\begin{aligned} \lambda^2 &\equiv -2E \\ a &\equiv l + 1 - \frac{Z}{\lambda} \\ b &\equiv 2(l+1), \end{aligned} \tag{B.2.4}$$

and B.2.3 becomes

$$x\frac{d^2}{dx^2}\left[f(x) \right] + (b - x)\frac{d}{dx}\left[f(x) \right] - a f(x) = 0. \tag{B.2.5}$$

Equation B.2.5 is known as Kummer's equation, and it has solutions

$$f(x) = \begin{cases} {}_1F_1(a; b; x) \\ U(a, b, x) \end{cases} \tag{B.2.6}$$

where ${}_1F_1(a; b; x)$ and $U(a, b, x)$ are the confluent hypergeometric functions of the first and second kinds, respectively. The first of these behaves as a polynomial in x:

$${}_1F_1(a; b; x) = \sum_{k=0}^{\infty} \left(\frac{(a)_k}{(b)_k} \frac{x^k}{k!} \right),$$

where $(a)_k$ and $(b)_k$ are Pochhammer symbols

$$(a)_n \equiv \frac{\Gamma(a+n)}{\Gamma(a)}.$$

As such, ${}_1F_1$ is regular at the origin. In the asymptotic limit of $x \to \infty$, the confluent hypergeometric function behaves as an increasing exponential

$$\lim_{x\to\infty}\left[{}_1F_1(a;b;x)\right] = \frac{\Gamma(b)}{\Gamma(a)}e^x x^{a-b},$$

which is not conducive to physical wavefunctions, except in the case that the coefficient can be made to vanish, as well. The gamma function has no zeros, but it does diverge for non-positive integer arguments, i.e., $\Gamma(-n_r) \to \infty$. This quickly imposes a restriction on the arguments of ${}_1F_1$, namely

$$a = -n_r, \quad n_r \in \left\{\mathbb{Z}^-, 0\right\},$$

where n_r is the radial quantum number, which indicates the number of radial nodes in the wavefunction. Inserting the scaling definitions from B.2.4 gives

$$\begin{aligned} a &= -n_r \\ l+1-\frac{Z}{\lambda} &= -n_r \\ \lambda &= \frac{Z}{n_r+l+1}. \end{aligned} \tag{B.2.7}$$

A quantity n is defined so that $n \equiv n_r + l + 1$, allowing B.2.7 to be written in terms of a single quantum number n:

$$\lambda = \frac{Z}{n},$$

where n is known as the principle quantum number. Because λ is a scaling of the energy (B.2.4), this restriction dictates allowed energy values

$$\begin{aligned} E_n &= -\frac{\lambda_n^2}{2} \\ &= -\frac{Z^2}{2n^2}. \end{aligned}$$

This further places a restriction on the angular momentum in that there are exactly n degenerate wavefunctions for each energy E_n, these corresponding to angular momentum

quantum number values of

$$l \in \left\{ \mathbb{Z}^+, 0 : 0 \leq l \leq n-1 \right\}. \tag{B.2.8}$$

It bears mentioning that B.2.8 places a stronger restriction on l than an integer requirement, in that negative integer values are excluded.
The confluent hypergeometric function of the second kind can be expressed in terms of its counterpart

$$U(a,b,x) = \frac{\Gamma(1-b)}{\Gamma(a-b+1)} \left[{}_1F_1(a;b;x) \right] + \frac{\Gamma(b-1)}{\Gamma(a)} x^{1-b} \left[{}_1F_1(a-b+1;2-b;x) \right], \tag{B.2.9}$$

which is, except in very specific cases, irregular at the origin. This irregularity causes $U(a,b,x)$ to be rejected as contributing to any bound radial wavefunction that extends to the origin, though it is kept as a second, linearly independent solution to B.2.5.

It is prudent, at this point, to mention that a scenario exists for which these two solutions are *not* linearly independent. The function $U(a,b,x)$ is written in terms of ${}_1F_1(a;b;x)$ by equation B.2.9 in such a way that the two are linearly independent so long as $b \neq 1$. This can be seen quickly by inspecting B.2.9 and examining the consequences of supposing exactly this condition. The exponent on x in the second term vanishes, and the arguments of the instances of ${}_1F_1$ become identical, i.e.,

$$\begin{aligned} a &= a - b + 1 \\ b &= 2 - b, \end{aligned}$$

so that

$$\begin{aligned} U(a,1,x) &= \left(\frac{\Gamma(0)}{\Gamma(a)} \right) {}_1F_1(a;1;x) + \left(\frac{\Gamma(0)}{\Gamma(a)} \right) {}_1F_1(a;1;x) \\ &= 2 \left(\frac{\Gamma(0)}{\Gamma(a)} \right) {}_1F_1(a;1;x), \end{aligned}$$

which would be problematic even if $\Gamma(0)$ did not diverge. However, to reach this result, it must be the case that $l = -1/2$, which, as was stated previously, is a scenario that is ruled out by angular momentum restrictions.

Thus, the radial wavefunction for the bound states of the Coulomb potential, as per

equations 2.1.7, B.2.2, B.2.4,and B.2.6, is

$$\begin{aligned}\mathscr{R}(r) &= r \cdot u(r) \\ &= N_{nl} \left(\frac{2Zr}{n}\right)^{l+1} e^{-Zr/n} \left[{}_1F_1\left((-n+l+1);(2l+2);(2Zr/n)\right)\right], \end{aligned} \tag{B.2.10}$$

where N_{nl} is a normalization constant.

B.3 Normalizing the Wavefunction

With the radial wavefunction individually normalized, N_{nl} may be determined by normalizing the radial wavefunction alone:

$$\begin{aligned}1 &= \int_{r=0}^{\infty} \left(\frac{u(r)}{r}\right)^* \left(\frac{u(r)}{r}\right) \cdot r^2 dr \\ &= |N_{nl}|^2 \int_{r=0}^{\infty} \left(\left(\frac{2Zr}{n}\right)^{2l+2} e^{-2Zr/n} \left[{}_1F_1\left((-n+l+1);(2l+2);\frac{2Zr}{n}\right)\right]^2 \right) dr.\end{aligned}$$

The integral may be evaluated analytically to give

$$\begin{aligned}1 &= |N_{nl}|^2 \left(n \cdot \Gamma(2l+2)\right)^2 \frac{\Gamma(n-l)}{Z\Gamma(n+l+1)} \\ N_{nl} &= \frac{1}{n \cdot \Gamma(2l+2)} \sqrt{\frac{Z \cdot \Gamma(n+l+1)}{\Gamma(n-l)}}. \end{aligned} \tag{B.3.1}$$

Finally, with both the radial and angular portions of the wavefunction determined, the total electronic wavefunction is found by compiling equations B.3.1 and B.2.10, along with the properties of the spherical harmonics:

$$\psi_{nlm}(r,\theta,\phi) = A_{nlm} \cdot \frac{1}{\sin^m\theta} \left(\frac{2Zr}{n}\right)^{l+1} e^{-Zr/n} {}_1F_1(a;b;2\lambda r) \left[\frac{d}{d(\cos\theta)}\right]^{l-m} \left(\sin^{2l}\theta\right), \tag{B.3.2}$$

where

$$
\begin{aligned}
A_{nlm} &= \frac{(-1)^m}{n \cdot l! \cdot 2^l \cdot \Gamma(2l+2)} \sqrt{\frac{Z \cdot \Gamma(n+l+1) \cdot (2l+1)(l+m)!}{4\pi(l-m)! \cdot \Gamma(n-l)}} \\
a &= l + 1 - \frac{Z}{\lambda} \\
b &= 2(l+1) \\
\lambda^2 &= -2E.
\end{aligned}
\tag{B.3.3}
$$

Thus the total wavefunction for an electron in a bare Coulomb potential is parameterized by three quantum numbers, n, l, and m. The energy of the state is determined by the principle quantum number n, the total angular momentum by the angular momentum quantum number l, and the z-component of angular momentum, and thereby the orientation of the atomic orbital, by the magnetic quantum number m.

C

R-Matrix: A Simple Example

Prior to beginning work on the photoionization of N_2, it was particularly beneficial to consider a simple, single-channel illustration of the R-matrix method. An electron is subject to a long-range Coulomb potential. Within this Coulomb field, let there exist a step function of magnitude V_0, so that the total potential total potential, in atomic units, is given by

$$V(r) = -\frac{Z}{r} + V_{step}(r), \tag{C.1.1}$$

where Z is the charge of the nucleus producing the Coulombic field, and V_{step} is the step function

$$V_{step}(r) = \begin{cases} -V_0 & r < a \\ 0 & r > a \end{cases} \tag{C.1.2}$$

with $r = a$ demarking the radius of the potential "box." The Hamiltonian, then, is

$$\hat{\mathscr{H}} = -\frac{1}{2}\vec{\nabla}^2 - \frac{Z}{r} + V_{step}(r),$$

so that the Schrödinger equation reads

$$\left[-\frac{1}{2}\vec{\nabla}^2 - \frac{Z}{r} + V_{step}(r) - E\right]\psi(r) = 0. \tag{C.1.3}$$

As in Section 2.1, this potential is spherically symmetric, so that the angular portion of the electron's wavefunction will be manifest in spherical harmonics $Y_{lm}(\theta, \phi)$. The angular momentum is incorporated into the radial Schrödinger equation , so that C.1.3 is written in the same way as 2.1.12 and 2.1.13, except that the additional potential "step" must be included. This suggests a natural separation of space into an inner region $(r < a)$, in which the potential "step" has effect, and an outer region $(r > a)$, in which it does not.

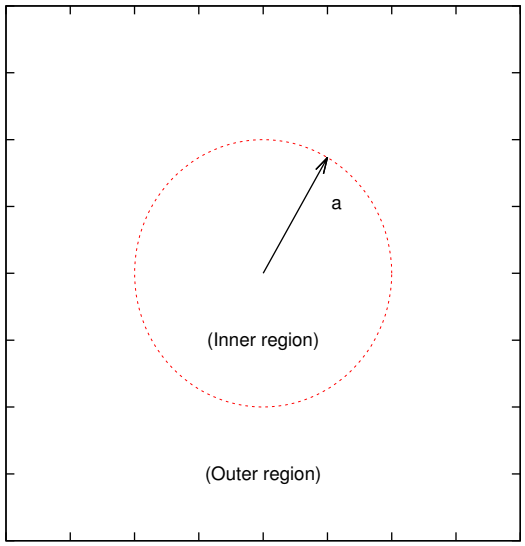

Figure C.1.1: The inner and outer regions. The electron experiences a different potential in different regions of space. The discontinuity in the potential, as given by C.1.2 and shown in Figure C.1.2, provides a natural division of space into an inner region and an outer region.

After having separated variables, the angular momentum contribution adds a centrifugal barrier term $V_{\text{(centrifugal)}}$ for all nonzero angular momentum states, so that an effective potential $V_{eff}(r)$ may be defined

$$\begin{aligned} V_{eff}(r) &\equiv V(r) + V_{\text{(centrifugal)}} \\ &= V(r) + \frac{l(l+1)}{2r^2}. \end{aligned} \tag{C.1.4}$$

This total effective potential is shown in Figure C.1.2.

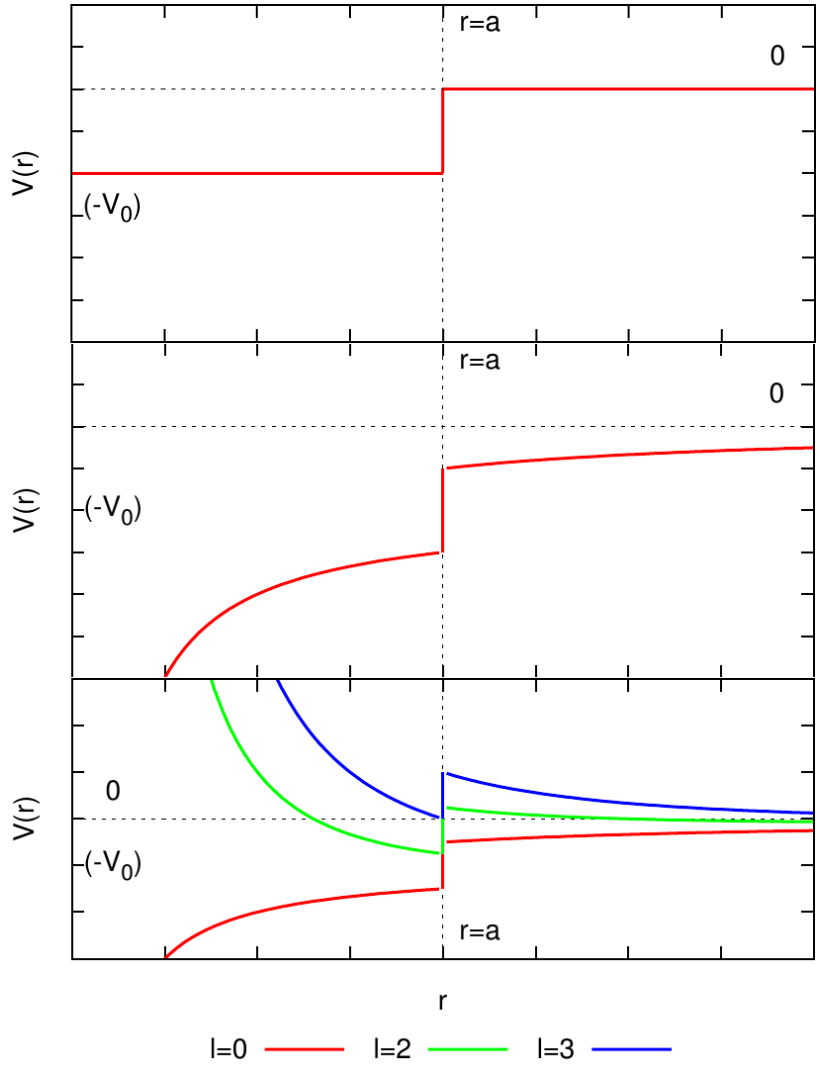

Figure C.1.2: A spherical square well in a Coulomb potential. Top: The simple potential step function V_{step} from C.1.2. Middle: The total potential $V(r)$ from C.1.1 with no angular momentum. Note the discontinuity at $r = a$. Bottom: The total effective potential $V_{eff}(r)$ for angular momentum quantum numbers $l = 0$, $l = 2$, and $l = 3$, as shown in C.1.4. Note that the centrifugal barrier is absent for $l = 0$.

Again as in Section 2.1, the solutions to C.1.3 are the regular and irregular Coulomb functions from 2.1.14

$$u(r, E) = a_l \cdot S_l(\eta, \rho) + b_l \cdot C_l(\eta, \rho)$$

with scaled quantities

$$\begin{aligned} \rho &\equiv \sqrt{2E} \cdot r \\ \eta &\equiv \frac{Z}{\sqrt{2E}}. \end{aligned} \tag{C.1.5}$$

Boundary conditions dictate that the wavefunction must vanish at the origin, i.e.,

$$\lim_{r \to 0} \Big[u(r, E) \Big] = 0,$$

so that only the regular Coulomb function $S_l(\eta, \rho)$ may contribute to the wavefunction in the inner region. In the outer region, however, there is no such restriction, so that the outer region wavefunction is, in general, a linear combination of regular and irregular Coulomb functions

$$\begin{aligned} u_{(in)}(r, E) &= a_l^{(in)} \cdot S_l(\eta_{(in)}, \rho_{(in)}) \\ u_{(out)}(r, E) &= a_l^{(out)} \cdot S_l(\eta_{(out)}, \rho_{(out)}) + b_l^{(out)} \cdot C_l(\eta_{(out)}, \rho_{(out)}) \end{aligned} \tag{C.1.6}$$

The difference between this square well problem and the Coulomb scattering problem discussed in Section 2.1, then, is not in the form of the solutions, but in the scaled quantities ρ and η. In the outer region, these quantities remain unchanged, but in the inner region, where the potential has been lowered by V_0, the energy in C.1.5 is replaced by $E + V_0$, so that the scaling quantities differ by region, as shown in the table.

Inner region	Outer region
$\rho^{(in)} = \sqrt{2(E + V_0)r}$	$\rho^{(out)} = \sqrt{2Er}$
$\eta^{(in)} = \dfrac{Z}{\sqrt{2(E + V_0)}}$	$\eta^{(out)} = \dfrac{Z}{\sqrt{2E}}$

The task, now, is to match the logarithmic derivative of the inner region wavefunction $u_{(in)}$ to that of the outer region wavefunction $u_{(out)}$ at the boundary $r = a$. While this can be done by adjusting the parameters a_l and b_l, these coefficients offer very little

insight. Instead, the wavefunctions may be rewritten so as to give more meaning to the coefficients. Defining the quantities k and κ such that

$$\begin{aligned} k &\equiv \sqrt{2E} \cdot r \\ \kappa &\equiv \sqrt{2(E+V_0)} \cdot r, \end{aligned}$$

a shorthand notation may be adopted

$$\begin{aligned} S_l(\kappa r) &\equiv S_l\left(\eta_{(in)}, \rho_{(in)}\right) \\ S_l(kr) &\equiv S_l\left(\eta_{(out)}, \rho_{(out)}\right), \end{aligned}$$

as carrying the explicit arguments will otherwise become rather cumbersome. The inner and outer region wavefunctions, then, are

$$\begin{aligned} u^{(in)} &= d_l S_l(\kappa r) \\ u^{(out)} &= a_l S_l(kr) + b_l C_l(kr). \end{aligned}$$

The outer region wavefunction may be expressed in terms of a phase shift δ_l

$$\begin{aligned} u^{(out)} &= a_l S_l(kr) + b_l C_l(kr) \\ &= [\cos\delta_l]\, S_l(kr) + [\sin\delta_l]\, C_l(kr). \end{aligned}$$

This allows the wavefunction to be matched by varying the amplitude d_l of the inner region function, and the phase shift δ_l of the outer region wavefunction, as shown in Figure C.1.3. The matching process is performed by means of the R-matrix. The R-matrix is defined as the logarithmic derivative of the inner region wavefunction, and evaluated at the boundary

$$\begin{aligned} \underline{\underline{\mathbf{R}}}(a) &\equiv \frac{u(\kappa a)}{u'(\kappa a)} \\ &= \frac{S_l(\kappa a)}{\kappa S_l'(\kappa a)}. \end{aligned} \tag{C.1.7}$$

While expressed as a matrix in C.1.7, for this single-channel problem, the R-matrix consists of a single element, i.e., is a 1×1 matrix.

The outer region wavefunction may then be matched to the R-matrix at the boundary

$$\begin{aligned}\underline{\underline{\mathbf{R}}}(a) &= \frac{u(ka)}{u'(ka)} \\ &= \frac{[\cos\delta_l]\, S_l(ka) + [\sin\delta_l]\, C_l(ka)}{k\left([\cos\delta_l]\, S_l'(ka) + [\sin\delta_l]\, C_l'(ka)\right)}.\end{aligned}$$

This may be equivalently written

$$\underline{\underline{\mathbf{R}}}(a) = \frac{S_l(ka) + [\tan\delta_l]\, C_l(ka)}{k\left(S_l'(ka) + [\tan\delta_l]\, C_l'(ka)\right)}, \tag{C.1.8}$$

a form which lends itself to applications to more complex problems. The tangent of the phase shift, as it appears in C.1.8, is, strictly speaking, the reactance matrix $\underline{\underline{\mathbf{K}}}$ for this single-channel problem, though be it a 1×1 matrix

$$\underline{\underline{\mathbf{K}}} = \tan\delta_l. \tag{C.1.9}$$

Finally, the cross section may be found from this phase shift

$$\sigma_l = \frac{1}{k^2}\left(\frac{4\pi}{2l+1}\right)\sin^2\delta_l. \tag{C.1.10}$$

The matching process is illustrated in Figures C.1.3 and C.1.4 for several potential well depths and angular momentum quantum numbers.

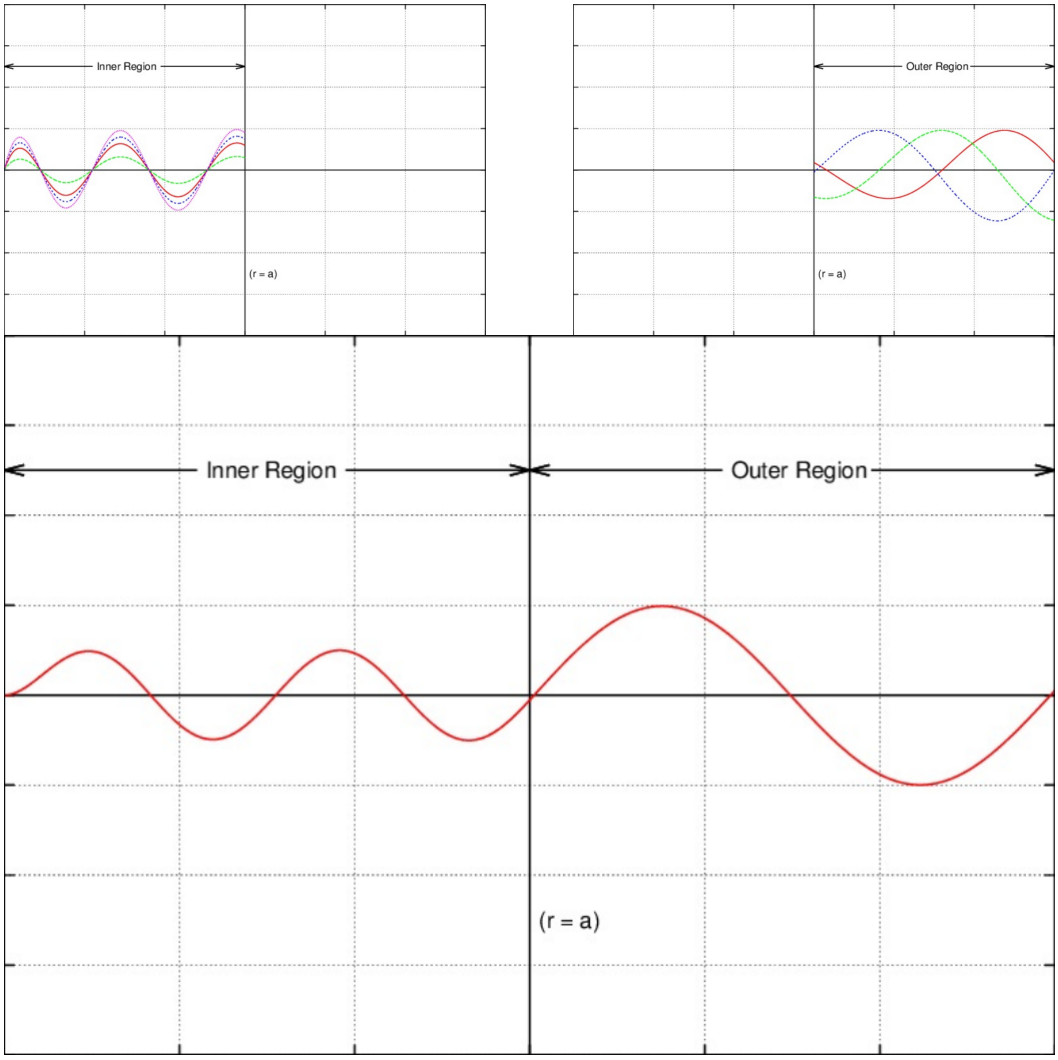

Figure C.1.3: Matching the inner and outer regions. The amplitude d_l of the inner region wavefunction, and the phase shift δ_l of the outer region wavefunction are varied so that the wavefunction and its spatial derivative are continuous at the boundary $r = a$.

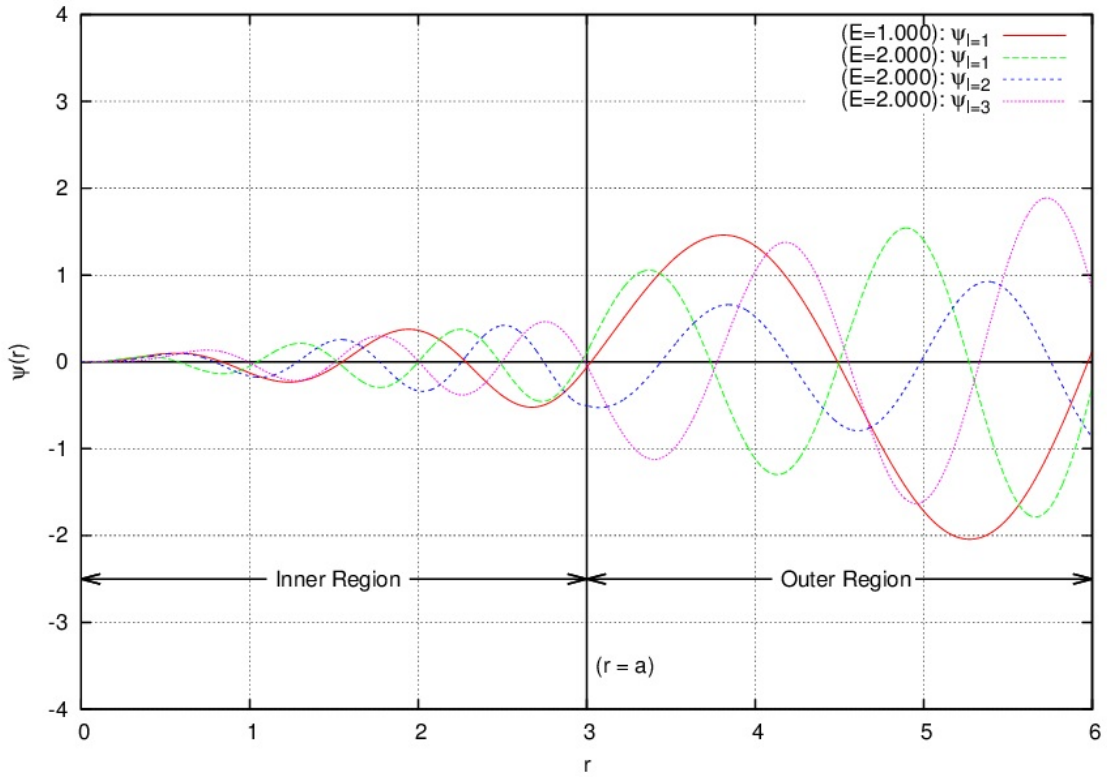

Figure C.1.4: The (unnormalized) wavefunction $\psi = r \cdot u(r)$ for varying parameters. The full radial wavefunction is plotted for two energies: $E = 1.00\ a.u.$ and $E = 2.00\ a.u.$, as well as for three different angular momentum values $l = 1$, $l = 2$, and $l = 3$. The square well "step" is set at $V_0 = 3.0\ a.u.$, and the well width is set at $a = 3.0$ bohr.

Finally, the photoabsorption cross section is shown for several angular momentum values in Figure C.1.5, showing a shape resonance that shifts toward higher energies for larger angular momenta.

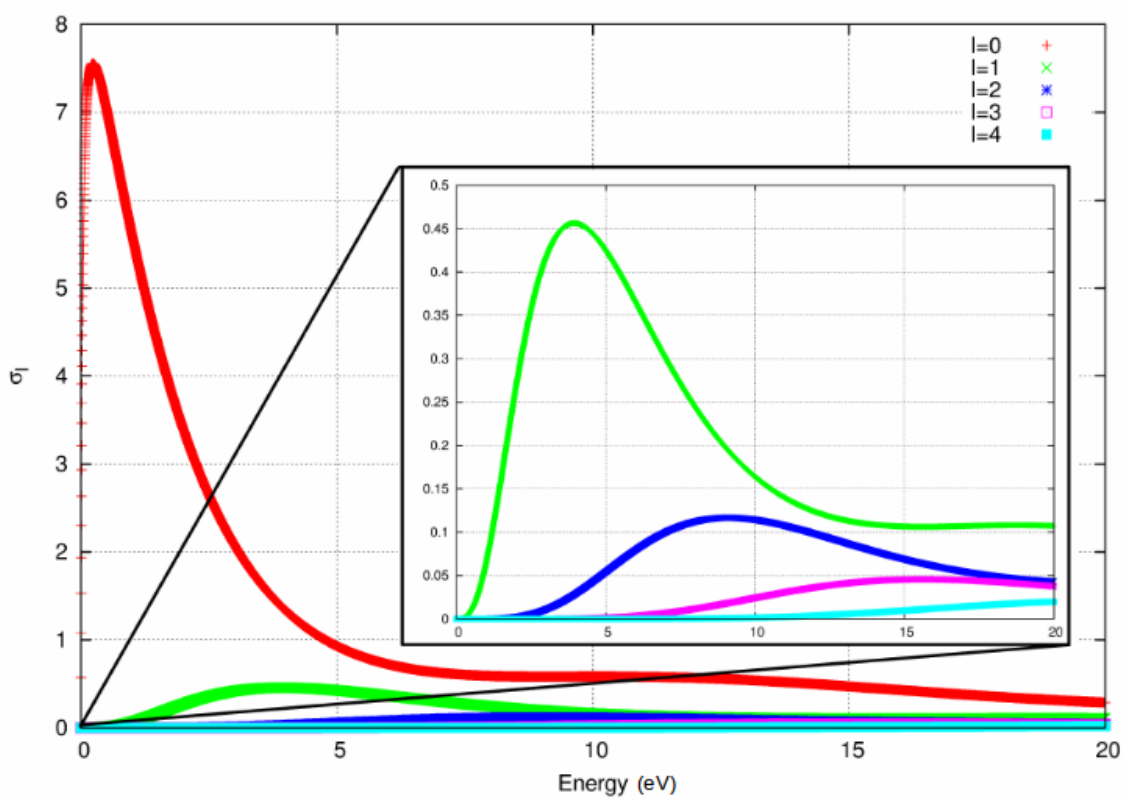

Figure C.1.5: Photoabsorption cross section for the spherical square well. The photoabsorption cross section is shown for several angular momenta. The indicated region is expanded for nonzero angular momentum waves, and a shape resonance may be seen shifting toward higher energies for larger angular momentum values.

D

The Morse Potential: A Derivation

As stated in Section 2.11.2, the Morse potential is given by 2.11.4 and reproduced here:

$$\begin{aligned} V(R) &= D\left(\left(1-e^{-\alpha(R-Req)/R_{eq}}\right)^2-1\right) \\ &= D\left(e^{-2\alpha(R-Req)/R_{eq}}-2e^{-\alpha(R-Req)/R_{eq}}\right), \end{aligned}$$

so that the one-dimensional, time-independent Schrödinger equation for the vibrational wavefunctions , in atomic units, is

$$\left(-\frac{1}{2m}\frac{\partial^2}{\partial R^2}+V(R)\right)\chi = E\chi,$$

where, again, χ are the radial wavefunctions.

Eigenfunctions

A scaling in the spatial coordinate is adopted, so that

$$x \equiv \frac{R-R_{eq}}{R_{eq}}. \tag{D.1.1}$$

The Schrödinger equation (2.11.5) then becomes

$$\left[-\frac{1}{2\mu R_{eq}^2}\frac{\partial^2}{\partial x^2} + D\left(e^{-2\alpha x} - 2e^{-\alpha x}\right) - E\right]\chi = 0$$
$$\left[\frac{\partial^2}{\partial x^2} - 2mR_{eq}^2 D\left(e^{-2\alpha x} - 2e^{-\alpha x}\right) + 2mR_{eq}^2 E\right]\chi = 0. \tag{D.1.2}$$

The form of D.1.2 suggests a set of energy scalings

$$\gamma^2 \equiv 2mR_{eq}^2 D$$
$$\beta^2 \equiv -2mR_{eq}^2 E. \tag{D.1.3}$$

For separation distances in the vicinity of R_{eq}, the nuclei exhibit vibrational energy levels that fall far short of the dissociation energy. These states are bound, i.e., $E < 0$, so that $\beta^2 > 0$, and β is real. With D.1.3, the Hamiltonian D.1.2 is written

$$\left[\frac{\partial^2}{\partial x^2} - \gamma^2\left(e^{-2\alpha x} - 2e^{-\alpha x}\right) - \beta^2\right]\chi = 0. \tag{D.1.4}$$

Again, a substitution is suggested by the form of the Hamiltonian. The natural choice is to introduce a scaled quantity z such that

$$z \equiv e^{-\alpha x}. \tag{D.1.5}$$

Inserting z into D.1.4 yields

$$\left[\alpha^2 z^2\frac{\partial^2}{\partial z^2} + \alpha^2 z\frac{\partial}{\partial z} - \gamma^2 z^2 + 2\gamma^2 z - \beta^2\right]\chi = 0$$
$$\left[z^2\frac{\partial^2}{\partial z^2} + z\frac{\partial}{\partial z} - \frac{\gamma^2}{\alpha^2}z^2 + \frac{2\gamma^2}{\alpha^2}z - \frac{\beta^2}{\alpha^2}\right]\chi = 0,$$

which is further simplified with the additional scaling

$$y \equiv \frac{2\gamma}{\alpha}z \tag{D.1.6}$$

to read

$$\left[y^2\frac{\partial^2}{\partial y^2} + y\frac{\partial}{\partial y} - \frac{1}{4}y^2 + \frac{\gamma}{\alpha}y - \frac{\beta^2}{\alpha^2}\right]\chi = 0$$
$$\left[\frac{\partial^2}{\partial y^2} + \frac{1}{y}\frac{\partial}{\partial y} - \frac{1}{4} + \frac{\gamma}{\alpha}\frac{1}{y} - \frac{\beta^2}{\alpha^2}\frac{1}{y^2}\right]\chi = 0. \tag{D.1.7}$$

As with the treatment of the Coulomb potential, the asymptotic behavior of this differential equation is inspected. The large-y behavior is extracted first:

$$\lim_{y\to\infty}\Big[(D.1.7)\Big] = \left(\frac{\partial^2}{\partial y^2} - \frac{1}{4}\right)\chi = 0$$
$$\left[\frac{\partial^2}{\partial y^2} - \left(\frac{1}{2}\right)^2\right]\chi = 0,$$

which gives solutions of

$$\lim_{y\to\infty}\Big[\chi\Big] = Ae^{-y/2} + Be^{+y/2}.$$

Because the wavefunction must vanish for $y \to \infty$, the increasing exponential must not contribute, so that

$$\lim_{y\to\infty}\Big[\chi\Big] \sim e^{-y/2}. \tag{D.1.8}$$

The small-y behavior is considered next. Near $y = 0$, the wavefunction is expanded in a polynomial series in y. Only the leading term survives, leaving:

$$\lim_{y\to 0}\Big[(D.1.7)\Big] = \left[y^2\frac{\partial^2}{\partial y^2} + y\frac{\partial}{\partial y} - \frac{\beta^2}{\alpha^2}\right]\chi = 0,$$

again giving two possible solutions

$$\lim_{y\to 0}\Big[\chi = Ay^{-\beta/\alpha} + By^{+\beta/\alpha}\Big].$$

For small y, however, it is the first term that must not contribute, so that the asymptotic behavior of χ is

$$\lim_{y\to 0}\Big[\chi\Big] \sim y^{+\beta/\alpha}. \tag{D.1.9}$$

Having secured the form of χ at both limits, D.1.8 and D.1.9 are combined to construct a functional form for the wavefunction

$$\chi = y^{\beta/\alpha}e^{-y/2}f(y), \tag{D.1.10}$$

where $f(y)$ is an unknown function of y. Note that, at this point, a choice is made to leave χ unnormalized, a situation which will later be remedied. It remains, then, to find

$f(y)$. The general form of χ presented in D.1.10 is used in D.1.7

$$\left[\frac{\partial^2}{\partial y^2} + \frac{1}{y}\frac{\partial}{\partial y} - \frac{1}{4} + \frac{\gamma}{\alpha}\frac{1}{y} - \frac{\beta^2}{\alpha^2}\frac{1}{y^2}\right]\left(y^{\beta/\alpha}e^{-y/2}f(y)\right) = 0. \tag{D.1.11}$$

It will become rather cumbersome to carry out the following procedure as written, so a more concise notation will be used

$$\begin{aligned} f &\equiv f(y) \\ \lambda &\equiv \frac{\beta}{\alpha}. \end{aligned} \tag{D.1.12}$$

Using these, D.1.11 becomes

$$\left[\frac{\partial^2}{\partial y^2} + \frac{1}{y}\frac{\partial}{\partial y} - \frac{1}{4} + \frac{\gamma}{\alpha}\frac{1}{y} - \lambda^2\frac{1}{y^2}\right]\left(y^{\lambda}e^{-y/2}f\right) = 0. \tag{D.1.13}$$

The derivatives are quite straightforward, if tedious. The resulting expression is

$$\left[y\frac{\partial^2}{\partial y^2} + (2\lambda + 1 - y)\frac{\partial}{\partial y} - \left(\lambda + \frac{1}{2} - \frac{\gamma}{\alpha}\right)\right] f = 0, \tag{D.1.14}$$

which, with a final set of substitutions

$$\begin{aligned} c &\equiv 2\lambda + 1 \\ a &\equiv \lambda + \frac{1}{2} - \frac{\gamma}{\alpha} \end{aligned} \tag{D.1.15}$$

takes a seemingly simple form

$$y\frac{\partial^2}{\partial y^2}f + (c - y)\frac{\partial}{\partial y}f - af = 0. \tag{D.1.16}$$

This form is exactly the same as B.2.5, which was previously encountered during the analysis of the Coulomb potential, and has the confluent hypergeometric functions ${}_1F_1(a; c; y)$ and $U(a, c, y)$ as its solutions. Once again, the confluent hypergeometric function of the second kind $U(a, c, y)$ is unphysical at the origin. Compiling the confluent hypergeometric functions with equation D.1.10 gives an unnormalized vibrational wavefunction

$$\chi(y) = y^{\lambda}e^{-y/2}{}_1F_1(a; c; y), \tag{D.1.17}$$

where the scaling factors are retraced through equations D.1.15,D.1.12, D.1.6, D.1.5, D.1.3, D.1.1, and 2.11.6.

Energies

As with the Coulomb potential solutions discussed in Section 2.1.2, there is a restriction imposed on a so that the wavefunction does not diverge for large y

$$a = -n_y.$$

Following the scaling factors from D.1.15, D.1.13, and D.1.3, this introduces a quantization of the energy levels

$$\begin{aligned} a &= -n_y \\ \lambda + \frac{1}{2} - \frac{\gamma}{\alpha} &= -n_y \\ \frac{\beta}{\alpha} + \frac{1}{2} - \frac{\gamma}{\alpha} &= -n_y \\ \frac{\sqrt{-2mR_{eq}^2 E}}{\alpha} + \frac{1}{2} - \frac{\sqrt{2mR_{eq}^2 D}}{\alpha} &= -n_y, \end{aligned} \tag{D.1.18}$$

so that

$$\begin{aligned} E &= -\frac{\left[\sqrt{2mR_{eq}^2 D} - \left(n_y + \frac{1}{2}\right)\alpha\right]^2}{2mR_{eq}^2} \\ &= D\left[2b\left(n_y + \frac{1}{2}\right) - b^2\left(n_y + \frac{1}{2}\right)^2 - 1\right], \end{aligned} \tag{D.1.19}$$

with

$$b \equiv \frac{\alpha}{\sqrt{2mR_{eq}^2 D}}. \tag{D.1.20}$$

These energy levels become more dense for increasing n_y, but there is a limit beyond which the model breaks down. The Morse potential has a finite number of bound states, which is, of course, inconsistent with actual molecular dynamics. However, for low-lying energy states, i.e., near-equilibrium internuclear separation, the energies predicted by the Morse potential are a good approximation.

Normalizing the Wavefunctions

Finally, it remains to normalize the Morse wavefunctions. The form of the wavefunction D.1.17 is very like that of the Coulomb wavefunction (B.2.10), and this similarity may be exploited to determine the normalization constant. While this form is convenient for normalizing, the wavefunction is typically expressed in terms of the generalized Laguerre polynomials. These are related to the confluent hypergeometric functions by

$$L_n^k(x) = \frac{\Gamma(k+n+1)}{\Gamma(n+1)\Gamma(k+1)} {}_1F_1(-n, k+1, x).$$

Since the vibrational wavefunctions are, to this point, unnormalized, the proportionality D.1.17 may be written

$$\chi(y) = y^\lambda e^{-y/2} L_n^{2\lambda}(y), \tag{D.1.21}$$

where $L_n^{2\lambda}(y)$ are the generalized Laguerre polynomials

$$L_n^{2\lambda}(y) \equiv \frac{1}{n!} \sum_{i=0}^{n} \left[\frac{n!}{i!} \binom{2\lambda+n}{n-i} (-y)^i \right], \tag{D.1.22}$$

with the binomial coefficient

$$\binom{2\lambda+n}{n-i} \equiv {}_{(2\lambda+n)}C_{(n-i)} \equiv \frac{(2\lambda+n)!}{(2\lambda+i)\,!\,(n-i)\,!}.$$

This gives a total, normalized wavefunction of

$$\chi_n(y) = \sqrt{\frac{n!\,(2\lambda)!}{\Gamma\,(2\lambda+n+1)}} \cdot y^\lambda e^{-y/2} L_n^{2\lambda}(y). \tag{D.1.23}$$

The subscript n in D.1.23 is understood to be the n_y from D.1.18 in the previous section, and the scaled quantities are as defined in the previous sections

$$\begin{aligned}
\gamma^2 &\equiv 2mR_{eq}^2 D \\
\beta^2 &\equiv -2mR_{eq}^2 E \\
\lambda &\equiv \frac{\beta}{\alpha} \\
y &\equiv \left(\frac{2\gamma}{\alpha}\right) e^{-\alpha(R-R_{eq})/R_{eq}} \\
-n &\equiv \lambda + \frac{1}{2} - \frac{\gamma}{\alpha}.
\end{aligned}$$

References

[1] M. Born and R. Oppenheimer, Annalen der Physik **389**, 457–484 (1927).

[2] B. Bransden and C. Joachain, *Physics of atoms and molecules*, Pearson Education (Longman, 1983).

[3] J. Tennyson, Journal of Physics B Atomic Molecular Physics **19**, 4255–4263December (1986).

[4] J. Tennyson and C. J. Noble, Journal of Physics B Atomic Molecular Physics **19**, 4025–4033December (1986).

[5] C. J. Gillan, P. G. Burke, O. Nagy, L. A. Morgan, and C. J. Noble, Journal of Physics B Atomic Molecular Physics **20**, 4585–4603September (1987).

[6] C. J. Gillan, C. J. Noble, and P. G. Burke, Journal of Physics B Atomic Molecular Physics **21**, L53–L59February (1988).

[7] C. J. Gillan, P. G. Burke, and C. J. Noble, Journal of Physics B Atomic Molecular Physics **23**, L407–L413August (1990).

[8] P. G. Burke, *R-Matrix Theory of Atomic Collisions: Application to Atomic, Molecular and Optical Processes, Springer Series on Atomic, Optical, and Plasma Physics, Volume 61. ISBN 978-3-642-15930-5. Springer-Verlag Berlin Heidelberg, 2011* (2011).

[9] M. Tashiro, J. Chem. Phys. **132**, p. 134306April (2010), arXiv:1003.2261 [physics.chem-ph] .

[10] C. Greene, U. Fano, and G. Strinati, Phys. Rev. A **19**, 1485–1509April (1979).

[11] C. H. Greene, A. R. P. Rau, and U. Fano, Phys. Rev. A **26**, 2441–2459November (1982).

[12] M. J. Seaton, Reports on Progress in Physics **46**, 167–257February (1983).

[13] P. O'Keeffe, P. Bolognesi, A. Moise, R. Richter, Y. Ovcharenko, and L. Avaldi, J. Chem. Phys. **136**, p. 104307March (2012).

[14] A. Heays, (2015), unpublished Soleil data (private communication).

[15] A. Lofthus and P. H. Krupenie, Journal of Physical and Chemical Reference Data **6**, 113–307January (1977).

[16] X. Li and J. Paldus, J. Chem. Phys. **129**, 054104–054104August (2008).

[17] K. P. Huber and C. Jungen, J. Chem. Phys. **92**, 850–861January (1990).

[18] C. Jungen, K. P. Huber, M. Jungen, and G. Stark, J. Chem. Phys. **118**, 4517–4538March (2003).

[19] P. L. Kapur and R. Peierls, Proceedings of the Royal Society of London Series A **166**, 277–295May (1938).

[20] E. P. Wigner and L. Eisenbud, Physical Review **72**, 29–41July (1947).

[21] A. M. Lane and R. G. Thomas, Reviews of Modern Physics **30**, 257–353April (1958).

[22] C. Bloch, Nuc. Phys. A **4**, 503–528November (1957).

[23] M. E. Haglund and D. Robson, Physics Letters **14**, 225–227February (1965).

[24] P. J. Buttle, Physical Review **160**, 719–729August (1967).

[25] P. Descouvemont and D. Baye, Reports on Progress in Physics **73**, p. 036301March (2010), arXiv:1001.0678 [nucl-th] .

[26] C. H. Greene, Phys. Rev. A **28**, 2209–2216October (1983).

[27] C. H. Greene, Phys. Rev. A **32**, 1880–1882September (1985).

[28] C. H. Greene and L. Kim, Phys. Rev. A **38**, 5953–5956December (1988).

[29] U. Fano, Physical Review **124**, 1866–1878December (1961).

[30] J. W. Cooper, U. Fano, and F. Prats, Physical Review Letters **10**, 518–521June (1963).

[31] P. G. Burke, A. Hibbert, and W. D. Robb, Journal of Physics B Atomic Molecular Physics **4**, 153–161February (1971).

[32] P. G. Burke, Advances in Atomic and Molecular Physics **4**, 173–219 (1968).

[33] P. G. Burke, Computational Physics (Inst. Phys. and Phys. Soc., London p. 9 (1970).

[34] P. G. Burke, Comm. At. Mol. Phys. **4**, p. 157 (1973).

[35] P. G. Burke, Comput. Phys. Commun. **6**, p. 288 (1974).

[36] P. G. Burke, *Potential Scattering in Atomic Physics* (Plenum Press, New York, NY and London, 1977).

[37] D. C. S. Allison, P. G. Burke, and W. D. Robb, Journal of Physics B Atomic Molecular Physics **5**, 55–65January (1972).

[38] D. C. S. Allison, P. G. Burke, and W. D. Robb, Journal of Physics B Atomic Molecular Physics **5**, 1431–1438August (1972).

[39] W. D. Robb, Journal of Physics B Atomic Molecular Physics **6**, 945–953June (1973).

[40] P. G. Burke and K. T. Taylor, Journal of Physics B Atomic Molecular Physics **8**, 2620–2639November (1975).

[41] B. Schneider, Chemical Physics Letters **31**, 237–241March (1975).

[42] B. I. Schneider, Phys. Rev. A **11**, 1957–1962June (1975).

[43] B. I. Schneider and P. J. Hay, Phys. Rev. A **13**, 2049–2056June (1976).

[44] P. G. Burke, I. Mackey, and I. Shimamura, Journal of Physics B Atomic Molecular Physics **10**, 2497–2512August (1977).

[45] R. F. Barrett, B. A. Robson, and W. Tobocman, Reviews of Modern Physics **55**, 155–243January (1983).

[46] M. Aymar, C. H. Greene, and E. Luc-Koenig, Reviews of Modern Physics **68**, 1015–1123October (1996).

[47] P. G. Burke and W. D. Robb, Advances in Atomic and Molecular Physics **11**, 143–214 (1976).

[48] J. R. Rydberg, K. Svenska Vetenskaps Akad. Handlinger **23**, 1–155 (1890).

[49] M. J. Seaton, C.R. Acad. Sci., Paris **240**, 1317–1318 (1955).

[50] M. J. Seaton, Mon. Not. R. Astr. Soc. **118**, p. 504 (1958).

[51] M. J. Seaton, Reviews of Modern Physics **30**, 979–991July (1958).

[52] M. J. Seaton, Proceedings of the Physical Society **88**, 801–814August (1966).

[53] Physics Today **41**, p. 120 (1988).

[54] D. R. Hartree, Proceedings of the Cambridge Philosophical Society **24**, p. 89 (1928).

[55] D. R. Hartree, Proceedings of the Cambridge Philosophical Society **24**, p. 111 (1928).

[56] D. R. Hartree, Proceedings of the Cambridge Philosophical Society **24**, p. 426 (1928).

[57] D. R. Hartree, Proceedings of the Cambridge Philosophical Society **25**, p. 310 (1929).

[58] F. S. Ham (Academic Press, 1955), pp. 127 – 192.

[59] A. Burgess and M. J. Seaton, Mon. Not. R. Astr. Soc. **120**, p. 121 (1960).

[60] M. H. Ross and G. L. Shaw, Annals of Physics **13**, 147–186May (1961).

[61] M. Gailitis, Soviet Physics-JETP **17**, 1328–1332 (1963).

[62] O. Bely, D. Moores, and M. J. Seaton, "Many-channel quantum defect theory," in *Atomic Collision Processes*, edited by M. R. C. McDowell (1964) p. 304.

[63] U. Fano, Phys. Rev. A **2**, 353–365August (1970).

[64] U. Fano, Journal of the Optical Society of America **65**, 979–987 (1975).

[65] O. Atabek and C. Jungen, "Quantum Defect Theory of Excited $^1\Sigma^+{}_u$ Levels of H_2," in *Electron and Photon Interactions with Atoms*, edited by H. Kleinpoppen and M. R. C. McDowell (1976) p. 613.

[66] C. Jungen and O. Atabek, J. Chem. Phys. **66**, 5584–5609June (1977).

[67] O. Atabek, D. Dill, and C. Jungen, Physical Review Letters **33**, 123–126July (1974).

[68] P. M. Dehmer and W. A. Chupka, J. Chem. Phys. **65**, 2243–2273September (1976).

[69] C. Jungen and D. Dill, J. Chem. Phys **73**, 3338–3345October (1980).

[70] C. Jungen, Physical Review Letters **53**, 2394–2397December (1984).

[71] J. A. Stephens and C. H. Greene, J. Chem. Phys. **103**, 5470–5475October (1995).

[72] C. H. Greene and C. Jungene, Advances in Atomic and Molecular Physics **21**, 51–121 (1985).

[73] J. Tennyson, Journal of Physics B Atomic Molecular Physics **21**, 805–816March (1988).

[74] I. Shimamura, C. J. Noble, and P. G. Burke, Physical Review A **41**, 3545–3554April (1990).

[75] B. Yoo, "Theoretical Description of Doubly Excited States of Molecular Hydrogen." Ph.D. thesis, THE LOUISIANA STATE UNIVERSITY AND AGRICULTURAL AND MECHANICAL COL.. 1990.

[76] D. A. Little, K. Chakrabarti, J. Z. Mezei, I. F. Schneider, and J. Tennyson, Physical Review A **90**, p. 052705November (2014).

[77] R. Čurík and C. H. Greene, Physical Review Letters **98**, p. 173201April (2007).

[78] M. Hiyama and N. Kosugi, Journal of Physics B Atomic Molecular Physics **39**, 1797–1811April (2006).

[79] M. Telmini, S. Bezzaouia, and C. Jungen, International Journal of Quantum Chemistry **104**, 530–537 (2005).

[80] D. Haxton and C. Greene, "Multichannel quantum defect studies of e^- + LiH_2^+ and e^- + NO_2^+," in *APS Division of Atomic, Molecular and Optical Physics Meeting Abstracts* (2008).

[81] P. F. O'mahony and F. Mota-Furtado, Physical Review Letters **67**, 2283–2286October (1991).

[82] M. Abramowitz and I. A. Stegun, *Handbook of Mathematical Functions, New York: Dover, 1972* (1972).

[83] S. Altunata, *Generalized Quantum Defect Methods in Quantum Chemistry* (Massachusetts Institute of Technology, Department of Chemistry, 2006).

[84] H. Goldstein, C. Poole, and J. Safko, *Classical mechanics (3rd ed.) by H. Goldstein, C. Poolo, and J. Safko. San Francisco: Addison-Wesley, 2002.* (2002).

[85] E. Merzbacher, *Quantum Mechanics, 3rd Edition, by Eugen Merzbacher, pp. 672. ISBN 0-471-88702-1. Wiley-VCH , December 1997.* (1997).

[86] W. Demtröder, *Molecular Physics: Theoretical Principles and Experimental Methods, by Wolfgang Demtröder, pp. 484. ISBN 3-527-40566-6. Wiley-VCH , November 2005.* (2005).

[87] A. M. Lane, Journal of Physics B Atomic Molecular Physics **19**, 253–257January (1986).

[88] P. G. Burke, I. Mackey, and I. Shimamura, Journal of Physics B Atomic Molecular Physics **10**, 2497–2512August (1977).

[89] P. G. Burke and J. Tennyson, Molecular Physics **103**, 2537–2548 (2005).

[90] A. G. Harvey, D. S. Brambila, F. Morales, and O. Smirnova, Journal of Physics B Atomic Molecular Physics **47**, p. 215005November (2014).

[91] O. Nagy, C. P. Ballance, K. A. Berrington, P. G. Burke, and B. M. McLaughlin, Journal of Physics B Atomic Molecular Physics **32**, L469–L477August (1999).

[92] H. S. W. Massey and C. B. O. Mohr, Proceedings of the Royal Society of London Series A **136**, 289–311May (1932).

[93] H. S. W. Massey and C. B. O. Mohr, Proceedings of the Royal Society of London Series A **139**, 187–201January (1933).

[94] N. F. Mott and H. S. W. Massey, *The theory of atomic collisions, by Mott, N. F.; Massey, Harrie Stewart Wilson. Oxford, Clarendon Press, 1949.* (1949).

[95] M. J. Seaton, Philosophical Transactions of the Royal Society of London Series A **245**, 469–499February (1953).

[96] A. Faure, J. D. Gorfinkiel, L. A. Morgan, and J. Tennyson, Computer Physics Communications **144**, 224–241April (2002).

[97] A. G. Harvey, D. S. Brambila, F. Morales, and O. Smirnova, ArXiv e-prints December (2014), arXiv:1401.0229 [physics.chem-ph] .

[98] C. Jungen, Optics & Photonics News **9**, p. 47October (1998).

[99] E. S. Chang and U. Fano, Phys. Rev. A **6**, 173–185July (1972).

[100] R. S. Mulliken, Physical Review **136**, 962–965November (1964).

[101] C. Ballance, Personal Communications, 2013-2016.

[102] J. Kobus, H. M. Quiney, and S. Wilson, Journal of Physics B Atomic Molecular Physics **34**, 2045–2056May (2001).

[103] D. E. Woon and T. H. Dunning, Jr., J. Chem. Phys. **103**, 4572–4585September (1995).

[104] E. W. Plummer, T. Gustafsson, W. Gudat, and D. E. Eastman, Phys. Rev. A **15**, 2339–2355June (1977).

[105] P. J. Linstrom and W. G. Mallard, eds., *NIST Chemistry WebBook, NIST Standard Reference Database Number 69* (National Institute of Standards and Technology, Gaithersburg MD, 20899, 2005).

[106] C. H. Greene, Phys. Rev. A **22**, 149–157July (1980).

[107] A. M. Mukhamedzhanov and M. Akin, European Physical Journal A **37**, p. 185July (2008), nucl-th/0602006